A NEW

TRANSFER FUNCTION ANALYSER

by

James R. Robertson.

A thesis submitted to
the University of Warwick
for the degree of
Doctor of Philosophy.

School of Engineering Science

April 1971.

ABSTRACT

This thesis investigates the concept and design of a portable on-line transfer function analyser (TFA). It is eminently suitable for the identification of plants and other controlled feedback systems in which normal operating records are available.

A point by point representation in the frequency domain, requiring a maximum of three records, allows Nyquist plots to be carried out, either visually or by plotter facilities. The basic theory relies heavily upon statistical concepts whereby, least squares estimates of the transfer function are obtained from a combination of heterodyning, exact filtering and adaptive loops. The resultant output, on both channels (real and imaginary), is the culmination of the solution to two linear differential equations with stochastic coefficients, so mechanised when the adaptive loops reach a stable equilibrium.

Throughout, emphasis is placed upon the electronics combining the best of analog and digital techniques, in order that six parallel paths may be analysed in similar mode. This is especially true of the heterodyning and filtering operations. Practical shortcomings of the instrument are noted by comparing estimates with those from the best currently available commercial apparatus, operating on deterministic signals. Examples of a feedback loop, subjected to both deterministic and random stimulii, with and without the presence of extraneous noise sources, are used to illustrate the ease and simplicity by which the instrument can be used in place of complex computing schemes, which tend, in consequence, to be solely of local academic interest.

The practical features of the thesis have led to the submission

of four papers to the technical press. Two of them deal, exclusively, with a capacitor ratio commutated filter - not apparently described in publications to date - which is also the subject of a proposed patent application in conjunction with NRDC. It is intended, in the near future, to submit the complete instrument as the basis for a second patent proposal.

ACKNOWLEDGEMENTS

This thesis represents work carried out at the University of Warwick, by the author, during the period October 1968 to December 1970. It was solely conducted by him, except where due acknowledgement has been made to references.

During this period, he was financed by the Science Research Council to develop a new method of transfer function analysis and is, accordingly, greatly indebted for their assistance.

He expresses his thanks to the School of Engineering Science for the experimental equipment available and to his supervisor, Dr. M. T. G. Hughes, for his initiation and helpful discussions of the project.

Finally, he appreciates the competence of his Senior Technician, Mr. M. P. Bell, whose interest in printed circuit boards allowed a compact instrument to be built.

James R Robertson

CONTENTS

GLOSSARY OF PRINCIPAL SYMBOLS

CHAPTER TWO

A	Amplitude of signal.
$Av[\ ]$	Average or expected value of.
A_{yx}	Real part of true cross-spectral density function - S_{yx}.
$b[\ ]$	Bias of.
BT	Bandwidth - time product relating to the evaluation of co-variance matrix.
B_{yx}	Imaginary part of true cross-spectral density function - S_{yx}.
$Cov[\ ]$	Covariance of.
$C_{ye}(jw)$	Estimate of cross-spectral density function - $S_{ye}(jw)$.
e_f, x_f, y_f	Abbreviated notation for filtered portions of signals fed to the instrument.
e_c, x_c, y_c	Real part of above filtered signals.
e_s, x_s, y_s	Imaginary part of above filtered signals.
e^1_f, y^1_f	Complex products obtained by multiplying e_f, y_f by x_f.
$e(t)$	Error signal in feedback system.
$f(\varepsilon_m)$	Scalar function of model error.
$g(\psi)$	Impulse response of forward path.
$G(jw)$	Fourier transform of $g(\psi)$.
$h(\sigma)$	Impulse response of feedback path.
$H(jw)$	Fourier transform of $h(\sigma)$.
I_1, I_2, I_3	Abbreviated notation for evaluation of integrals.
j	$\sqrt{-1}$.
K	Real part of S_{yx} / S_{ex}.

K_a	Gain of adaptive loop.
L	Imaginary part of S_{yx} / S_{ex}.
m(t)	Additive noise signal in feedback path.
n	Integer.
n(t)	Additive noise signal in forward path.
$p(\psi)$	Impulse response of circuit between noise and output of forward path.
$q(\sigma)$	Impulse response of circuit between noise and output of feedback path.
$R_{ye}(\tau)$	Cross-correlation function between y(t) and e(t) as a function of time delay.
s	Complex frequency variable in Laplacian notation.
$S_{ye}(jw)$	Fourier transform of $R_{ye}(\tau)$ - true cross-spectral density function.
t	Time variable.
u_1, u_2, u_3, u_4	Variables of integration.
U_m	Real part of model transfer function.
Var [ ]	Variance of.
V_m	Imaginary part of model transfer function.
w	Frequency variable (radians per second).
w_c	Bandwidth of analysis filters.
w_e	"Equivalent bandwidth" of w_c.
w_o	Heterodyning frequency.
x(t)	Input signal.
y(t)	Output signal.
z(t)	Output signal from feedback path.
Z, Y, X, Q, P, N, M	Abbreviated notation for Fourier transform of the respective time signals.
γ^2_e	Coherency function at point e with respect to x.

CHAPTER THREE

$\alpha(t)$	Modulating function.
a_o, a_i, b_i	Fourier coefficients of $\alpha(t)$.
C	Capacitance.
C_p	Generalisation of cosine value at p^{th} iteration.
f_s	Sampling frequency (cycles per second).
F_k	Discrete weight of $\alpha(t)$.
Hz	Frequency.
i,k	Integers.
i(t)	Current.
K_p	Generalisation of the weights of a digital counter.
m(t)	Modulating function.
q	Radix to power n.
r	Radix.
R	Resistance.
S_p	Generalisation of sine value at p^{th} iteration.
T	Period of $\alpha(t)$.
u(t)	Heaviside step function.
v,V	Voltages.
w_a	Analogue frequency variable.
w_d	Digital frequency variable.
z	Z transform variable.
Z	Impedance.
ε	Error.
θ	Angle.
Ω	Ohms.
Ω_s	Normalised sampling frequency.
λ	Segment of modulating function.

CHAPTER ONE

Introduction

The thesis proposes to investigate a branch of control theory which deals with system identification. This topic may be understood as an experimental attempt, by control engineers, to formulate the unknown behaviour of a controlled system in mathematical terms or graphical displays. His objective usually stems from the desire to improve the performance of the system plant in question, when his knowledge may be limited through either

1) the plant being a new and untried piece of commercial hardware or
2) he not being fully conversant with all the system constants that he requires for his model.

The study must be observed in the time domain but the outcome of the identification may be realised in either the time or frequency domain. Choosing between the two, is a matter of personal preference, depending on the ease and familiarity with which the display can be interpreted.

The experimental data may be the result of observing the response to closely defined inputs such as sinusoids and impulses. Unfortunately, industrial operations cannot always permit such experiments, which corrupt the reference signals. In addition, it may be too expensive to conduct controlled experiments, with the plant disengaged from the production line. Hence, modern thinking has been prejudiced to provide answers to the identification problem, by employing the random data observed on the reference levels, with the process working under normal operating conditions. In some cases, this has not proved to be a success and control engineers have resorted to imposing a well defined signal of low amplitude upon the random data, whilst the system is operating

normally. Collection of the data when the plant is running normally, is given the title of "on-line" or "in-situ" measurements.

However, if the system is stimulated by a stochastic or random, rather than deterministic signal, problems in the collection of data will arise. In particular, measurements will be time consuming, since consistent evaluation of the data can only be performed using averaging techniques. Due to this inherent time lag, immediate corrective action to the system cannot be taken, if the random data analysis reveals an inadequate performance. In addition, the system must be linear and time - invariant, over at least the duration of the complete analysis, for the results to make sense.

The relative importance of the subject can be assessed by browsing through the contents of one IFAC Conference (Prague 1967). Papers by Cuenod and Sage (1) and Eykhoff (2) give useful introductions, whilst a recent comprehensive review has been provided by Balakrishnan (3). Identification techniques are important not only to the control field. Communication systems (4), medical techniques (5), mechanical vibrations (6), oceanic (7) and atmospheric disturbances (8) all benefit from the same analysis. In each case, the problem may be generalised to estimating the system behaviour, when the measurement points are known to contain "additive noise".

The basic mathematical concepts involved were evaluated in the early part of this century but it was not until the work of Rice (9) and Wiener (10), that the treatment of noise problems was firmly established. In this thesis, use of their techniques will be applied to the on-line estimation of frequency response functions in continuous form.

1.1 Review of Continuous Frequency Response Estimation using Computational Methods.

One of the earliest examples of identifying a system from

normal operating records originates from work carried out by Goodman and Reswick (11). Although their approach was essentially based in the time domain using correlation studies, it revealed how modelling techniques could manipulate stationary second-order amplitude processes, to simulate an impulse response, evaluated at specific units of delay. Manipulation of the weights of a delay line were performed manually via visual comparison of the model and system cross-correlation functions. The frequency response followed naturally using Fourier transformation.

With the advent of spectral analysis in 1958, dynamic modelling was not to gain much favour after the initial impetus. Blackman and Tukey (12) rationalised the smoothing of time series by spectral methods, to show that computerised techniques could successfully eliminate all special purpose hardware, the "smoothing windows" and time-frequency transformations being implicit via the skill of the programmer. Concurrently, using the above methods, Goodman (13) developed a regression procedure for estimating the open-loop transfer function of a system when the driving and additive output noise disturbances were assumed uncorrelated. This method was effectively the dual technique to (11). Goodman et al (14) successfully demonstrated the use of the former's approach, by applying stationary noise to simulated versions of a blending operation and a stirred tank reactor, to extract gain and phase information. Jenkins (15), without adding to the general theory, conducted similar experiments when evaluating the performance of a heat exchanger. A joint conclusion from these two papers appears to be, that conventional industrial plant self-generates insufficient uncorrelated disturbances of the input variables, to provide a foundation for spectral analysis. Stanton (16,17) obtained very useful results for turboalternator data, whilst attempting to estimate transfer functions for power station equipment but believed his results to be influenced more by inadequate power-system

instrumentation rather than insufficient data power.

Unfortunately, the above use of spectral techniques is inapplicable for a system with feedback loops contaminated by noise. However, Akaike (18) showed that, excessive bias, in the estimates for the feedback case, could be alleviated by referring to a signal external to the control loop, which was uncorrelated with the stochastic disturbances. In doing so, he further advanced the problem (19) of how best to make a two-point estimation of the forward path transfer function, when this reference signal was not present. The method relied upon "mixed spectra" whereby the output noise from the controller was assumed stationary and non-Gaussian, whereas the random disturbances and measurement errors were assumed to consist of traditional second-order statistics - a not very practical situation. It appears that this problem yet remains unsolved.

With the realisation of model-reference control systems (20), it was recognised that these techniques could be utilised for identification purposes. In particular, they are very useful (21) when updating of the estimation is required due to time variations in the system. The method relies upon some "a priori" knowledge of the system order, expressed as a polynomial in the frequency domain, the polynomial coefficients being adjusted to minimise an error criterion between the system and model, usually based on gradient techniques. Both linear and non-linear systems with single-valued non-linearities (22) may be identified to advantage. In particular, use of analogue computer simulations, in combination with a suitable adjustment algorithm can replace the costly computing facilities required by spectral analysis techniques.

1.2 Review of Continuous Frequency Response Estimation using Special Purpose Hardware.

The techniques applied here tend to be sequential in nature, since ease of use and low cost is being traded for the large storage

facilities provided by a computer. The simplest schemes are based upon the injection of a sinusoidal stimulus into the system and the output response evaluated by correlation techniques, to remove errors due to noise - a case of linear regression. Indeed, resolution of the response into its constituent real and imaginary portions, in combination with the above techniques, was used by Dwyer (23) for the construction of two differential equations for continuous single point estimation. When the equations reached their steady state, the response was directly interpreted as a measure of the system's component gains. It was further claimed to evaluate the system impulse response, at regular time intervals, when random data was used. However, unless use was made of spectrum analysis, via evaluating the signal power content through narrow-band filters, assuming knowledge of the input spectra to be "white", very little progress had been made in this direction, until a paper was presented by Hughes and May (24). It revealed that, using analogue computer simulation, random data around a specific region, could be extracted in blocks using filtering techniques, manipulated by hardware in the form of a first-order stochastic differential equation and in the steady state, produce reliable estimates of the system's real and imaginary gains. A hardware algorithm was based upon gradient techniques. The study was later to become the basis of a special purpose analyser for open-loop estimation (25).

1.3 Motivation of Thesis.

Although analysis is possible and more practically viable in the time domain, this thesis aims to implement a special purpose instrument which will advance the approach to on-line estimation in the frequency domain, with the presence of feedback loops. On-line correlators are commercially available but not for solving feedback problems, since they contain no mechanism to remove a bias caused by injected noise into the inner loop. As regards the use

of a suitable stimulus, sinusoids, steps and impulses are of limited use, if there is an obvious desire not to upset the system, once it has been started. To this end, the intended hardware must rely either upon injected random or pseudo - random data (26) or on self-evident uncorrelated processes, naturally occurring in the controlled plant. However, it is worthwhile to note that, when conditions are favourable, sinusoids do produce a high concentration of power in a very narrow bandwidth, so yielding robust estimates.

Applications would not be solely confined to identification of electrical and automatic control schemes. The instrument would be foreseen as invaluable to the whole field of frequency response analysis, which embraces random vibrations, biomedical applications and fluid mechanics. A consequence of its universal application in the engineering world would necessitate a design able to analyse frequences in a region as low as ·01Hz - for automatic control schemes - to 2KHZ, necessary for vibration analysis of machine tools. A corresponding amplitude range would involve orders of at least 60dB, in any one sweep, with the possible addition of another 60dB of external scaling. Responses of any plant, tool joint etc., would be displayed using Nyquist plots. Since the instrument would function, even if the plant input and output signals to it were interchanged, reciprocal identification is also feasible.

Arguments for such an instrument would find strong industrial appeal, due to the present limitation of current hardware. Indeed, applied sinusoids must corrupt the reference signal, giving rise to superimposed oscillation on the controlled output. Consequently, shut-down of the plant would appear inevitable, before a testing procedure could be instituted. Whereas, with a instrument relying solely upon random input signal features, it could be plugged on-line and with some variable controller in the plant loop, adjustments made to improve the system response, should such sophistication, over and above the identification procedure be so required. In particular, the instrument should possibly identify

hardware which is unstable in the open-loop case e.g. integrators. In this situation at present, known local feedback is administered before correlators can be used with random data.

To summarise, it would appear that known methods of identification are either too cumbersome, at present, to be of general industrial use, or cannot be used on-line in any feature. Hence, the intended instrument should be a valuable contribution to dynamic analysis in the frequency domain, being both practical and uncomplicated by large-scale computing schemes, which tend, in consequence, to be of local academic interest.

1.4 Contribution of Thesis.

Chapter two initially deals with the mathematical background to the problem in general terms. It reveals that, an unbiased estimator of the forward path transfer function may be obtained from a ratio of cross-spectra. In addition, a variance expression is deduced to reveal the effect of corrupting noise upon the derived estimate. The chapter then continues by explaining, mathematically, how the available data may be manipulated by the method of gradients to form a two-parameter model estimate of the desired transfer function, evaluated at single points in the frequency domain. Two first-order differential equations with stochastic coefficients are the outcome of the analysis. These may be solved in the mean, using a fourth-order integral expression. The parameter estimates are shown to converge exponentially and bias expressions are derived without recourse to the Fokker-Planck equation (25), in which the stochastic coefficients must be assumed macroscopically "white", in comparison to the averaging time of the adaptive loop.

Chapter three deals exclusively with two very important circuit features -heterodyning and filtering - showing, where necessary, the present limitations of the circuitry to date. Two important contributions have here been devised, using hybrid techniques

i.e. information is processed in an analogue manner under the influence of digital controls. Critical potentiometers are therefore no longer a source of concern for frequency sweeping. The heterodyning technique is based upon a recursion, for the trigonometrical functions sine and cosine, using identities similar to :-

$$\sin (A+B) = \sin A \cos B + \cos A \sin B$$

$$\sin (A+B+C) = \sin (A+B) \cos C + \cos(A+B) \sin C$$

This enables 360° to be evaluated in 64 discrete steps, without using nearly the same amount of individual resistor weights.

Secondly, a new form of filter has been conceived by the author, who is unaware of any other published reference to the topic. It has been designated the "Capacitor Ratio Commutated Filter" (CRCF) and basically relies upon capacitors and switches for its construction. Such an arrangement can produce filters whose cut-off points are a function of the commutating frequency and the ratio between the capacitors. In addition, these filters could theoretically be immune from temperature effects, if the capacitors have the same characteristics. This makes the technique feasible for integrated circuit manufacture. It is further revealed that, by recourse to established active filter networks, similar characteristics can be obtained by replacing the fixed resistors by commutated capacitors, thus giving continuous variation of the cut-off frequency, without using either decade switched capacitors or variable resistors. Although only low-pass shapes have been analysed, certain features have been observed, which makes the author suspect that the technique could also be applied to both band-pass and high-pass filters.

Chapter four explains the new transfer function analyser (TFA) in detail. It reveals that although being a complicated piece of hardware, the operator interference with the front panel controls has been kept to a minimum, by the use of thumbwheel switched controls and automatically sweeping facilities. The frequency

sweeping, heterodyning and filtering have all been locked to digitally derived clock waveforms.

Chapter five illustrates the performance of the instrument in practice. It shows the results of identifying transfer functions in either closed-loop or open-loop systems, using an injected stimulus stimulii based on sinusoids, pseudo-random sequences and Gaussian random data, the first two being implicitly derived test signals. An explanation of system errors completes the chapter and thesis apart from the conclusions of chapter six and following appendices.

CHAPTER TWO

Theoretical Study of a New Transfer Function Analyser

2.1 Introduction.

The previous chapter has highlighted the benefits and requirements of a portable on-line random data analyser. Here, a theoretical study reveals the fundamentals of such an instrument and illustrates the versatility of an adaptive loop to remove a practical drawback for low-signal-level transfer function analysis - that of division. In addition to developing the basic stochastic differential equations which govern the aforementioned loop, approximate solutions for the bias and rate of convergence of the adaptive loop are derived.

Theoretical expressions for the normalised variance of the real and imaginary portions of any forward path transfer function are derived. They reveal a strict dependency solely on the coherence of the error path.

2.2 Basic Concepts.

A schematic diagram is shown in Fig.(2.1). This depicts a generalised feedback system and the proposed instrument is intended to identify the forward or feedback transfer functions. The system is observed to consist of a forward path network of impulse response $g(\psi)$, the output of which is re-connected to the input via a feedback network of impulse response $h(\sigma)$. Each network is assumed linear and time invariant, although not necessarily stable in the open-loop condition. The signals $x(t)$, $e(t)$, $y(t)$ are assumed to consist of stationary random variables. In addition, stochastic disturbances $n(t)$, $m(t)$ when passed through unknown linear networks of impulse response $p(\psi)$, $q(\sigma)$ may interfere with measurements at the points indicated. The inputs $n(t)$, $m(t)$ are assumed to be additive noise sources, which are Gaussian with zero mean values and uncorrelated with $x(t)$, $e(t)$, $y(t)$, although they may be correlated with each other. Hence, it should be noted that a deterministic signal is

A "two-point" estimate of a transfer function is an estimate which is derived from two separate signals which are connected by that transfer function.

not necessarily assumed present. The problem, then, is to measure either G(jw) or H(jw) - the fourier transforms of $g(\psi)$, $h(\sigma)$ respectively - by applying spectral analysis techniques.

No claim will be established for the use of the instrument to solve the "two-point"* feedback estimation problem posed by Akaike (18) and Priestley (27), whereby $x(t) \equiv 0$, i.e. x(t) cannot in any way be reckoned as a source of information.

Consider first the time-domain approach.

$$y(t) = \int_{-\infty}^{+\infty} g(\psi)e(t-\psi)d\psi + \int_{-\infty}^{+\infty} p(\psi)n(t-\psi)d\psi \qquad (2.1)$$

$$z(t) = \int_{-\infty}^{+\infty} h(\sigma)y(t-\sigma)d\sigma + \int_{-\infty}^{+\infty} q(\sigma)m(t-\sigma)d\sigma \qquad (2.2)$$

$$e(t) = x(t) - z(t) \qquad (2.3)$$

It is thus observed that the various time functions are related by convolution integrals, whose lower limits will be zero if we consider conditions of physical realisability. These imply that the impulse responses $g(\psi)$, $h(\sigma)$ are zero before the application of a source at time t = 0. In addition, it is assumed that $|g(\psi)|$, $|g(\psi)|^2$, $|p(\psi)|$, $|p(\psi)|^2$, $|h(\sigma)|$, $|h(\sigma)|^2$, $|q(\sigma)|$, $|q(\sigma)|^2$, are integrable. Under these conditions, the equations (2.1) to (2.3) may be Fourier transformed into the frequency domain such that

$$Y(jw) = G(jw)\,E(jw) + P(jw)\,N(jw) \qquad (2.4)$$

and similarly for Z(jw), E(jw), where w is the frequency in radians per second and the symbol $j = \sqrt{-1}$.

Again viewing the approach in the time domain, it is possible to form correlation functions between the various signals. Such averaging techniques are required to reduce the corrupting effects of noise (11). If we consider e(t), y(t) to be real variables, then it may be said that

$R_{ye}(\tau) = \overline{y(t+\tau)e(t)}$ where the bar indicates the averaging

operator, R the cross-correlation function. This technique, which is applied for the analysis of stable systems, when used in combination with (2.1) yields

$$R_{ye}(\tau) = \int_{-\infty}^{+\infty} R_{ee}(\tau-\psi)\, g(\psi)d\psi + \int_{-\infty}^{+\infty} R_{ne}(\tau-\psi)p(\psi)d\psi \qquad (2.5)$$

Using the well-known one-to-one correspondence of correlation and spectral density functions, it may be stated that

$$S_{ye}(jw) = S_{ee}(jw)\, G(jw) + S_{ne}(jw)\, P(jw) \qquad (2.6)$$

where S represents the double-sided spectral density function which may be real or complex. With stochastic signals, it is apparent that the forward path transfer function is readily identifiable as $S_{ne}(jw)$ or $P(jw)$ tend to zero.

2.2.1 Bias Aspects of Cross-Spectral Identification.

From (2.6), an estimate of the forward path transfer function may be obtained by saying

$$\hat{G}(jw) = \frac{C_{ye}(jw)}{C_{ee}(jw)} - \frac{P(jw)\, C_{ne}(jw)}{C_{ee}(jw)} \qquad (2.7)$$

where the circumflex indicates an estimator and C an approximation to the true spectral density S, by virtue of finite averaging. The expected value of $\hat{G}(jw)$ will be unbiased if the signals n(t), e(t) are uncorrelated and the ratio $\left[C_{ye}(jw)\right]\left[C_{ee}(jw)\right]^{-1}$ is itself unbiased. One instance occurs when the feedback path is open-circuited. Unfortunately, as seen from Fig.(2.1), the interfering disturbance, n(t), must correlate with the error signal and thus a biased estimate results. How may this be removed? From the notation developed for (2.4), using capital letters as an implied function of (jw), we may formally say

$$Y = GE + PN \qquad (2.8)$$

$$E = X - Z \qquad (2.9)$$

$$Z = HY + QM \tag{2.10}$$

$$\therefore E = X - (HY + QM) \tag{2.11}$$

and (2.7) gives :-

$$Y = G\left[X - (HY + QM)\right] + PN$$

$$\therefore Y(1 + GH) = GX - GQM + PN \tag{2.12}$$

Similarly

$$E(1 + GH) = X - HPN - QM \tag{2.13}$$

Let us take an information point external to the loop, say X and disregard the effects of non-ideal filtering of the data.

Therefore from (2.12) and (2.13) :-

$$C_{yx} = \frac{G\,C_{xx}}{1+GH} - \frac{GQC_{mx}}{1+GH} + \frac{PC_{nx}}{1+GH} \tag{2.14}$$

$$C_{ex} = \frac{C_{xx}}{1+GH} - \frac{HPC_{nx}}{1+GH} - \frac{QC_{mx}}{1+GH} \tag{2.15}$$

$$\therefore \frac{C_{yx}}{C_{ex}} = \frac{GC_{xx} - GQC_{mx} + PC_{nx}}{C_{xx} - HPC_{nx} - QC_{mx}} \tag{2.16}$$

Hence, from the initially assumed zero correlation between the disturbances and the random signal x(t), the estimate, after ensemble averaging of both numerator and denominator yields

$$\frac{S_{yx}}{S_{ex}} = G \tag{2.17}$$

and an unbiased result is obtained. A variance component will of course remain. Akaike (18) has in fact suggested that, viewing of the signal external to the loop is not a necessary prerequisite for an unbiased estimate. All that is required, is information which correlates with this reference signal. The instrument, described in this thesis, will exploit this fact to simplify its operation.

If we return to (2.7), it was noted that a biased estimator of G (jw) is obtained from a two point analysis. How severe is this ?

From (2.8) to (2.13) the equivalent spectral density equations result :-

$$C_{yy} = |G|^2 C_{ee} + |P|^2 C_{nn} + GC_{en} P^* + P C_{ne} G^* \quad (2.18)$$

$$C_{en} = C_{xn} - HC_{yn} - QC_{mn} \quad (2.19)$$

$$C_{yn} = GC_{en} + PC_{nn} \quad (2.20)$$

where the asterisk signifies a complex conjugate.

Making use of (2.7) an estimate of the bias yields :-

$$\frac{PC_{ne}}{C_{ee}} = \frac{\left[C_{yy} - |G|^2 C_{ee} - |P|^2 C_{nn} - GC_{en} P^*\right]}{C_{ee} G^*}$$

By taking expected values throughout, it can be seen that

$$b\left[\hat{G}\right] = \frac{\left[S_{yy} - |G|^2 S_{ee} - |P|^2 S_{nn} (1+GH)^{-1}\right]}{S_{ee} G^*} \quad (2.21)$$

assuming x, m, n are all mutually uncorrelated and b symbolises the bias term. The value of the bias can be made equal to zero, either when no noise source n(t) is present, or the feedback loop is open-circuited. An interesting sidelight of (2.21) further reveals that although introduction of the feedback noise source, m(t), inflates S_{yy} and S_{ee}, it cannot affect the bias term when $S_{nn} = 0$. For this situation, $S_{yy} = |G|^2 S_{ee}$ and therefore $b\left[\hat{G}\right] = 0$.

Using a similar derivation of the result in (2.16), an unbiased estimator of H could be obtained by using the ratio $(C_{zx})(C_{yx})^{-1}$. If the estimator was obtained using only the signals z(t), y(t), an equivalent bias term to (2.21) would prevail, except that the expression would be influenced more by m(t), due to the effective roles of m(t) and n(t) being interchanged in the analysis.

2.2.2 Variance Aspects of Cross-Spectral Identification.

Although an unbiased result for $\hat{G}$ may be readily obtained, the question remains as to the scatter of these estimated points around the mean. For the convenience in implementing the

instrument, the value of $\hat{G}$ is required in orthogonal co-ordinates such that

$$\hat{K} = \text{Real part of } C_{yx} / C_{ex}$$

$$\hat{L} = \text{Quadrature part of } C_{yx} / C_{ex}$$

and C_{yx}, C_{ex} can be split into co and quadrature spectral density components $\hat{A}$, $\hat{B}$ respectively.

$$\therefore \hat{K} = \frac{\hat{A}_{yx}\hat{A}_{ex} + \hat{B}_{yx}\hat{B}_{ex}}{\hat{A}_{ex}^2 + \hat{B}_{ex}^2} = RP\,\frac{C_{yx}\,C_{ex}^*}{C_{ex}\,C_{ex}^*} \qquad (2.22)$$

$$\hat{L} = \frac{\hat{A}_{yx}\hat{B}_{ex} - \hat{A}_{ex}\hat{B}_{yx}}{\hat{A}_{ex}^2 + \hat{B}_{ex}^2} = Im\,P\,\frac{C_{yx}\,C_{ex}^*}{C_{ex}\,C_{ex}^*} \qquad (2.23)$$

Now consider small perturbations $\delta\hat{A}$, $\delta\hat{B}$ about the expected or average values.

$$Av\left[\hat{A}\right] = A, \quad Av\left[\hat{B}\right] = B \text{ so that}$$

$$\hat{A}_{yx} = A_{yx} + \delta\hat{A}_{yx}$$

$$\hat{B}_{yx} = B_{yx} + \delta\hat{B}_{yx}$$

$$\hat{A}_{ex} = A_{ex} + \delta\hat{A}_{ex}$$

$$\hat{B}_{ex} = B_{ex} + \delta\hat{B}_{ex}$$

Further define:-

$$Av\left[\delta\hat{A}_{yx}\right] = Av\left[\delta\hat{B}_{yx}\right] = Av\left[\delta\hat{A}_{ex}\right] = Av\left[\delta\hat{B}_{ex}\right] = 0$$

and

$$Av\left[\delta\hat{A}_{yx}^2\right] = Var\left[\hat{A}_{yx}\right]$$

$$Av\left[\delta\hat{A}_{yx}\,\delta\hat{B}_{yx}\right] = Cov\left[\hat{A}_{yx}, \hat{B}_{yx}\right] \text{ etc.}$$

Equation (2.22) may be expanded as a Taylor series (28) to include only terms of first order, if the number of degrees of freedom are such that $Var\left[\hat{A}_{yx}\right]$ etc., are small in comparison to the mean value of the estimate.

Hence,

$$\hat{K} = \frac{\left[(A_{yx} + \delta\hat{A}_{yx})(A_{ex} + \delta\hat{A}_{ex}) + (B_{yx} + \delta\hat{B}_{yx})(B_{ex} + \delta\hat{B}_{ex})\right]}{(A_{ex} + \delta\hat{A}_{ex})^2 + (B_{ex} + \delta\hat{B}_{ex})^2} \quad (2.24)$$

$$\hat{L} = \frac{\left[(A_{yx} + \delta\hat{A}_{yx})(B_{ex} + \delta\hat{B}_{ex}) - (A_{ex} + \delta\hat{A}_{ex})(B_{yx} + \delta\hat{B}_{yx})\right]}{(A_{ex} + \delta\hat{A}_{ex})^2 + (B_{ex} + \delta\hat{B}_{ex})^2} \quad (2.25)$$

A Taylor series expansion of a non-linear function $g(X_1, X_2, X_3 \ldots X_n)$ of random variables $(X_1, X_2, X_3 \ldots X_n)$ may be written about the point $(a_1, a_2, a_3 \ldots a_n)$ as:-

$$g(X_1, X_2, X_3 \ldots X_n) \approx g(a_1, a_2, a_3 \ldots a_n) + \sum_{i=1}^{n} \left[\frac{\partial g}{\partial X_i}\right]_{X_i = a_i} (X_i - a_i) \quad (2.26)$$

This is performed in Appendix One for $\hat{K}$ and due to the similarity between (2.24) and (2.25), inferred for $\hat{L}$. Consequently, it is observed from (A1.3) and (A1.7) that

$$\text{Av}\left[\hat{K}\right] = \text{Re Part} \frac{S_{yx} S_{ex}^*}{S_{ex} S_{ex}^*} \quad (2.27)$$

$$\text{Av}\left[\hat{L}\right] = \text{Im Part} \frac{S_{yx} S_{ex}^*}{S_{ex} S_{ex}^*} \quad (2.28)$$

$$\frac{\text{Var}\left[\hat{K}\right]}{K^2} = \frac{\text{Var}\left[\hat{L}\right]}{L^2} \approx \frac{4}{2BT}\left[\frac{1}{\gamma_{\delta\epsilon}^2} - 1\right] \quad (2.29)$$

where $\gamma_{\delta\epsilon}^2$ by (A1.8) is the coherency function, a real number such that $0 \leq \gamma_{\delta\epsilon}^2 \leq 1$ - and is defined by Enochson (29). It directly gives a measure of signal/noise power ratio at the measurement points e and x. When no noise is present, there is no variance in the estimates of K and L. Goodman's (13) work on the open-loop estimate resulted in confidence expressions depending on γ_{y}^2. It would be interesting to find out whether γ_{ϵ}^2 and γ_{y}^2 are similar in the closed-loop case, since similar confidence statements might be applicable.

Using (2.12 to 2.15) it can be said:-

$$C_{yy}\,|1+GH|^2 = |G|^2C_{xx} + |GQ|^2C_{mm} + |P|^2C_{nn} - |G|^2Q^*C_{xm} + GP^*C_{xn} - |G|^2QC_{mx} - GQP^*C_{mn} + G^*PC_{nx} - PG^*Q^*C_{nm} \quad (2.30)$$

Taking expected values of (2.30) assuming x,m,n to be mutually uncorrelated

$$S_{yy}\,|1+GH|^2 = |G|^2S_{xx} + |GQ|^2S_{mm} + |P|^2S_{nn} \quad (2.31)$$

Also

$$C_{ee}\,|1+GH|^2 = C_{xx} + |HP|^2C_{nn} + |Q|^2C_{mm} - H^*P^*C_{xn} - Q^*C_{xm} - HP\,C_{nx} + HPQ^*C_{nm} - QC_{mx} + QH^*P^*C_{mn} \quad (2.32)$$

Hence, by expected values:-

$$S_{ee}\,|1+GH|^2 = S_{xx} + |HP|^2S_{nn} + |Q|^2S_{mm} \quad (2.33)$$

Further

$$|S_{yx}|^2 = \frac{|G|^2S_{xx}^2}{|1+GH|^2} \quad (2.34)$$

$$|S_{ex}|^2 = \frac{S_{xx}^2}{|1+GH|^2} \quad (2.35)$$

Using (2.31) to (2.35)

$$\gamma_{\hat{y}}^2 = \frac{|S_{yx}|^2}{S_{yy}S_{xx}} = \frac{|G|^2S_{xx}^2}{(|G|^2S_{xx} + |GQ|^2S_{mm} + |P|^2S_{nn})\,S_{xx}} \quad (2.36)$$

$$\gamma_{\hat{e}}^2 = \frac{|S_{ex}|^2}{S_{ee}S_{xx}} = \frac{S_{xx}^2}{(S_{xx} + |Q|^2S_{mm} + |HP|^2S_{nn})\,S_{xx}} \quad (2.37)$$

From (2.36) and (2.37) it is observed that $\gamma_{\hat{y}}^2 = \gamma_{\hat{e}}^2$, when either $S_{nn} = 0$ or $|H|^2 = 1$. The importance of the coherency function of

the error to that of the output, stems from a desire to circumvent the necessity for evaluating the probability density distributions of the required estimators. If these coherency functions in the closed-loop case are identical, an equivalent open-loop model may be derived for the closed-loop system. Use may then be made of Goodman's work to evaluate the confidence intervals for the estimators. Wellstead (30) pursued this approach when trying to identify the magnitude and phase of a forward path transfer function, using $S_{mm} = 0$ and $|H|^2 = 1$. Equations (2.36) and (2.37) agree with his analysis but also reveal that it may be further advanced to cope with feedback noise as well, with the proviso that either $|H|^2 = 1$ or $S_{nn} = 0$. No further attempt will be made in this thesis to develop the necessary confidence intervals, since much experimental data would be necessary to justify the theory.

2.3 An Adaptive Modelling Technique.

The technique relies upon the fact that the response of a linear time-invariant system to a complex exponential stimulus, results in an output which is characterised both by the system resolved gain factors, in the frequency domain and the resolved components of the input signal. Thus, if the input is of the form $e(t) = Ae^{jwt}$, the steady-state output will be

$$y(t) = A\left[\cos wt + j \sin wt\right]\left[U(w) + jV(w)\right] \qquad (2.38)$$

where U(w) and V(w) are the real and imaginary portions of G(jw) respectively.

If we refer to Fig. (2.2) and assume the effective value of x(t) temporarily $\equiv 1$, the signal e(t) may be resolved and the separate components applied to a two dimensional model of the system, evaluated at a particular frequency and the resultant output compared with that of the true system. An error measure ε_m will result, which may be used, automatically, to adjust the gain model parameters, such that the model $\left[\hat{U}_m(w,t) + j\hat{V}_m(w,t)\right]$ compares favourably with the system, according to an acceptable

error criterion. Dwyer (23) arrived at this technique via regression analysis for the special case of sinusoidal data and zero feedback. It is to be noted that the model will be obtained using point-to-point plotting in the frequency domain and hence is necessarily time consuming. This would appear to be the price to pay, if one requires portability. Otherwise, with storage techniques, a polynomial model, expressed in the "s-plane", would have been ideal, although requiring more than two parameters to be optimised. These have already been discussed in Chapter One, where it was observed that such techniques require extensive computational facilities.

If we are to apply the above technique to modelling the response of a system to random data, the signals from the system will initially, have to be accurately filtered. This necessity stems from Rice's (9) representation of random data, as a finite sum of sinusoids, whose frequencies are multiples of a frequency, w_n and related to the duration of the analysis. Consequently, a signal of very low power content would be the result of trying to analyse any one particular frequency. Therefore, in accordance with recognised techniques of power spectral estimation (31), an assessment of the average power is taken by viewing adjacent frequency components in addition to the component of interest. The assumption is made, that the spectral densities of these surrounding components are "white". Filtering is therefore required, the merits and practical realisation of which will be covered in Chapter Three. Meanwhile, it remains to state that after resolving the data, it has been thought better to manipulate the signal around zero frequency and hence the filter structures will be of the low-pass variety and not directly band-pass, as illustrated in Fig. (2.2).

2.3.1 Parameter Adjustment.

A powerful technique for adaptive parameter adjustment, or

hill-climbing, is known as the method of gradients. This permits parameter adjustments to be made, which are proportional to the local gradient of a suitable error function. The technique appears to have advanced from studies at M.I.T.(20). In context, let us use the symbols :-

$f(\varepsilon_m)$ to denote a scalar function of the error between the system resolved outputs and those of the model.

$\hat{U}_m(w,t)$, $\hat{V}_m(w,t)$ to denote estimates of the model gains $U(w)$, $V(w)$ respectively.

K_a to denote the gain of each adaptive loop.

Therefore,
$$\frac{d\hat{U}_m(w,t)}{dt} = -\frac{1}{2} K_a \frac{\partial f\left[\varepsilon_m(t)\right]}{\partial \hat{U}_m(w,t)} \tag{2.39}$$

$$\frac{d\hat{V}_m(w,t)}{dt} = -\frac{1}{2} K_a \frac{\partial f\left[\varepsilon_m(t)\right]}{\partial \hat{V}_m(w,t)} \tag{2.40}$$

From now onwards, explicit use of the independent variables w,t will be dropped when the text is not ambiguous.

Referring to (2.17),

$$S_{yx} = (U_m + j\, V_m)\, S_{ex} \tag{2.41}$$

is the result which we hope to instrument, based upon the error function $|\varepsilon_m|^2 = \varepsilon_m \varepsilon_m^*$. This composition of error variables has been shown by May (25) to result in a set of linear equations with stochastic coefficients. Equation (2.41) implies that the input signal to the model must be a complex function of the signals e and x, with the complementary output being a similar complex function of y and x. The generalised diagram of Fig.(2.2) may now be fully symbolised as follows. Consider each of the signals x,e,y to be resolved and filtered such that

$$\left.\begin{aligned} x_f &= x_c + jx_s \\ e_f &= e_c + je_s \\ y_f &= y_c + jy_s \end{aligned}\right\} \tag{2.42}$$

where the subscript f implies filtered data

where the subscript c implies in-phase component relative to an arbitrary clock reference.

where the subscript s implies quadrature-phase component.

Since x_f, e_f, y_f are inputs to complex multipliers, we may further define e^1_f and y^1_f to consist, also, of pairs of signals.

Therefore
$$e^1_f = e^1_{fc} + je^1_{fs}$$
$$= (e_c + je_s)(x_c + jx_s)$$
$$= (e_c x_c - e_s x_s) + j(e_s x_c + e_c x_s) \quad (2.43)$$

$$y^1_f = y^1_{fc} + jy^1_{fs}$$
$$= (y_c + jy_s)(x_c + jx_s)$$
$$= (y_c x_c - y_s x_s) + j(y_s x_c + y_c x_s) \quad (2.44)$$

Hence from Fig. (2.2),

$$\varepsilon_m = y^1_f - e^1_f(\hat{U}_m + j\hat{V}_m) \quad (2.45)$$

$$\varepsilon_m^* = y^1_f{}^* - e^1_f{}^*(\hat{U}_m - j\hat{V}_m) \quad (2.46)$$

Referring to the parameter adjustment equations (2.39), (2.40)

$$\frac{d\hat{U}_m}{dt} = -\frac{K_a}{2}\left[-\varepsilon_m e^1_f{}^* - \varepsilon_m^* e^1_f\right] \quad (2.47)$$

$$\frac{d\hat{V}_m}{dt} = -\frac{K_a}{2}\left[j\varepsilon_m e^1_f{}^* - j\varepsilon_m^* e^1_f\right] \quad (2.48)$$

Since $j(\varepsilon_m e^1_f{}^*) = j(\varepsilon_m^* e^1_f)^*$, equations (2.47), (2.48) can be further simplified to the following forms.

$$\frac{d\hat{U}_m}{dt} = K_a \,\mathrm{Real}\left[\varepsilon_m^* e^1_f\right]$$
$$= K_a\left[\varepsilon_{mc} e^1_{fc} + \varepsilon_{ms} e^1_{fs}\right] \quad (2.49)$$

Similarly

$$\frac{d\hat{V}_m}{dt} = jK_a \,\mathrm{Imag}\left[\varepsilon_m^* e^1_f\right]$$
$$= K_a\left[\varepsilon_{mc} e^1_{fc} - \varepsilon_{ms} e^1_{fs}\right] \quad (2.50)$$

Equations (2.49), (2.50) so form the differential equations, from which the model gains are obtained. In addition, they will

further determine the manner of convergence of the estimates of the parameters U_m and V_m. Unfortunately, the arrangement is not conducive to forming an impression of the convergence in terms of the stimulating random signals. This may be accomplished by substituting for ε_m as follows:-

$$\dot{\hat{U}}_m = K_a\left[\begin{array}{l}(y^1_{fc} - e^1_{fc}\hat{U}_m + e^1_{fs}\hat{V}_m)\,e^1_{fc} \\ +\,(y^1_{fs} - e^1_{fs}\hat{U}_m - e^1_{fc}\hat{V}_m)\,e^1_{fs}\end{array}\right]$$

$$\text{i.e.}\quad \dot{\hat{U}}_m = K_a\left[y^1_{fc}\,e^1_{fc} + y^1_{fs}\,e^1_{fs} - \hat{U}_m(e^{1\,2}_{fc} + e^{1\,2}_{fs})\right] \qquad (2.51)$$

In passing, it is worthwhile to note for future reference that

$$y^1_{fc}\,e^1_{fc} + y^1_{fs}\,e^1_{fs} = \tfrac{1}{2}\left[(y_c+jy_s)(e_c-je_s)+(e_c+je_s)(y_c-jy_s)\right] \times (x_s^2 + x_c^2) \qquad (2.52)$$

Similarly to (2.51),

$$\dot{\hat{V}}_m = K_a\left[y^1_{fs}\,e^1_{fc} - y^1_{fc}\,e^1_{fs} - \hat{V}_m(e^{1\,2}_{fc} + e^{1\,2}_{fs})\right] \qquad (2.53)$$

where the dot notation indicates differentiation with respect to time.

Hence two first-order linear differential equations with stochastic coefficients have resulted. These, together with the complex notation developed in this section, completely define the organisation of the parameter adjustment loops and the arrangement is depicted in Fig. (2.3), in which the synchrodyning waveform is taken to be of unit amplitude.

2.4 Statistics of an Adaptive Loop Transfer Function Analyser.

Although an adaptive modelling technique has shown to be theoretically possible, questions remain as to the rate of convergence of the model gains, whether the estimates will be biased and to what degree will the points be scattered around the mean, with or without superimposed random noise at the observation points. In short, what degree of confidence may one place in the model parameters? This will depend on both frequency and time

averaging but should be independent of signal levels. It would greatly simplify the organisation of the instrument, if the response time of the adaptive loops was also independent of signal levels. Unfortunately, since stochastic differential equations are involved, the analysis may be awkward, especially since $\hat{U}_m$, $\hat{V}_m$ are non-stationary random functions. In consequence, an approximate solution is advanced, which assumes sufficient degrees of freedom present in the averaging circuits, such that the model gains and the stochastic coefficients can be considered independent. The resultant answers produce no less insight of the exact solution, than had recourse been made to a simulation based upon the Fokker-Planck equation (25). The reason for this, is due to the implicit requirements of the Fokker-Planck equation to have its stochastic coefficients macroscopically "white", in comparison to the model gains. One extra condition, not highlighted in (25), is that the extent of the "whiteness" must be expressly interpreted from the problem. This is of paramount importance, since an infinite noise spectrum must be treated differently to the band-limited case. An excellent discussion of the matter has been given in a paper by Caughey and Dienes (32).

For the approximate solution, a feature of the mathematics will be the requirement to evaluate integrals of a fourth-order moment.

2.4.1. An Approximation to the Mean Solution of the Model Gains.

Let us take equation (2.51) as an example and view the expectation of the first-order linear differential equation in the mean. An assumption, necessary to allow a simple evaluation, proceeds from the physical nature of the adaptive loop. Since this is essentially an averaging operation, used to smooth out the high frequency components of the adaptive error, the filtering parameters are assumed virtually independent of the stimulating data.

Hence:-

$$\dot{\hat{U}}_m = K_a \left[\overline{y^1_{fc}\, e^1_{fc} + y^1_{fs}\, e^1_{fs}} - \hat{U}_m \, \overline{(e^{1\,2}_{fc} + e^{1\,2}_{fs})} \right] \qquad (2.54)$$

where the bar signifies ensemble averaging.

In the steady state, the solution must therefore tend towards

$$Av\left[\hat{U}_m\right] = \frac{Av\left[y^1_{fc}\, e^1_{fc} + y^1_{fs}\, e^1_{fs}\right]}{Av\left[e^{1\,2}_{fc} + e^{1\,2}_{fs}\right]} \qquad (2.55)$$

Similarly,

$$Av\left[\hat{V}_m\right] = \frac{Av\left[y^1_{fs}\, e^1_{fc} - y^1_{fc}\, e^1_{fs}\right]}{Av\left[e^{1\,2}_{fc} + e^{1\,2}_{fs}\right]} \qquad (2.56)$$

From both (2.55) and (2.56) the estimate of the model parameters, in the mean, is shown to depend on moments of a fourth-order process. A typical expression can be generalised to one of evaluating the fourth-order moment of the signals $\left[a^*_f, b_f, c^*_f, d_f\right]$, where a_f, b_f, c_f, d_f, are outcomes of the process generated via the heterodyning and filter operations.

For example,

$a_f = \int_0^\infty a(t-u_1) \exp jw_o(t-u_1)\, h(u_1)\, du_1$ represents the signal, a, to be rotated via a complex exponential of frequency w_o radians per second and convolved with a low-pass filter of impulse response $h(u_1)$.

Consequently,

$$a^*_f b_f c^*_f d_f = \int_0^\infty\int_0^\infty\int_0^\infty\int_0^\infty a(t-u_1)b(t-u_2)c(t-u_3)d(t-u_4)x\, h(u_1)h(u_2)h(u_3)h(u_4)x \exp -jw_o(u_1-u_2+u_3-u_4)\, du_1 du_2 du_3 du_4 \qquad (2.57)$$

Taking expected values of the above equations, results in moments of a fourth-order integrand consisting of Gaussian processes. By manipulation of the variables and changes in the order of integration, an evaluation in Appendix Three leaves the result that:-

$$Av\left[a_f^* b_f c_f^* d_f\right] = I(U) = I_1(U) + I_2(U) + I_3(U) \qquad (2.58)$$

$$= \frac{1}{4\pi^2}\int_{-\infty}^{+\infty} S_{cd}(w-w_o)H_4^*(jw)H_3(jw)dw \int_{-\infty}^{+\infty} S_{ab}(w-w_o)H_2^*(jw)H_1(jw)dw$$

$$+ \frac{1}{4\pi^2}\int_{-\infty}^{+\infty} S_{bd}(w-w_o)H_4^*(jw)H_2(jw-j2w_o)dw \int_{-\infty}^{+\infty} S_{ac}(w-w_o)H_3^*(jw-j2w_o) \times H_1(jw)dw$$

$$+ \frac{1}{4\pi^2}\int_{-\infty}^{+\infty} S_{ad}(w-w_o)H_4^*(jw)H_1(jw)dw \int_{-\infty}^{+\infty} S_{bc}(w-w_o)H_3^*(jw-j2w_o) \times H_2(jw-j2w_o)dw \qquad (2.59)$$

where S_{ij} is the double-sided power spectral density function of the respective signals and H(jw) the Fourier transform of h(u).

At first sight, the above expression would appear to be rather involved in comparison to the original equation (2.57). However, after a moment's deliberation over Fig. (2.4), the composition $I_1(U), I_2(U), I_3(U)$ visually illustrates how simple the final result will become. In Fig.(2.4), the filter transfer functions $H_1(jw), H_2(jw), H_3(jw), H_4(jw)$ are taken to be identical - a practical result of requiring six very closely controlled data reduction channels. In addition, they are illustrated as having perfect attenuation beyond the cut-off point $w = w_c$.

Therefore,

$$Av\left[a_f^* b_f c_f^* d_f\right] \simeq \frac{1}{4\pi^2}\left[\left\{S_{cd}(w_o)\int_{-\infty}^{+\infty}|H(jw)|^2 dw\right\} x\left\{S_{ab}(w_o)\int_{-\infty}^{+\infty}|H(jw)|^2 dw\right\}\right] \qquad (2.60)$$

as $w_c \longrightarrow 0$

assuming the relevent power spectral density functions to be virtually constant and $w_o - w_c > 0$.

Dividing throughout by the product of the two integrals, each defined by both Bendat and Piersol (33) and Jenkins and Watts (34) as "the equivalent bandwidth" of the data filters, we are left, in the limit as $w_c \rightarrow 0$ with an estimate which reduces to the product of the power spectral densities of the relevant signals at the heterodyning frequency w_o, as $S_{cd}(w_o)S_{ab}(w_o)$.

Hence, we may now revert to (2.55) and (2.56) to discuss the evaluation of Av $\left[\hat{U}_m\right]$, Av $\left[\hat{V}_m\right]$. Quantities of interest are:-

$$y^1_{fc}e^1_{fc}+y^1_{fs}e^1_{fs} = \tfrac{1}{2}\left[(y_c+jy_s)(e_c-je_s)+(e_c+je_s)(y_c-jy_s)\right]\left[x_c^2+x_s^2\right] \quad (2.61)$$

$$y^1_{fs}e^1_{fc}-y^1_{fc}e^1_{fs} = \tfrac{1}{2}\left[(y_c+jy_s)(e_c-je_s)-(e_c+je_s)(y_c-jy_s)\right] \times\left[(x_c+jx_s).(x_c-jx_s)\right] \quad (2.62)$$

$$e^{1\,2}_{fc} + e^{1\,2}_{fs} = \left[(e_c+je_s)(e_c-je_s)(x_c+jx_s)(x_c-jx_s)\right] \quad (2.63)$$

Substitution of (2.61) and (2.63) into (2.55) yields

$$\text{Av}\left[\hat{U}_m\right] = \frac{\tfrac{1}{2}\,\text{Av}\left[x_f^* e_f y_f^* x_f + x_f^* y_f e_f^* x_f\right]}{\text{Av}\left[x_f^* e_f\, e_f^* x_f\right]}$$

$$\therefore \quad \text{Av}\left[\hat{U}_m\right] = \frac{\tfrac{1}{2}\left[S_{yx}S_{xe}+S_{ex}S_{xy}\right]}{S_{ex}S_{xe}} \quad (2.64)$$

assuming the effective bandwidths of the data channels to be well matched and their heterodyned power spectral density functions to be virtually constant, over the bandwidths of the filters as $w_c \to 0$.

$$\text{i.e.} \quad \text{Av}\left[\hat{U}_m\right] = \text{Real Part of } \frac{S_{yx}S^*_{ex}}{S_{ex}S^*_{ex}} \quad (2.65)$$

which will be remembered as the desired theoretical result of (2.27).

$$\text{Similarly,} \quad \text{Av}\left[\hat{V}_m\right] = \text{Imag Part of } \frac{S_{yx}S^*_{ex}}{S_{ex}S^*_{ex}} \quad (2.66)$$

which itself corresponds to (2.28) and consequently, an on-line transfer function analyser operating on random data has been, at least, theoretically synthesised.

2.4.2 <u>An Approximate Discussion of Bias.</u>

From the analysis requiring fourth-order moments, it is now obvious that as long as there are no marked fluctuations in the

spectral density functions - and this may be controlled by astute selection of filters - a virtually unbiased estimate of the analysed transfer function must be so obtained. Unfortunately, referring to the joint integral I(U) (2.59) and Fig.(2.4), it is observed that further terms in the expectation will be involved, namely when $w_o \leqslant w_c$. From Fig.(2.4)(c,d,e,f), the spectral windows H(jw), H(jw -j2w_o) will begin to overlap, adding additional terms to both numerator and denominator. Therefore, both cross-spectral estimates will be themselves seperately biased, irrespective of how narrow is the filter bandwidth. In the case of perfect attenuation, the analysis for a strictly unbiased estimate, assuming w_c to be narrow, is confined to the region $w_o > w_c$. Imperfect filtering will, however, produce a "tail" to the filter responses and it is suggested that a safety factor equivalent to $w_c \gtrsim \frac{1}{2}w_o$ should be employed. For a spectral window consisting of two second-order Butterworth structures in cascade, approximately 20dB of attenuation will have occurred in each spectral window, before interaction takes place, if the latter inequality is satisfied.

2.4.3 An Approximate Discussion of Convergence.

The expressions for $\hat{U}_m$ and $\hat{V}_m$ could not be originally evaluated, since the coefficients were stochastic. However, by taking expected values, a deterministic orientation, in terms of mean values, remains to be solved using standard techniques applicable to equations with constant coefficients. To simplify matters, w_e will be the "equivalent bandwidth" and for the instrument, corresponds to two second-order Butterworth structures in cascade. Tables of standard integrals are reproduced in Shinners' book (35) and in Appendix Four, the resultant value of $w_e = w_c/\sqrt{2}$ is obtained. Laplace transformation of(2.54) and evaluating the step response, leads to the expression :-

$$\hat{\bar{U}}_m(s,w_o)\left[s + K_a w_{e2}^2 |S_{ex}|^2\right] = \hat{\bar{U}}_m(0)+\left[K_a w_{e1}^2 S_{yx} S_{ex}^*\right] /s \qquad (2.67)$$

$\hat{\bar{U}}_m(0)$ is the previous evaluation of $\hat{\bar{U}}_m$ i.e. at $(w-w_o+\delta w_o)$

$$= \hat{\bar{U}}_m(0,w_o-\delta w_o)$$

$\hat{\bar{U}}_m(0)$ thus indicates the "a priori" knowledge of the previous estimate at $(w_o-\delta w_o)$, where w_o is the present heterodyning frequency. Inverse transformation of (2.67) and using partial fractions, it is readily apparent that $\hat{\bar{U}}_m(w_o)$ tends towards the real part of S_{yx}/S_{ex} according to $1- \exp\left[- K_a w_e^2 |S_{ex}|^2 t\right]$. Likewise, $\hat{\bar{V}}_m(w_o)$ will converge to the imaginary part of S_{yx}/S_{ex}.

Therefore, the time constant of adaptation depends on both signal power and averaging parameters. One source of error depends upon the filtered channels being well matched. If this is not so, then $\hat{\bar{U}}_m(w_o)$, $\hat{\bar{V}}_m(w_o)$ are each inflated according to $(w_{e1}/w_{e2})^2$.

One final point to notice, stems from the solution of (2.67). $\hat{\bar{U}}_m(0)$ will decay exponentially, according to the time constant $\left[K_a w_{e2}^2 |S_{ex}|^2\right]^{-1}$ seconds. Hence, the previous knowledge of $\hat{\bar{U}}_m(w_o - \delta w_o)$ cannot be used in any way to speed up the convergence to the final value of $\hat{\bar{U}}_m(w_o)$, since $\hat{\bar{U}}_m(w_o - \delta w_o)$ will, by then, have decayed to zero.

This chapter has revealed the theoretical basis of a practical transfer function analyser, suitable for the on-line analysis of random data. Sufficient equations have been developed to show that the instrument could be simulated, if desired, on an analogue computer, since the basic building blocks are resolvers, filters, multipliers and summing junctions. The next chapter will deal exclusively with a novel resolver and filter, which were both found to be necessary, due to the limitations of current techniques.

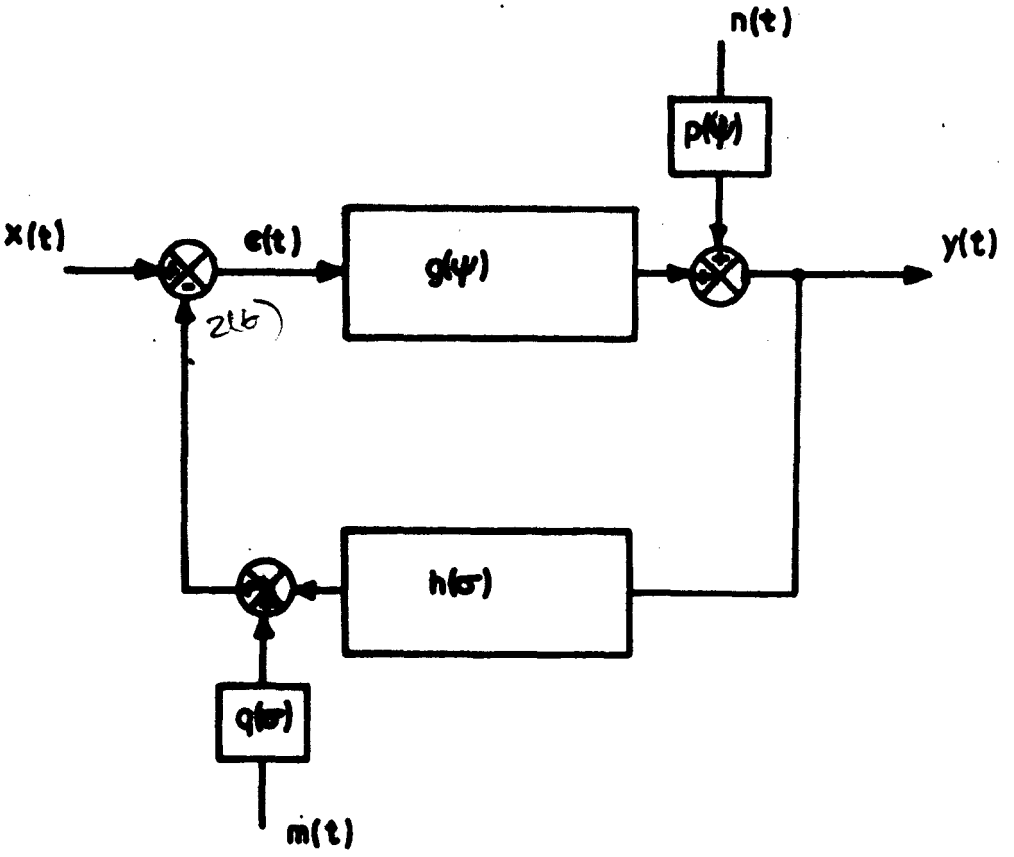

FIG. 2.1 GENERALISED FEEDBACK SYSTEM

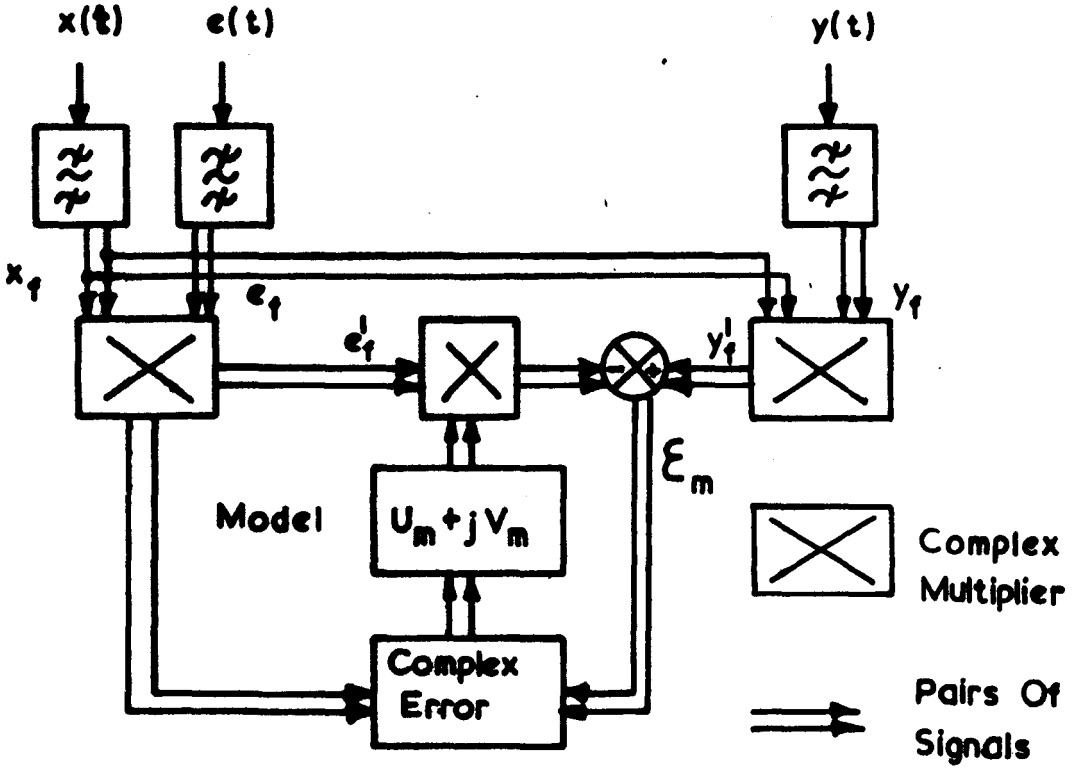

FIG. 2.2 GENERALISED MODEL IDENTIFICATION SCHEME

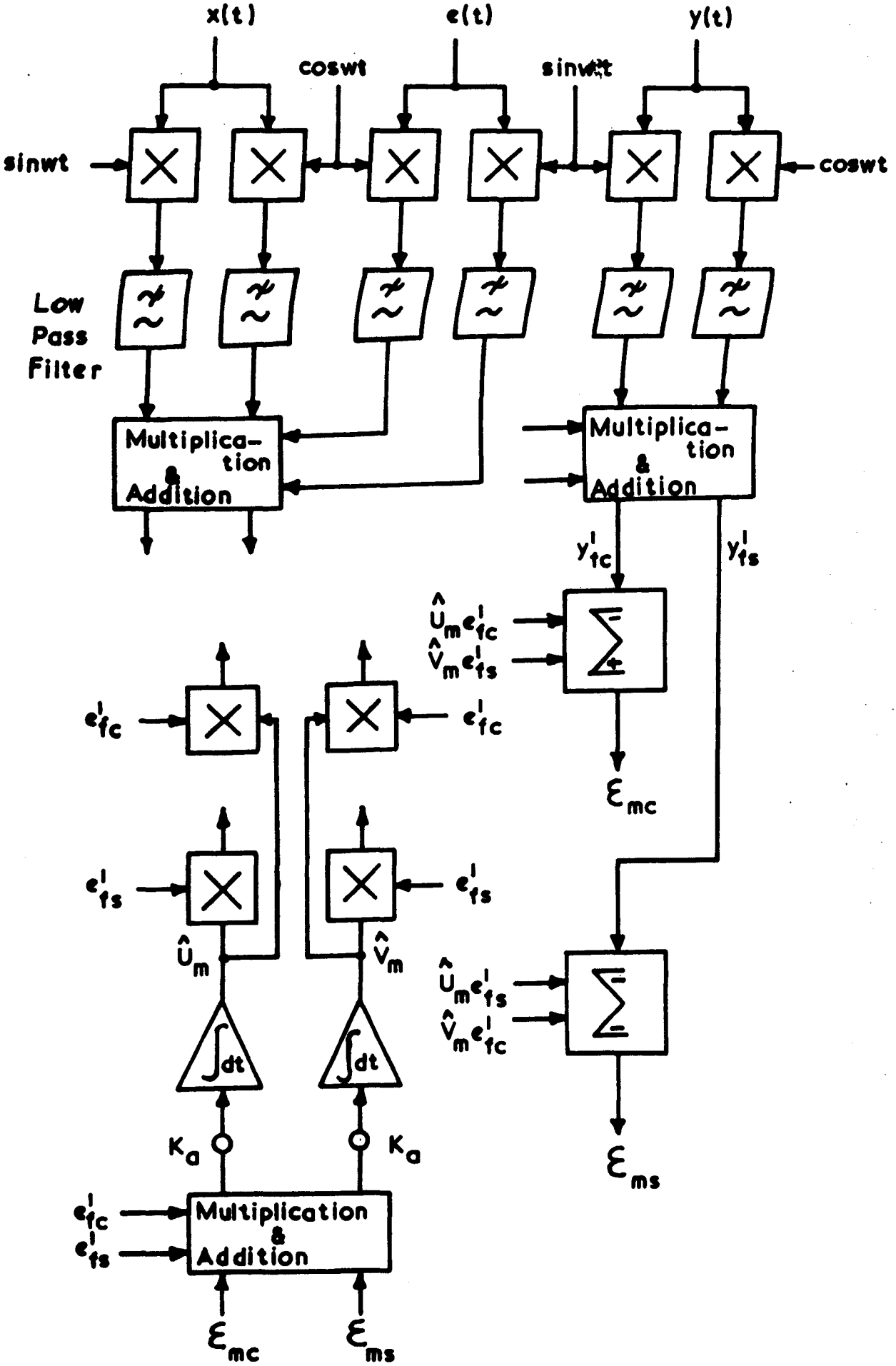

FIG. 2.3 AN ADAPTIVE LOOP TRANSFER FUNCTION ANALYSER

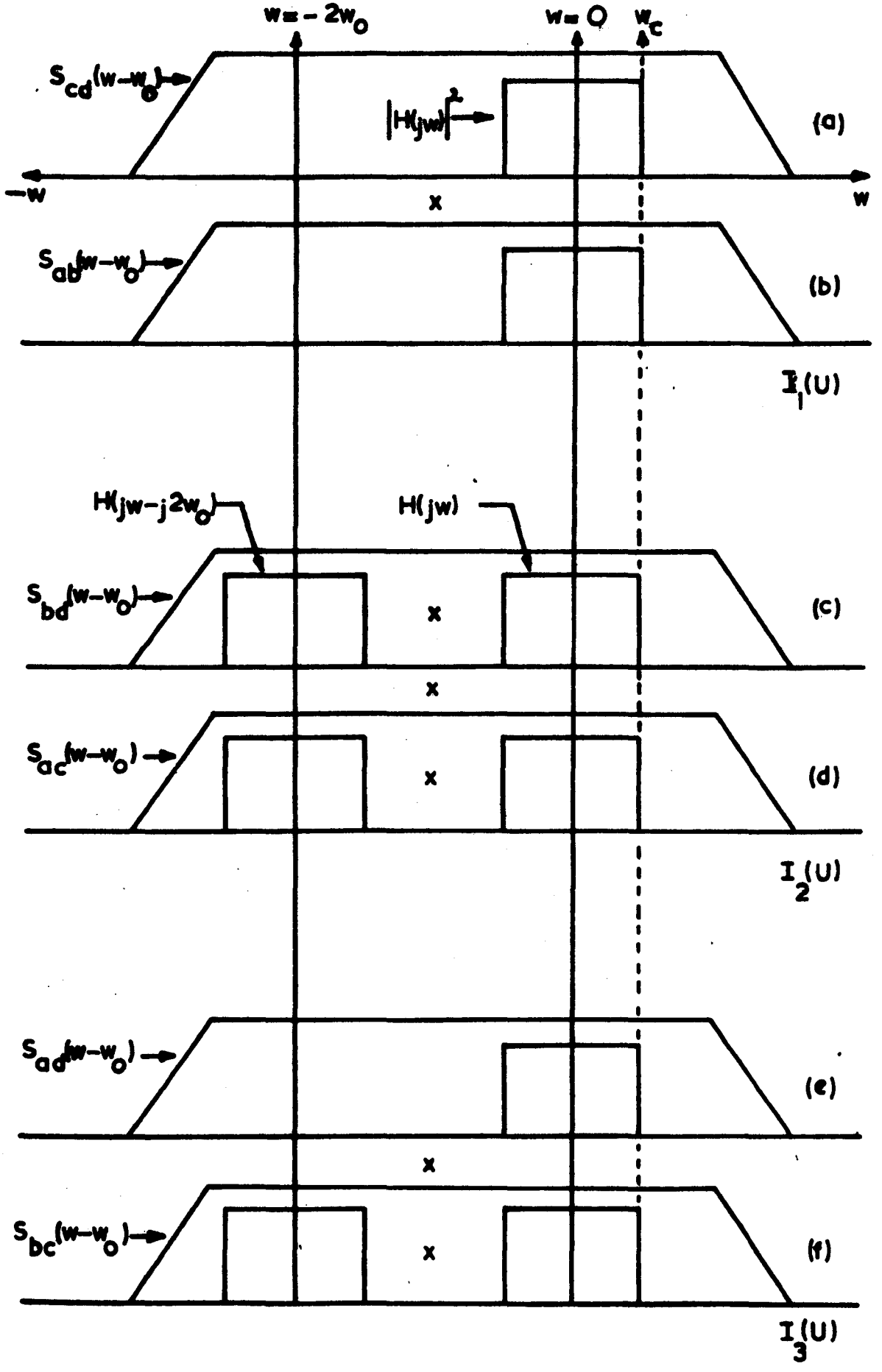

FIG. 2.4 GRAPHICAL EVALUATION OF I(U)

CHAPTER THREE

NOVEL ELECTRONIC FILTERING TECHNIQUES

3.1 Introduction

This chapter has been isolated from a discussion of the complete instrument, since new methods of tracking and filtering of the observed random data are claimed. These include a superior form of heterodyning, based on recursion techniques, as compared to R. May (25) and a revolutionary form of filter, which relies upon commutating techniques. The chapter is split into two parts. The first, based upon the heterodyning operation, emphasises how such a modulator may be controlled by digital techniques to produce an analogue circuit of high accuracy and repeatability. Resolution of the data into two components phase displaced by $\pi/2$ radians results. The latter part illustrates the filtering operation upon such resolved data. Use again, is made of digitally controlled networks, since six identical channels must be aligned, regarding both amplitude and phase characteristics. Resultant performance allows the alignment to $\pm$ 1% again yielding continuous repeatability.

3.2 Aspects of the Resolver.

The instrument must be capable of identifying all the available frequencies, the tracking time being bounded by the instrument's natural response or the statistical estimation time, whichever is the greater. A scheme of identification must either :-

a) Track simultaneously each of the frequencies stimulating the system or

b) Translate them to a specific narrowly defined band, where they will be viewed to the best advantage and appropriately analysed. The merits of the two techniques using narrow-band responses have been well analysed in the literature (36,37). Summarised as follows, it may be said :-

a) Analogue real-time analysis requires multiple filters for spectrum estimation. However, the expense of combing the spectrum up to 2KHz using bandwidths of 1Hz would be prohibitive. Further, high resolution -required for independent samples- is impractical due to imperfect out-of-band attenuation. In addition, the requirement for progressively higher "Q" tuned filters, when analysing constant increments of frequency, completely eliminates this technique for the instrument.

b) Heterodyning is the principle of modulating a known sinusoidal carrier by an arbitrary signal, such that the desired spectral portion, centred around the carrier frequency, is translated to a fixed narrow band-pass filter region, where the information is extracted. Sometimes, recording of the original sample together with repeated playback is used but in any case, real-time analysis is not possible due to the sequencing properties of the heterodyne. A distinct advantage arises, however, in that the sequencing properties will precipitate a more sophisticated design of the single filter, in comparison to the fixed bandwidths usual in the real-time analysis.

For the application under consideration, the modulated carrier will be of the same frequency as the signal component being analysed. This component will now be available at zero and double frequency and consequently, synchronous demodulation should be taken as a more descriptive term for the process. Estimates of the power spectral density properties are readily obtainable from the d.c. terms. This is preferable to using the double frequency sideband since :-

a) Extra circuitry is required to seperate the in-phase and quadrature phased components.

b) Difficulty of synthesising high "Q" filters with variable bandwidth properties.

How can the characteristics of a digitally switched resolver be best formed to generate the orthogonal sine/cosine pair which will make available the tandem information paths ? It is based upon an arrangement (38) which made use of recursive methods. The basic components are operational amplifiers, high grade resistors, field-effect transistors (FETS) and binary elements. In the respect that no frequency sensitive passive components are used and that the method relies upon the accuracy of resistance ratios and not absolute values, allows it to be possibly manufactured as an integrated circuit. The idea is akin to (39) whereby, simple frequency generation of sinusoidal and triangular waveforms have been obtained from a weighted chain of resistors attached to an operational amplifier and interrogated by a binary counter, to yield a multilevel signal in response to the counter outputs. The resultant synthesised functions will of necessity be stepped and decisions on the size of counter will have to be made with regard to the smoothness of the function. The method adopted here has an advantage over the others, due to the employment of a recursive strategy. It allows full use of the n stages of the counter to be made without redundancy. Hence, 2^n permissable states are available as opposed to 2n suggested in one application using a ring counter (40).

Further, in this application, the counter state acts as a modulating function upon the impressed analogue signal source and is not the source itself, hence eliminating the requirement for conversion of the counter output to stable analogue reference levels.

3.3 Theory of the Resolver.

The n-stage binary counter proposed by Hughes (38) resolves 360° into segments each of $2\pi/2^n$ radians. Each counter stage manipulates a weighted resistor either into or out of the recursion, as a clock line changes state. The recursion is based on well-

known summation rules - the count progressing upwards -

$$\sin (A+B) = \sin A \cos B + \cos A \sin B$$

$$\cos (A+B) = \cos A \cos B - \sin A \sin B$$

Simple resistance ratios could be employed but an n-stage counter requires the same number of recursions, each one being followed by an appropriate $\pm$ sign, depending as to whether the sine or cosine is being computed. On this basis, the idea was subsequently developed using a radix of four and the general theory is given below.

Consider 2π radians = r^n, a counter of n stages each to radix r.

Basic resolved segment = $2\pi r^{-n}$ rads.

At any instant of time, an equivalent angle θ can be specified:-

$$\theta = 2\pi r^{-n} \left[K_o r^o + K_1 r^1 + K_2 r^2 + \ldots\ldots + K_{n-1} r^{n-1} \right] \quad (3.1)$$

$$\text{i.e. } \theta = 2\pi r^{-n} \sum_{p=0}^{n-1} K_p r^p \quad (3.2)$$

and K_p varies sequentially from 0 to r - 1.

Consider sufficient clock pulses only to fill the first two stages of the counter. Then,

$$S_1 = \sin (K_o R^o + K_1 R^1) = \sin K_o R^o \cos K_1 R^1 + \cos K_o R^o \sin K_1 R^1 \quad (3.3)$$

where $R^p = r^p \, 2\pi r^{-n}$ rads.

Therefore, the sine value of the angle, represented by the count in the first two stages, is expressed as a summation of two fixed products.

Similarly,

$$C_1 = \cos (K_o R^o + K_1 R^1) = \cos K_o R^o \cos K_1 R^1 - \sin K_o R^o \sin K_1 R^1 \quad (3.4)$$

For a continuous clock of period τ and expressing the value when the third stage is being filled ;

$$S_2 = \sin (K_o R^o + K_1 R^1 + K_2 R^2) = S_1 \cos K_2 R^2 + C_1 \sin K_2 R^2 \quad (3.5)$$

This will be the value for time $t = r^2\tau \leqslant t \leqslant (r^3 - 1)\tau$ and hence recursions within these periods of time again only involve multiplication of one variable by a following fixed value.

In general, when the p^{th} most significant stage is in operation, we have at time

$$r^p\tau \leqslant t \leqslant (r^{p+1}-1)\tau$$

$$\text{Sin} \sum K_p R^p = S_p = S_{p-1} \cos K_p R^p + C_{p-1} \sin K_p R^p \qquad (3.6)$$

$$S_{p-1} = S_{p-2} \cos K_{p-1} R^{p-1} + C_{p-2} \sin K_{p-1} R^{p-1} \qquad (3.7)$$

$$S_{p-2} = S_{p-3} \cos K_{p-2} R^{p-2} + C_{p-3} \sin K_{p-2} R^{p-2} \qquad (3.8)$$

$$\vdots$$

$$S_1 = S_o \cos K_1 R^1 + C_o \sin K_1 R^1$$

Cosine values may be similarly expressed. In matrix form, the recursion can be summarised as :-

$$\begin{bmatrix} S_p \\ C_p \end{bmatrix} = \begin{bmatrix} S_{p-1} & C_{p-1} \\ C_{p-1} & -S_{p-1} \end{bmatrix} \begin{bmatrix} \cos K_p R^p \\ \sin K_p R^p \end{bmatrix} \qquad (3.9)$$

3.4 Practical Considerations.

From the equations (3.6 - 3.9), the spatial displacement would appear linked to the time sequence and hence, the physically arranged recursion must proceed in the direction S_o to S_p. However, remembering that only fixed ratios are to be used, the order between the computational blocks (ratio values and summation or subtraction) need not be the above. What does matter, is, that each spatially displaced block must be activated by the corresponding counter position. The physical arrangement must try to minimise both drift and spike interference, the latter due to the use of FETS for the analogue switching unit. A stepped output will result and the response to a d.c. signal level is shown in Fig.(3.1). Methods of generating sinusoidal functions

could have used diode function generators or digital methods, based on variable rate counters (41). In either case, performance as a resolver would have been difficult to orientate.

What determines the value of the radix and is there an optimum? Values of K_p lie in the range 0 to r-1, each value in the same stage being mutually exclusive. Analogue interaction must be precluded and thence the arrangement of the circuit is realisable by a system of time-division multiplex (TDM). Increasing the radix does so also to the branches of the multiplexer and reduces the total number of recursions, whilst reducing the radix, deteriorates the system accuracy according to the tolerance of the components used. Drift and offset could also accumulate but as opposed to a series of amplifiers, these problems are only evident in the final stage, since all previous stages will have ratios $\leqslant 1$, hence tending to alleviate the problem.

Consider 256 segments of the resolved waveform. Possible counter configurations are :-

a) Pure binary, involving eight distinct stage operations, each of the two branches being switched directly from the counter state.

b) Radix = 4. Hence four branches per stage and four recursions.

c) Radix = 256 and a single recursion. Accuracy here is obtained at the expense of a vast array of complex decoding gates and will almost certainly be rejected.

The overall design becomes a compromise between accuracy, decoding complexity and leakage problems of the TDM system. In conclusion, r = 2 requires one path to be inactive as far as information processing is concerned. In any computational block, should the value of $K_p = 0$, a redundant parallel path is required to pass on previously computed values. The redundancy, defined as r^{-1}, applies to any radix chosen and for r = 2, is obviously the highest.

3.5 Minimisation of Harmonics.

Consider the orthogonal sinusoidal functions to be synthesised by the formation of a number of discrete steps, which are repetitive over integral multiples of the angle 2π rads. The discontinuities of the waveform are most easily analysed by means of a Fourier series, since the segments will produce harmonics of the fundamental stepped waveform. However, appropriate adjustment of the weighted steps should cater for the removal of the lowest order harmonics.

Consider the modulating function existing either side of time t = 0.

$$\alpha(t) = \sum_{k=1}^{\frac{1}{2}r^n} F_k \left\{ u\left[t - (k-1)\lambda\right] - u\left[t - k\lambda\right] \right\} - \sum_{k=1}^{\frac{1}{2}r^n} F_k \left\{ u\left[t + (k-1)\lambda\right] - u\left[t + k\lambda\right] \right\} \quad (3.10)$$

where :-

u(t) is a sequence of Heaviside step functions.

F_k is the discrete weight.

λ is the segment = $2\pi r^{-n}$ rads.

Expanding (3.10) as a Fourier trigonometrical series

$$\alpha(t) = a_o + \sum_{i=1}^{\infty} a_i \cos \frac{2\pi i t}{T} + \sum_{i=1}^{\infty} b_i \sin \frac{2\pi i t}{T} \quad (3.11)$$

From the observed symmetry :-

a) No d.c. terms are involved.

b) $\alpha(t) = -\alpha(t + T/2)$, therefore only odd harmonics will prevail and they arise from two sources.

1) Variations in amplitude weights from the theoretical value.

2) Asymmetrical time segments but a digital clock will remove the latter; assuming the range of interest, for the shortest

dwell period, is within the frequency cut-off of the FETS (42).

For the example of the sinusoidal modulating function, only the harmonics b_i can be present. Further, due to symmetry, b_i may be evaluated in the first quadrant and the commutation is arranged palindromically as a result.

$$\text{Therefore } b_i = {}^4/_{\pi} \sum_{k=1}^{q/4} \int_{(k-1)2\pi q^{-1}}^{k.2\pi q^{-1}} F_k \sin \frac{2\pi it}{T} \, d\Theta \quad (3.12)$$

where $q = r^n$

Integrating and evaluating (3.12) for all k

$$b_i = {}^4/_{i\pi} \left\{ F_1(1 - \cos 2\pi i q^{-1}) + F_2(\cos 2\pi i q^{-1} - \cos 4\pi i q^{-1}) \right.$$
$$\left. + \cdots + F_{q/4} \left[\cos\left(\frac{q}{4} - 1\right) 2\pi i q^{-1} - \cos \frac{q}{4} 2\pi i q^{-1} \right] \right\} \quad (3.13)$$

In matrix form, (3.13) may be conveniently expressed as :-

$$\begin{bmatrix} b_1 \\ b_3 \\ b_5 \\ \\ b_{\left(\frac{q}{2}-1\right)} \end{bmatrix} = \frac{4}{i\pi} \begin{bmatrix} (1 - \cos 2\pi q^{-1}) & \cos\left(\frac{q}{4}-1\right)2\pi q^{-1} \\ (1 - \cos 32\pi q^{-1}) & \\ (1 - \cos 52\pi q^{-1}) & \\ \vdots & \\ 1 - \cos\left(\frac{q}{2}-1\right)2\pi q^{-1} & \cos\left(\frac{q}{4}-1\right)\cos\left(\frac{q}{2}-1\right)2\pi q^{-1} \end{bmatrix} \begin{bmatrix} F_1 \\ F_2 \\ \\ \\ F_{q/4} \end{bmatrix} = \begin{bmatrix} 1 \\ 0 \\ \\ \\ 0 \end{bmatrix}$$

(3.14)

For the instrument, 64 segments were used and the sixteen (F_1 - F_{16}) coefficients were evaluated by a computer. The values (F_1 - F_{16}) are sequenced left to right in Table (3.1), correct to the fifth decimal place.

Table 3.1

.04909	.14679	.24308	.33702	.42773
.51431	.59594	.67183	.74125	.80353
.85807	.90435	.94192	.97042	.98957
.99920				

With 64 steps per cycle, the lowest harmonics will be the 63^{rd} and 65^{th}, with amplitudes inversely proportional to the frequency. Should one however require more highly resolved segments, by extending the counter capacity, the calculations must become somewhat laborious. In trying to find a simpler solution, the immediate difficulty is to decide upon a criterion for the evaluation. If a smooth curve is to be placed through the stepped segments, to what value of Θ would F_k refer ?

Taking a mean square error criterion over the fundamental region $(0 \rightarrow \pi/2)$,

$$\varepsilon^2 = {}^2/_{\pi} \int_{0}^{\pi/2} \left[\sin\Theta - F_k(\Theta)\right]^2 d\Theta \qquad (3.15)$$

$$= {}^2/_{\pi} \sum_{k=1}^{q/4} \int_{(k-1)2\pi q^{-1}}^{k2\pi q^{-1}} \left[\sin\Theta - F_k(\Theta)\right]^2 d\Theta \qquad (3.16)$$

Differentiating (3.16) with respect to Θ and evaluating the integral for one segment,

$$\cos(k-1)2\pi q^{-1} - \cos k2\pi q^{-1} = F_k\, 2\pi q^{-1} \qquad (3.17)$$

$$\therefore\ 2\sin\frac{(2k-1)}{2} 2\pi q^{-1} \sin\frac{2\pi}{2} q^{-1} = F_k 2\pi q^{-1} \qquad (3.18)$$

For small increments, $\sin\Theta = \Theta$ and therefore

$$F_k = \sin\frac{(2k-1)}{2} 2\pi q^{-1} \qquad (3.19)$$

From (3.19), it has been shown that F_k must be evaluated at the angle $(k - \frac{1}{2})\, 2\pi q^{-1}$ rads. i.e. midway between the extremities of the step.

3.6 Operation of the Resolver.

Schematic diagrams are shown in Figs (3.2, 3.3). For q = 64, three recursions seem necessary but only two have been used, use being made of the symmetry of the sine and cosine waves throughout the four quadrants. This is the simplest way of avoiding the negative coefficients which are then required. Digital circuitry again maintains the recursive accuracy by being substituted for operational amplifiers.

Consider the sine function. During the period $0 \leqslant \theta \leqslant \pi/2$, the coefficients change in the order F_1' to F_8' and in the reverse sequence, $\pi/2 \leqslant \theta \leqslant \pi$. Four cycles of the r values of K_o are completed in the same time as one cycle of the r values of K_1. Witness the timing diagram of Fig.(3.4). Therefore, each quadrant is resolved into sixteen discrete steps. Finally during $\pi \leqslant \theta \leqslant 2\pi$, reversal of the coefficients is accomplished with the final stage of the counter triggering the SGN bit and switching ON the FET in the positive leg of the operational amplifier. During the previous half cycle, with the FET OFF, the operational amplifier was working in the common mode configuration, with feedback. Hence, output equals the input. Biasing unbalance, due to asymmetrical circuits being viewed by the bias current, was much more difficult to compensate for. More complicated FET circuits to give automatic correction can be used but a mean value not greater than 2mV was found to be possible with r.m.s.$\simeq$5mV. This is a minor carrier leak which will be filtered subsequently.

3.7 Factors Affecting Accuracy of the Resolver.

The resistance ratios were obtained by external connections to a high gain operational amplifier (MC 1433). Inaccuracies in the ratio established - apart from the tolerance of the resistors themselves - depend upon the loop gain of the amplifier in question. Hartley (43) has tabulated this error, which in the MC 1433 amounts to ·02%, when open-loop gain exceeds 80dB

and closed loop gain = - 1. This error can be neglected.

The search for a fast semiconductor switch with low loss characteristics, resulted in using a FET of epoxy construction. Even at 70°C, the ON resistance is not greater than 30Ω and the leakage current •2nA at 40V breakdown (Amelco U1897E). This FET was preferred to a normal switching transistor, both for leakage and not having a saturation voltage, although switching spikes are common to both but more likely to be less hazardous in the latter. Freeman (44) has given as analysis of the latter case.

For the FET, spikes arise due to the differentiating effect of the combined channel/transmission capacitance and the load resistance. In addition, a fast switching low ON resistance FET has voltage transition levels, at the gate control, approaching ten volts. Switching in a few microseconds, it is not surprising to encounter spikes of the order of one volt amplitude but low energy. Drive circuits are similar to Fig.(3.11).

Two spikes occur, one positive and the other negative, shared between the ON and OFF conditions. For the N-channel device used, the negative spike is the most serious. In effect, a time varying resistance parallel combination of channel resistance and load exists. This value is small when the gate level rises to make Vgs = 0 - the ON condition. The opposite occurs when the device is turned OFF. This hazard can produce a measurable D.C. effect with frequency and a graph is shown in Fig.(3.5). Variations in the rise time will produce proportional amplitude changes in the spike and hence, experiments were carried out for acceptable levels. Referring to a previous discussion (Chapter 3.4), it will be clear, that placing the most frequently switched components at the beginning of the recursive chain, will help to ameliorate the overall effect at the output terminal. Should the spike not reach its steady-state level quickly, an obvious inaccuracy must result.

For $C_{gd} = C_{gs} = 15$ pF and $R_L = 10$ KΩ, the time constant = ·15 microseconds. Seven time constants are necessary for the steady state to be reached, within ·1%. Hence, the maximum switching rate was chosen to be 64 x 2 KHz. Consideration of this time constant, plus a low value of R_{DS} ON/R_L, resulted in choosing ratios normalised to 10 KΩ. Errors due to the OFF impedance of the switch may also be neglected, since R_{DS} OFF $> 10^9 \Omega$, as far as leakage is concerned.

Finally in Appendix Five, a derivation of the balancing potentiometer value, to minimise the d.c. content of the carrier leak in the TDM branches, is given. The value is equal to the parallel combination of the branches.

3.8 Harmonic Breakthrough.

The above mentioned effect is a function of the deviation of the weights from the theoretical optimum. Component resistors were of the metal film construction and selected with nominal tolerance ± ·1%. Variation of the weights by computer programming, using both systematic and random techniques, revealed that a ± ·1% tolerance would be quite sufficient, should no allowance be made for a maximum of + ·3% deviation caused by the FET. A glance at Table (3.2) will reveal the maximum third harmonic, still, to be only ·1% of the fundamental. The table shows both the programmed weights correct to the fourth decimal place, with either a positive or negative bias and the principal harmonics, corresponding to the deviations, listed with their inverse amplitudes. Harmonics were evaluated to the 101st and in each case null variations observed for the 63rd and 65th.

MODIFIED WEIGHTING FACTORS (c.f. TABLE 3.1)

+ .3%	Alternate ± .3%	Random ± .3%
.0492	.0492(+)	.0492(+)
.1472	.1464(-)	.1472(+)
.2437	.2437(+)	.2437(+)
.3380	.3360(-)	.3360(-)
.4292	.4292(+)	.4292(+)
.5159	.5128(-)	.5128(-)
.5978	.5978(+)	.5978(+)
.6738	.6698(-)	.6738(+)
.7438	.7438(+)	.7390(-)
.8059	.8011(-)	.8011(-)
.8606	.8606(+)	.8606(+)
.9072	.9015(-)	.9015(-)
.9448	.9448(+)	.9448(+)
.9733	.9675(-)	.9675(-)
.9925	.9925(+)	.9865(-)
1.0022	.9962(-)	.9962(-)

RECIPROCAL HARMONIC LEVELS.

1st	1.0030	.9998	.9989
3rd	24723	4105	993.35
5th	21546(-)	4855(-)	2298(-)
7th	54897(-)	7089	2427
9th	37549(-)	5016(-)	1501(-)
11th	39444(-)	4873	1698
13th	70520(-)	3631(-)	1870

TABLE 3.2

3.9 Aspects of Filtering.

Having established the signal component of interest at zero frequency, how is this desired portion to be filtered out ? Absolute spectral analysis (45) requires averaging over frequency space, with essentially rectangular windows, if leakage from the unwanted "tail" region and hence, the bias, is to be minimised. Unfortunately, this is not possible, unless an infinite delay is practical! However, in transfer function analysis, a ratio of two spectral density functions is the complex random variable desired and hence, relative spectral analysis will suit the requirements. This is heuristically judged on the basis that, leakage components will be common to all channels and when normalised with respect to the desired spectral functions, should therefore tend to cancel. This also follows from equation (2.60). Strong variations may still remain in the smoothed data but filters with fourth-order cut-off slopes are thought to be satisfactory. Similarly, in assessing the pass-band structures, identical shapes are desirable for each of the six channels of signal processing in the instrument. The presence of either ripple characteristics (Chebyshev or Cauer) or flat characteristics as typified by Butterworth filters is immaterial, as long as there exists sufficient d.c. extraction gain. Consequently, the remaining stipulations of ease of manufacture, controllability, led to the use of Butterworth structures.

With the low-pass filter requirements of bandwidth variation between •01 and 10Hz, is it possible to form identical structures of six fourth-order devices, within 1% each to each economically ? Normal analogue techniques would consist of 24 ganged potentiometers and six ganged three-position decade switches for capacitor variations. Consequently, digital or hybrid techniques will be resorted to, the last described being

claimed as original in form and not at all seen by the author in publications to date. Both merits and disadvantages of possible filters are given, to show that a new device was required for the instrument.

3.9.1 Sampled Data Filters.

This is the technique, whereby, a selection of sample and hold devices plus delay elements, each controlled by binary computational elements, are arranged to form numerical difference equations which satisfy the filtering requirements in discrete time. Once sampled, the sums and differences may be manipulated by analog or digital techniques (46), the latter requiring an analog to digital (A/D) conversion. Only the former shall be considered, the A/D facilities are an unnecessary and expensive complication.

With sampling, the normalisation of the cut-off and band-pass characteristics relative to the sampling frequency is gained. Repeatability of the characteristics is therefore possible, since they would be locked to an externally applied digital clock frequency. Manipulation of the difference equation may be done recursively, whereby, functions of the output are fedback to the input. Alternatively, non-recursive or transversal techniques imply delay of each sample, with a weighted sequence to give approximations to the desired impulse response.

However, in the feedback case since the transfer response is synomonous with continuous s-plane filters, it would be very convenient if knowledge of the continuous frequency response could be transformed into the z-domain. A technique to do this was popularised (47) and known as the bilinear transform. A change of variable is made, such, that $s = \frac{2}{T}\left[\frac{z - 1}{z + 1}\right]$ (3.20) where T is the period according to the sampling rate. A polynomial in z results, which if accompanied by a low normalised cut-off, produces an identically transformed low-pass filter.

Unfortunately, as $z = e^{jw_d t}$ and $s = jw_a$, the equivalent analogue variable in radian measure, (3.20) reduces to (48),

$$w_a = \frac{w_s}{\pi} \tan \pi \frac{w_d}{w_s} \qquad (3.21)$$

where w_s is the sampling rate.

A subsequent warping of the frequency scales will result in the stop-band, alone, if the pass-band is achieved with a low normalised cut-off. A good practical example of the design of a Cauer filter has been given (49) with normalised cut-off about 13^{-1} . Accordingly, very good matched guard filters would be required to keep aliased spectra to low proportions in the instrument design. The disadvantages of decreasing the normalised value of w_d will be highlighted with an example.

Consider the normalised polynomial in the s-plane,

$$F(s) = \frac{w_o^2}{s^2 + \sqrt{2}s\, w_o + w_o^2} \qquad (3.22)$$

i.e. a second-order Butterworth structure.

Using (3.20) and the substitution $\tan \pi w_d / w_s = \pi w_d (w_s)^{-1}$, (3.22) becomes,

$$F(z) = \frac{w_d^2}{\left[\frac{2}{T} \cdot \frac{z-1}{z+1}\right]^2 + \sqrt{2} \cdot \frac{2}{T}\left[\frac{z-1}{z+1}\right] \cdot w_d + w_d^2} \qquad (3.23)$$

(3.23) may be re-arranged as a polynomial in z.

$$\therefore F(z) = \frac{(z+1)^2}{\left\{4(T^2 w_d^2)^{-1}(z^2-2z+1) + \sqrt{2} \cdot 2(Tw_d)^{-1}(z^2-1) + (z^2+2z+1)\right\}} \qquad (3.24)$$

Divide (3.24) throughout by z^2 and replace F(z) by the ratio of its output, $F_o(z)$, to its input, $F_1(z)$. Hence :-

$$F_o(z)\left[\frac{4}{T^2 w_d^{\,2}}(1-2z^{-1}+z^{-2})+\frac{2\sqrt{2}}{Tw_d}(1-z^{-2})+1+2z^{-1}+z^{-2}\right]$$

$$= F_1(z)\, z^{-2}\,(z+1)^2 \qquad (3.25)$$

Re-arranging into powers of z and using $\Omega_s = {}^{w_s}/_{w_d}$, we have :-

$$F_1(z)\left[1+2z^{-1}+z^{-2}\right] = F_o(z)\left[\begin{array}{l}(4\pi\Omega_s)^2 + \sqrt{2}.4\pi\Omega_s + 1 \\ -2z^{-1}\left[(4\pi\Omega_s)^2 + 1\right] \\ + z^{-2}\left[(4\pi\Omega_s)^2 - 4\sqrt{2}\Omega_s\pi + 1\right]\end{array}\right] \qquad (3.26)$$

Inverse transforming to the time domain, (3.26) becomes :-

$$F_o(nT) \sim \left[\frac{(4\pi\Omega_s)^2 2F_o(nT-T) - (4\pi\Omega_s)^2 F_o(nT-2T) + F_1(nT)}{(4\pi\Omega_s)^2} \right.$$

$$\left. \times \frac{+ 2F_1(nT-T) + F_1(nT-2T)}{(4\pi\Omega_s)^2}\right] \qquad (3.27)$$

where $\Omega_s \gg 1$.

It is now readily apparent that for a desired $\Omega_s \leq 100{:}1$, an extremely large attenuation factor is required to act upon the input signal, before the differencing operation begins. With operational amplifiers having a dynamic range of 1000:1, before the offset errors become appreciable in comparison to the differencing operations, it is just not feasible to have repeatable accuracies of the order desired. Using low values of Ω_s, the guard filters would require the same care in their design as for the analysing filters !

3.9.2. Commutated Filters.

Another recent technique made fashionable within the last decade (50) is a digital filter, known variously as the N-path, commutating or synchronous filter. With it came a new approach to the analysis of time - invariant subnetworks, whose constituent

parts are connected by means of switches. If a subnetwork is arranged by switches to be multi-port, a commutation network (CN) is involved (51). The electrical action of these switches upon an impressed signal is that of modulation and accordingly, the network may be arranged in series or shunt form. The latter type is depicted in Fig.(3.6), the time-invariant prototype being a simple RC lag network. Sequential switching gives rise to the commutation effect but more ingenious switching arrangements, such as derived from a ring counter, can give stepped approximations to sinusoidal modulation functions and so help to remove excess harmonics (52).

Before 1960, approximate analysis (53) had been developed but recent papers (51,54) had removed many approximations by the use of state-space analysis. Each was a development of the ideas of Desoer (55), who used the technique for simple switching circuits. State-space analysis allows for a loading of the CN to be catered for. Previous analysis normally relied upon an evaluation of the impulse response and Fourier transformation (56,57). An exponentially decaying envelope can be seen as the impulse response of Fig.(3.7). Other techniques (58), consider the network to be an equivalent circuit made up of two series modulators with the passive or active network sandwiched between them. The action of any CN is in general to produce a comb- like structure of responses, identical to that of the basic subnetwork but displaced at harmonics of the switching frequency. Care must be of course be taken to avoid aliasing. If the subnetwork is of the low-pass variety, high - Q tuned circuits are readily available (59 , 60). Hence, the network is very acceptable for band-pass analysis with simple guard filters. However, at low frequencies, to prevent interaction through aliasing, thorough protection is required.

By using the 180° of phase displacement (52,61) of an active CN, commutating band-stop filters have been derived to suppress

the bending modes in aircraft structures (62). Unfortunately, present research at low frequencies seems very restricted and even although various modulating functions, feedback CN's and second-order networks (63) were examined in view of the instruments requirements, no tangible foundation was revealed. In each case, it was apparent that analogue variation of the subnetwork parameters was required to change the overall pass-band characteristics. Switching only displaced the basic properties to another domain of the complex s-plane. In addition, the time waveform was most discouraging, due to R-C time constant transients and really requires following with a sample and hold device (64).

For obvious reasons, it would be ideal for the pass-band structures to be digitally controlled. This is not impossible, as resistance multiplication (65), transfer function variation (66), moving average (67) and integrator time constants(68) have illustrated. Unfortunately in (67), the subnetwork comprised two capacitors and to perform with a sampling rate/ filter cut-off frequency at a minimum of 100:1, would have necessitated a minimum of 100 switched capacitor segments !

These techniques had thus to be completely re-organised for the present need. Not unnaturally, the network devised, proved to be a combination of the above ideas. It can be re-arranged to produce digitally controlled parameters in either low-pass, high-pass or band-pass nominal structures of the subnetwork.

3.10 The Capacitor-Ratio Commutated Filter (CRCF)

Consider the network arrangement shown in Fig.(3.8). It consists of a series resistance R - which can include the output impedance of the step function driving source - a capacitor C, placed between a double-pole double-throw switch (DPDT) and a sink capacitor nC, where n is greater than one. The double-pole double-throw switch is assumed to consist of :-

1) Switches whose transients occur at very high frequencies, as opposed to the frequency content of the applied source.

2) Effectively zero leakage of current through switches in the OFF state.

3) An ON impedance which in no way limits the circuit current.

A current will exist in the circuit, arranged by the DPDT periodic switch to pass through the capacitor C in opposite directions. Correspondingly, a set of times T_1 and T_2 seconds will arise such that :-

$$i \in k\,T \leq t < k\,T + T_1 \text{ for direction } 1,1^1.$$

$$i \in k\,T + T_1 \leq t < (k+1)T \text{ for direction } 2,2^1.$$

where T is the period of the changeover, such that $T_1 + T_2 = T$ but T_1 is not necessarily equal to T_2 and k is an integer.

Consider a modulating function m(t), periodic in nature and resembling a jump function such that :-

$$\left.\begin{aligned} &a)\quad v(t) = m(t)\, v_c(t) \\ &b)\quad i(t) = m(t)\, i_c(t) \end{aligned}\right\} \qquad (3.28)$$

$$\text{where } m(t) = 1;\ kT \leq t < kT + T_1$$

$$m(t) = -1;\ kT + T_1 \leq t < (k+1)\,T$$

In addition, it must be observed that, irrespective of the switching time, should no applied stimulus prevail, the voltages around the loop must be in a state of mutual equilibrium, such that v and V are equal and opposite. Hence, summing the voltages around the network we have :-

$$Au(t) = i(t)\,R + m(t)\,v_c(t) + \frac{1}{nC}\int_{\tau}^{t} i(t)\,dt \qquad (3.29)$$

where τ indicates one of the base times of (3.28)

u(t) the Heaviside step function.

i.e. $$Au(t) = i(t)R + v_c(t) + \frac{1}{nC}\int_{KT}^{t} i(t)\,dt \quad \text{for } t \in T_1 \qquad (3.30)$$

$$Au(t) = i(t)R - v_c(t) + \frac{1}{nC}\int_{KT+T_1}^{t} i(t)\,dt \quad \text{for } t \in T_2 \qquad (3.31)$$

Expressed in general terms of v_c using (3.28) we have :-

$$Au(t) = m(t)CR\,\dot{v}_c(t) + m(t)v_c(t) + m(t)v_c(t)n^{-1} \qquad (3.32)$$

where $i_c = C\dot{v}_c$ and the dot notation indicates a derivative with respect to time.

Therefore

$$CR\dot{v}_c = m(t)^{-1}Au(t) - v_c(1 + {}^1/n) \qquad (3.33)$$

and the first state equation has revealed the voltage source to be modulated by the switching action. Similar equations thus result when compared with Desoer's method (55) of employing a complex exponential driving source, followed by a change of variable.

$$\therefore CR\dot{v}_c(t) = A\left[u(t) - u(t - T_1)\right] - v_c(1+{}^1/n),\ t \in T_1 \qquad (3.34)$$

$$\text{and}\quad CR\dot{v}_c(t) = -A\left[u(t - T_1) - u(t - T)\right] - v_c(1+{}^1/n), t \in T_2 \qquad (3.35)$$

Transforming (3.34) by the methods of Laplace and viewing v_c from time t = 0 :-

$$CR\left[sv_c(s) - v_c(o)\right] = A\left[1-e^{-sT_1}\right]s^{-1} - v_c(s)\left[1+{}^1/n\right] \qquad (3.36)$$

where $v_c(o)$ will be finite or zero, depending upon whether it is charged or not when the stimulus is applied. Also :-

$$CR\left[sv_c(s) - v_c(T_1)\right] = Ae^{-sT_1}\left[1-e^{-sT_2}\right]s^{-1} - v_c(s)\left[1+{}^1/n\right] \qquad (3.37)$$

Collecting terms and solving, we have from (3.36)

$$v_c(s)\left[sCR + (1+{}^1/n)\right] = CRv_c(o) + A\left[1-e^{-sT_1}\right]s^{-1} \qquad (3.38)$$

$$\therefore v_c(s) = \frac{v_c(o)}{s + a} + \frac{A\left[1 - e^{-sT_1}\right]}{sCR\,(s + a)} \qquad (3.39)$$

where $a = (n+1)(nCR)^{-1}$

Partial fractions may be used to separate the furthest right expression of (3.39) i.e.

$$\frac{1}{s(s+a)} = \frac{A}{s} + \frac{B}{s+a} = \frac{1}{as} - \frac{1}{a(s+a)}$$

$$\therefore v_c(T_1) = v_c(o)e^{-aT_1} + \frac{n}{n+1} A\left[1-e^{-aT_1}\right]\left[u(t)-u(t-T_1)\right] \qquad (3.40)$$

Since the CR product will be very small, to allow each capacitor to charge fully under a voltage source, the steady state will be reached very rapidly and hence

$$v_{css}(T_1) = \frac{n}{n+1} A \qquad (3.41)$$

$$\text{and } V_{ss}(T_1) = (n+1)^{-1} A \qquad (3.42)$$

These above values in (3.41), (3.42) will be pertinent, solely to the case where $v_c(o) = V(o) = 0$. Otherwise, they only constitute the part of the final steady state value due to the active expression (3.30), the other portion being the original steady state conditions at time t = 0. Hence, taking (3.41), (3.42) to be the final values, the circuit action will become more apparent by considering what occurs during T_2. The analysis will exploit the principles of superposition.

During time T_2, two events will occur.

1) $v(T_1)$ and $V(T_1)$ must redistribute their voltages at the moment of commutation and this can be seen by considering A not to be present.
2) The stimulus A will pump more current into the circuit to satisfy Kirchoff's law and maintain the distribution momentarily destroyed by 1). Hence, the steady state output voltages during T_2 are the sum of the actions 1) and 2).

For 1), $V_1(t) = V(T_1) + \frac{1}{nC}\int_o^{T_2} \frac{\left[v(T_1)-V(T_1)\right]}{R} \exp -t^1\left[\frac{(n+1)}{RnC}\right] dt^1$ (3.43)

$T_1 \leq t < T$

$$\therefore V_1(t) = V(T_1) + \frac{1}{(n+1)}\left[v(T_1) - V(T_1)\right]$$

$$\therefore V_1(T_2) = \frac{n}{(n+1)} V(T_1) + \frac{1}{(n+1)} v(T_1) = - v_1(T_2) \qquad (3.44)$$

For 2)

$$v_{c2}(T_2) = v_c(T_1)\, e^{-a(t-T_1)}\, u(t-T_1)$$

$$- \frac{n}{(n+1)} A \left[1-e^{-a(t-T_1)}\right] \left[u(t-T_1)-u(t-T)\right] \qquad (3.45)$$

Combining (3.44), (3.45) we have;

$$v_{css}(T_2) = - \frac{n}{(n+1)} \cdot A - v_1(T_2) \qquad (3.46)$$

$$\left.\begin{aligned} \text{But} \quad v(T_1) &= m^{-1}(t)\, v_c(T_1) = v_c(T_1) \\ v(T_2) &= m^{-1}(t)\, v_c(T_2) = -v_c(T_2) \end{aligned}\right\} \qquad (3.47)$$

$$\therefore v_{css}(T_2) = - \frac{n}{(n+1)} A + \frac{n}{(n+1)} V(T_1) + \frac{1}{(n+1)} v_c(T_1) \qquad (3.48)$$

$$\left.\begin{aligned} \text{Likewise} \quad v_{css}(T+T_1) &= \frac{n}{n+1} \cdot A - v_1(T+T_1) \\ \text{And} \quad v_{css}(2T) &= -\frac{n}{n+1} \cdot A - v_1(2T) \end{aligned}\right\} \qquad (3.49)$$

A diagram of the state voltage v_c is depicted in Fig.(3.8), minus the very sharp transients and drawn for $T_1 = T_2$. $v(t) = m(t)\, v_c(t)$ is readily calculated. When $v_{css}(t)$ is negative, the value of $v(t)$ will be multiplied by -1, giving the overall positive waveform shown in Fig.(3.8).

Returning to equations (3.41), (3.42) we have :-

$$\left.\begin{aligned} v_{css}(T_1) &= bA \\ V_{ss}(T_1) &= A(1-b) \end{aligned}\right\} \qquad (3.50)$$

where $b = n(n+1)^{-1}$

Substituting (3.50) into (3.48)

$$v_{css}(T_2) = -bA + bA(1-b) + (1-b)\,bA$$

$$= bA(1 - 2b)$$

$$\therefore v_{ss}(T_2) = bA(2b - 1)$$

$$V_{ss}(T_2) = A\left[1 + b - 2b^2\right] \qquad (3.51)$$

In general from the iterations (3.49)

$$v_{ss}(kT) = Ab(2b - 1)^{2k}$$

$$V_{ss}(kT) = A\left[1 - b(2b - 1)^{2k}\right] \qquad (3.52)$$

From these general formulations, we may observe the difference between any two transition states :-

$$v_{ss}(kT+T_1) - v_{ss}(kT) = bA(2b - 1)^{2k}\left[(2b - 1) - 1\right]$$

$$= bA(2b - 1)^{2k}\, 2(b - 1) \qquad (3.53)$$

From (3.53) it may now be concluded that the ratio between the difference of two following states and the initial one is a constant = $-\,{}^{2}/_{n+1}$

$$\text{i.e. } \frac{v_{ss}(kT+T_1) - v_{ss}(kT)}{v_{ss}(kT)} = \frac{-2}{n+1} \qquad (3.54)$$

(3.54) is the solution of a discrete exponential envelope, such that $v(t) = \exp\left[-2t/(n+1)T_1\right]$ and t is evaluated at the k values of T_1, T_2. Consequently, a time constant has been achieved digitally, such that the radian cut-off point is $4(n+1)^{-1}$ times the commutating frequency. The switched waveform is akin to a continuous exponential of the same time constant being applied to a sample and hold device. Aliasing must occur but this can be removed with simple guard filters, by making the sink capacitor as large as possible with regard to the commutated one.

3.11 Construction of a CRCF

From theory, two points are noted.

a) The voltage across the switched capacitor decays exponentially with an applied step change whilst

b) the voltage across the sink capacitor rises according to $1 - \exp\left[- t\ 4f_s(n+1)^{-1}\right]$.

Therefore, either low-pass or high-pass filters may be obtained. The action of the switch is to synthesise an equivalent resistance of the value $(n+1)\ T_1/2nC$ ohms. Further, during the stationary period, it is imperative that the commutated capacitor should not lose its charge through loading. Consequently, high impedance buffers are required, since one switched section may not be loaded by another.

The basic filter was taken to be a Butterworth voltage controlled source (69) of second-order polynomial, whose representation is depicted in Fig(3.9). Replacing each RC section with the switched segments, previously described but with the addition of buffering, changes were observed in the overall characteristics with a resultant peak around the cut-off point. Therefore, the filter structure is resynthesised in Appendix Six, using buffers and the basic and final configurations shown in Figs (3.10, 3.11).

Experiments were conducted with switching frequencies at 1.01 KHz, 101Hz. and 10.1Hz. In each case, at a frequency of 8.6, ·86, ·086Hz, the cut-off point was reached with an amplitude equivalent to $(\sqrt{2})^{-1}$ of the input signal. In addition, the equivalent phase change was a lag of 90°. It was noted that the maximum output was a constant within 2% of the input. This is equivalent to a 1% drop per stage.

With a sinusoidal input of 2 volts r.m.s. and n = 100:1, results were tabulated (Table 3.3) for each range of switching. The corresponding normalised graphs were plotted (Figs 3.12, 3.13) in dB's of attenuation relative to the cut-off point and in

degrees of phase lag against the same. It is readily observed that a second-order Butterworth filter of the low-pass variety has been synthesised, whose cut-off point is very easily controlled by digital switching, The asymptotic slope cut-off reaches -12 dB per octave as expected. Unfortunately, the phase lag for values of normalised frequency $> 10:1$ could not be reliably obtained from the Solartron TFA used for the experimental analysis.

The differential and switching FETS were Motorola 2N 5457, the former arrangement being matched to approximately 3% at the point of operation. It is worthwhile to note, that the maximum attenuation per first-order section is equivalent to $(n+1)^{-1}$ in the low-pass mode, i.e. when the signal frequency $\gg$ than the operation of the DPDT switch. A loading impedance of approximately $10^9 \Omega$ allows satisfactory operation to·01 Hz, especially if the drift voltage can be compensated for.

There is no reason to believe that with the use of a smaller switched capacitor and employing metal-oxide field-effect transistors (MOSFETS) as the buffering and switching devices, along with high quality polycarbonate capacitors, that the range could not be extended down by at least another two or three decades. With a 1 μF capacitor using conventional techniques, a 10^{10} ohm value would be completely impossible. This would apply, whether the configuration was chosen to be low-pass, high-pass, band-pass or a straight forward integrator, with the commutated capacitor replacing the resistor and a sink capacitor in the feedback loop of an operational amplifier.

From a temperature stability viewpoint, similar high quality capacitors would have the same temperature coefficient and hence, temperature variations common to both would be eradicated, since the time constant is only dependent on the ratio between the two values.

One final point concerns the analysis from a voltage source.

An infinite current will not flow with a small series resistance, due to the FET parameters saturating. The drain current under these conditions is such, that a limited current will flow but this must be sufficient to charge the small capacitor to the input voltage, when the highest switching frequency is present.

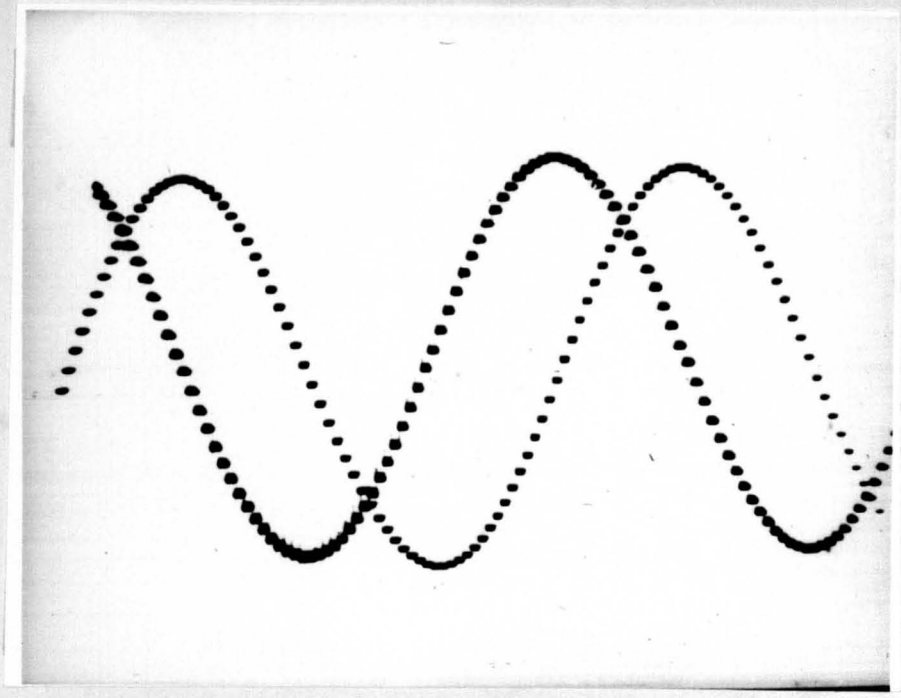

STEP RESPONSE OF RESOLVER AT 20 HZ

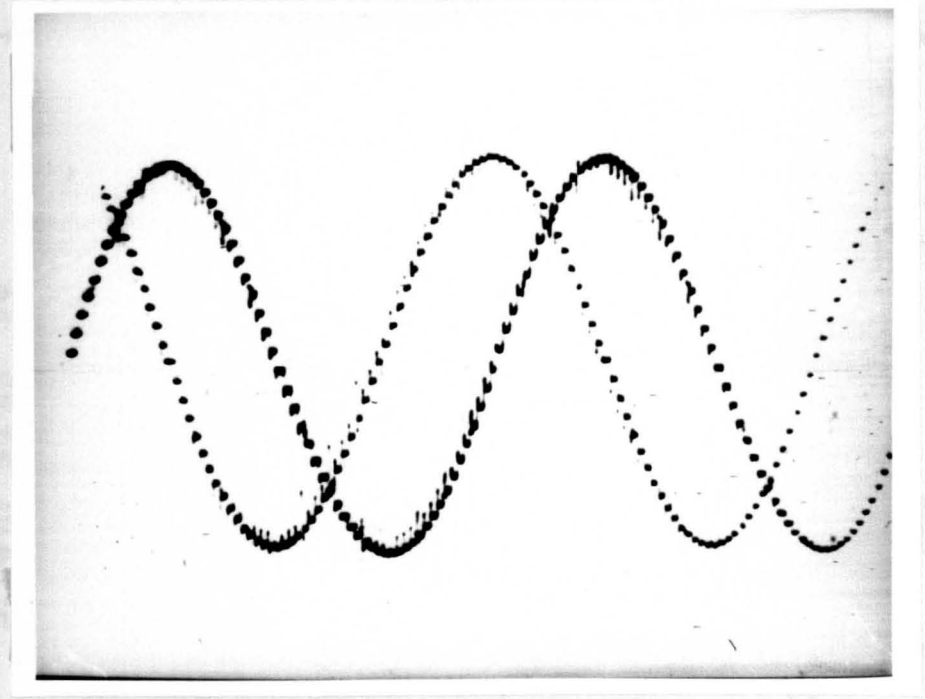

STEP RESPONSE OF RESOLVER AT 200HZ

FIG. 3.1

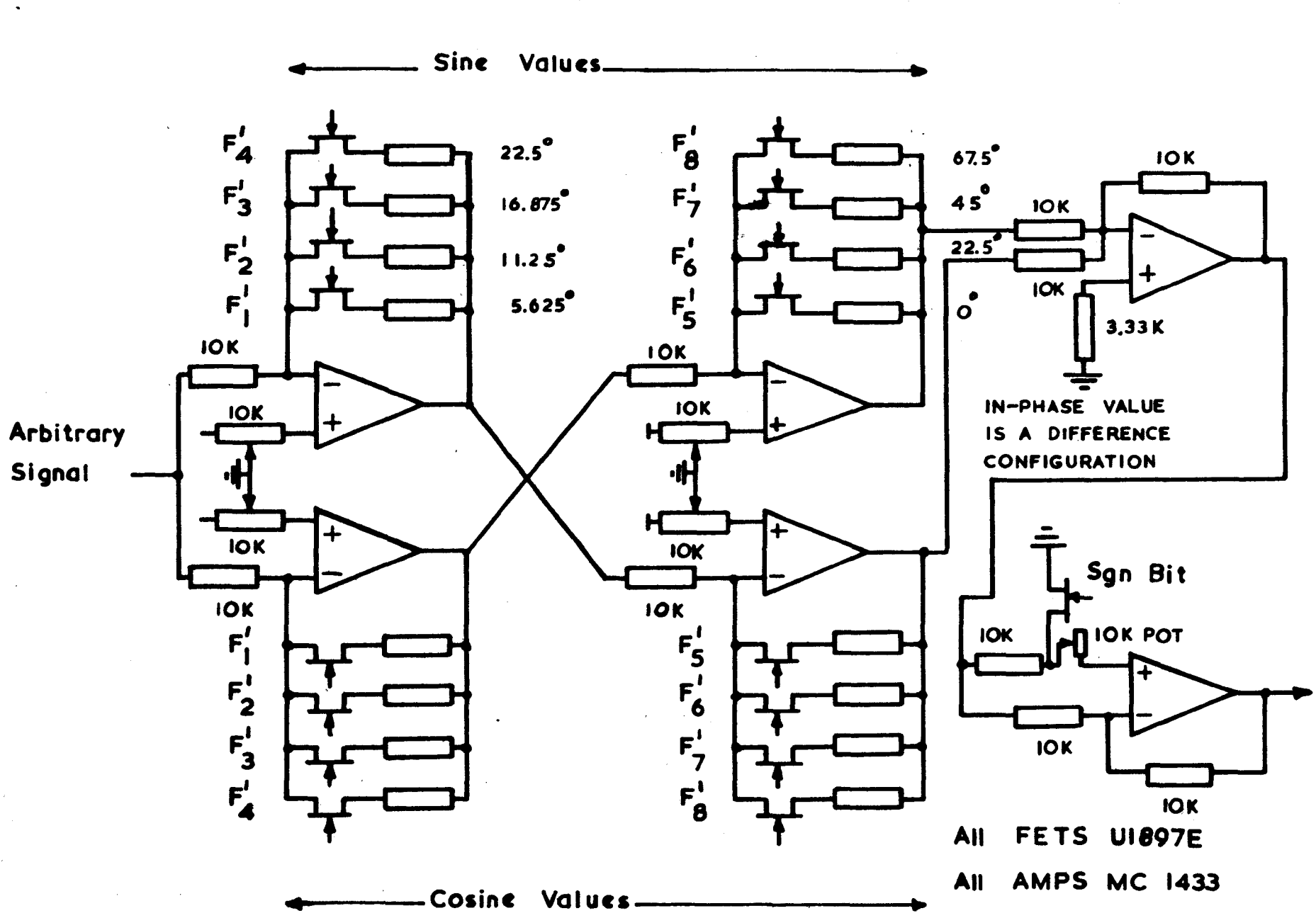

FIG. 3.2 RESOLVER QUADRATURE COMPONENT

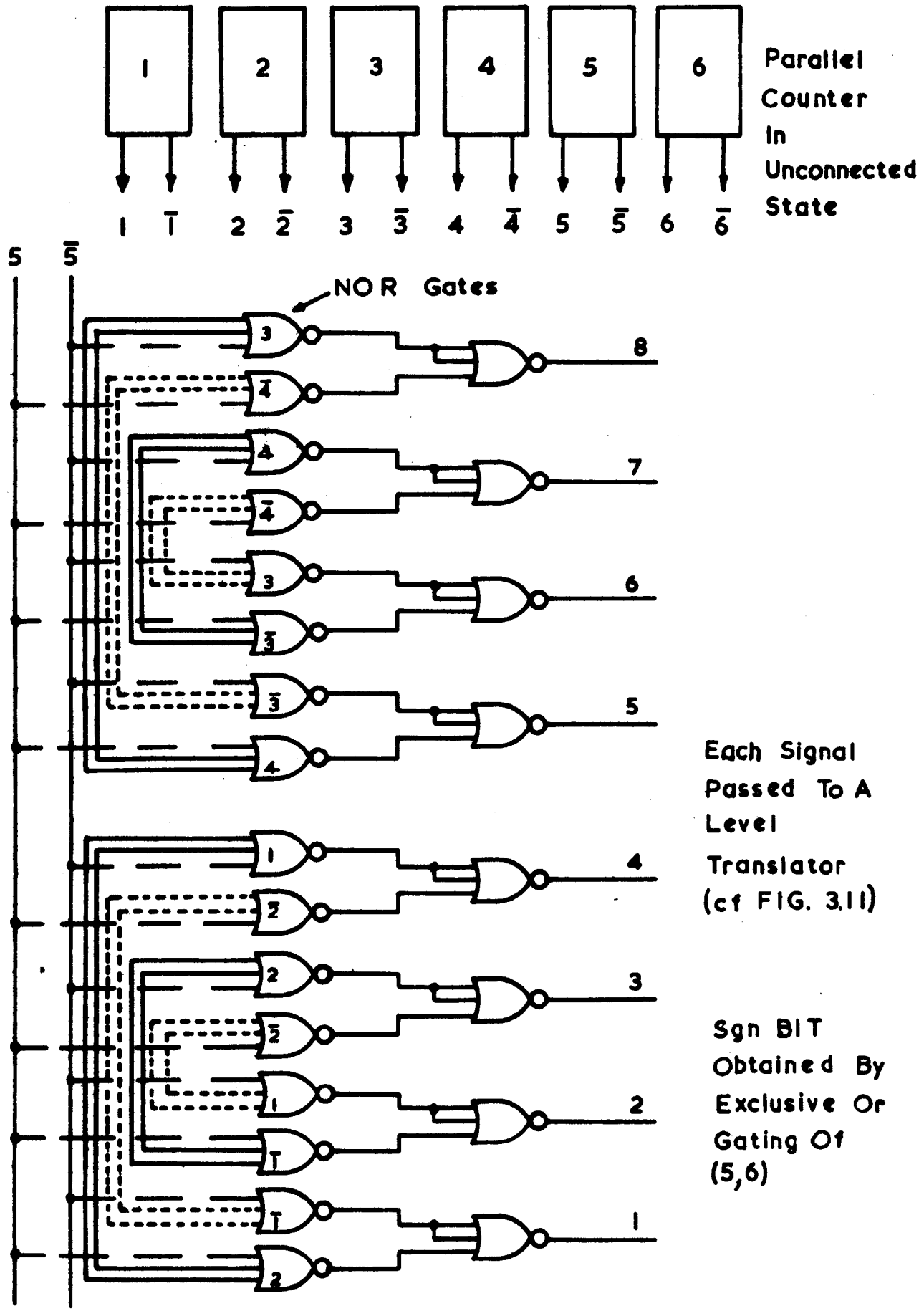

FIG. 3.3 TDM DECODING

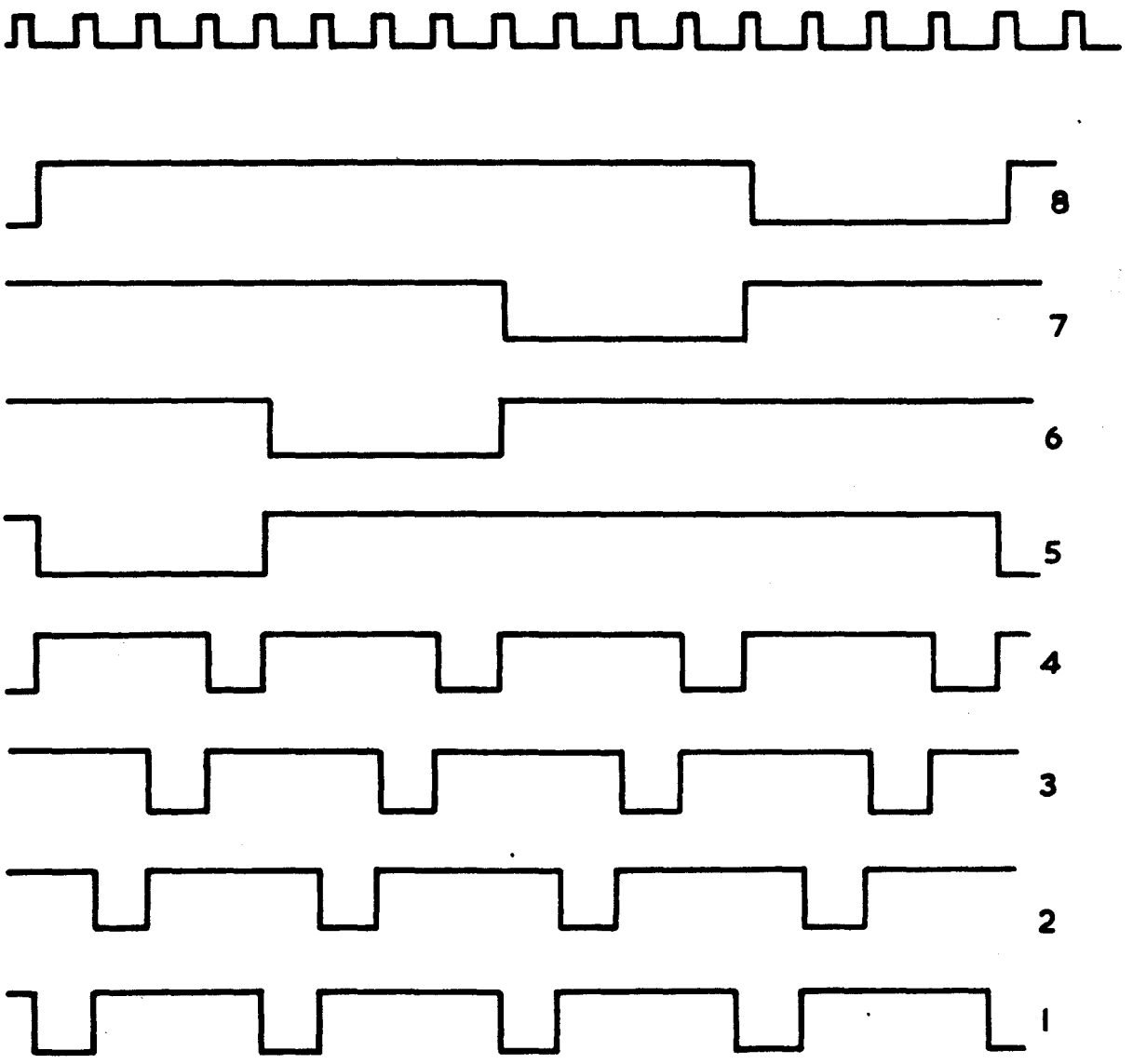

Timing Diagram For $0 < \theta < \pi/2$

For $\pi/2 < \theta < \pi$, Channels 8 And 4 Lead Their Respective Remaining Three

FIG. 3.4 RESOLVER TIMING

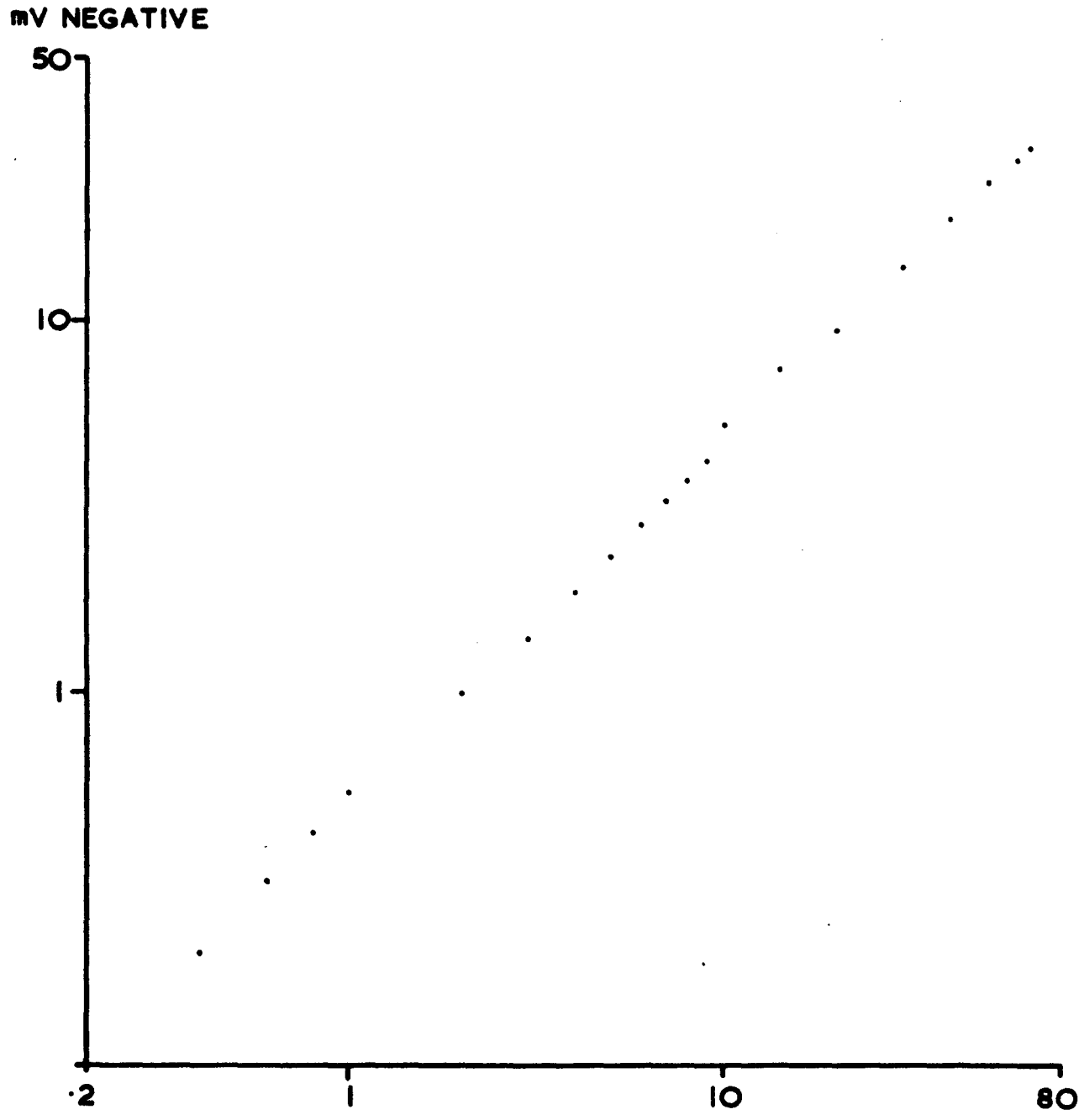

FIG. 3·5 DC OFFSET AGAINST FREQUENCY (KHz)
FOR N-CHANNEL F.E.T.

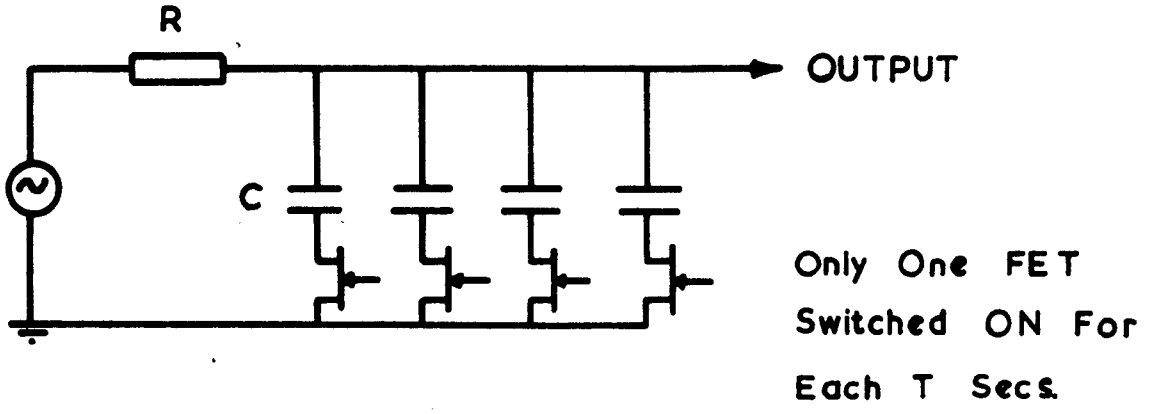

FIG. 3.6 SHUNT SWITCHED CN

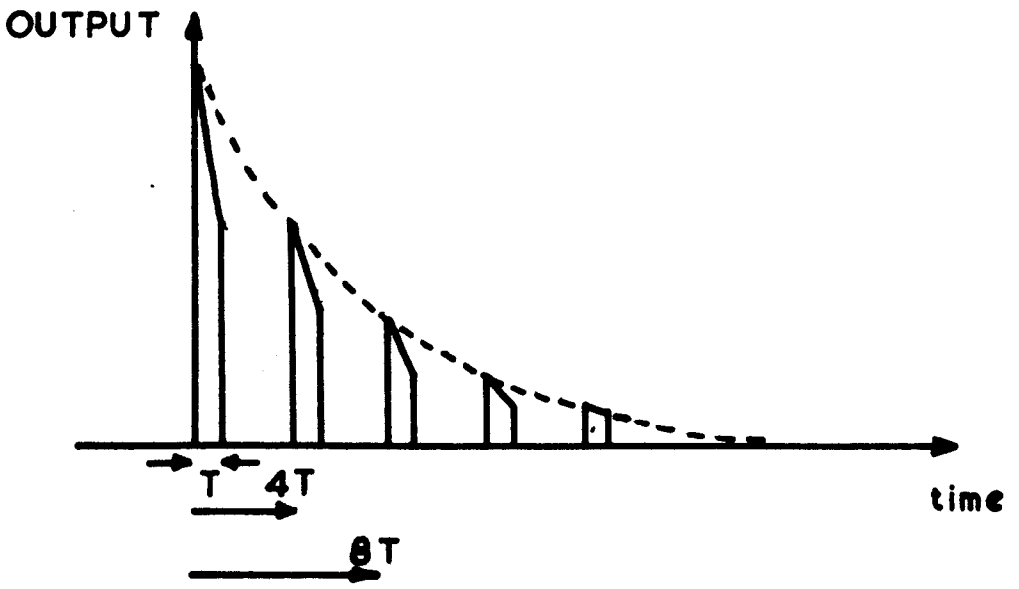

FIG. 3.7 PULSE RESPONSE OF THE ABOVE CN

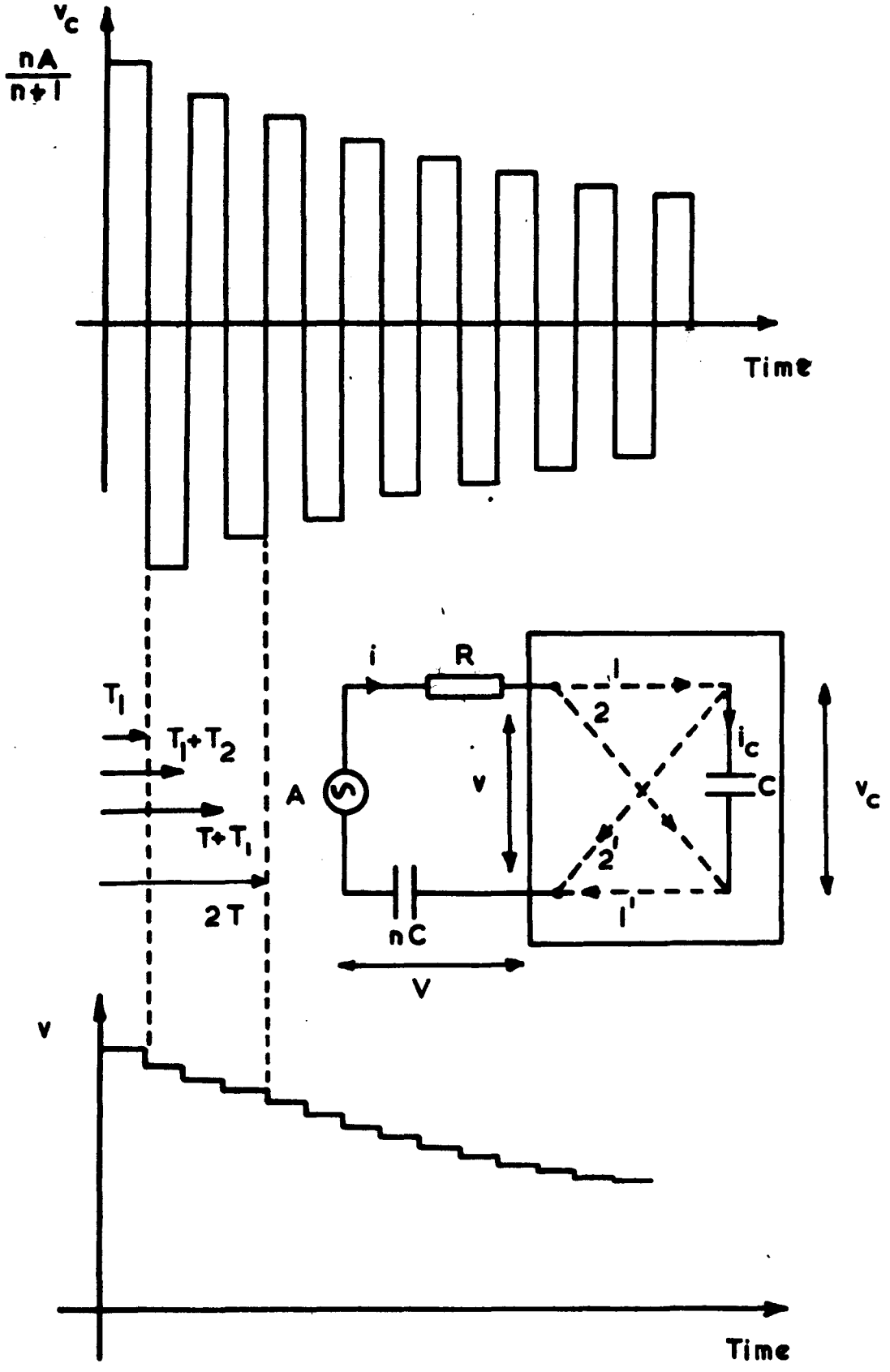

FIG. 3.8 BASIC CRCF AND RESPONSES TO STEP FUNCTION INPUT

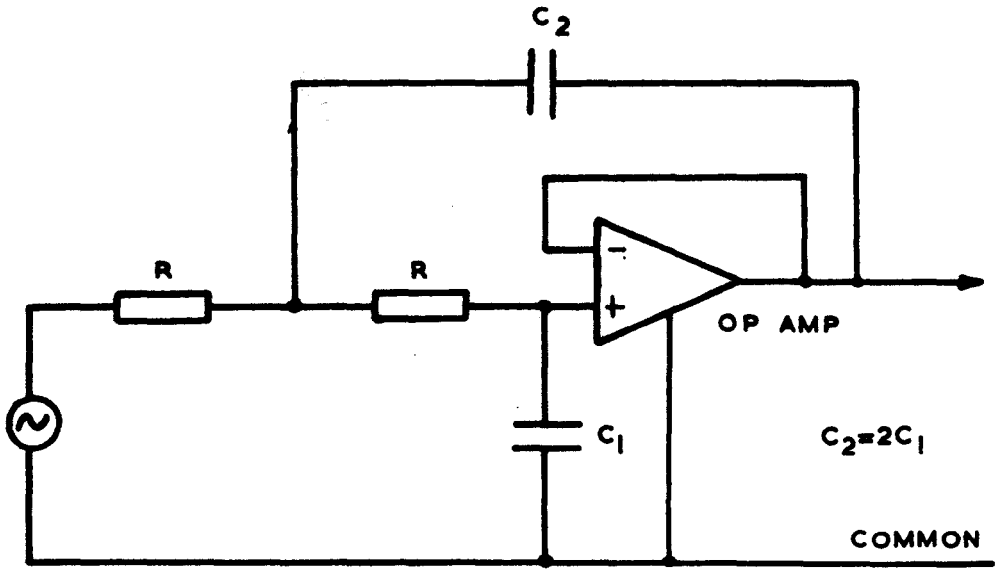

FIG. 3·9 BASIC 2nd ORDER BUTTERWORTH LOW PASS

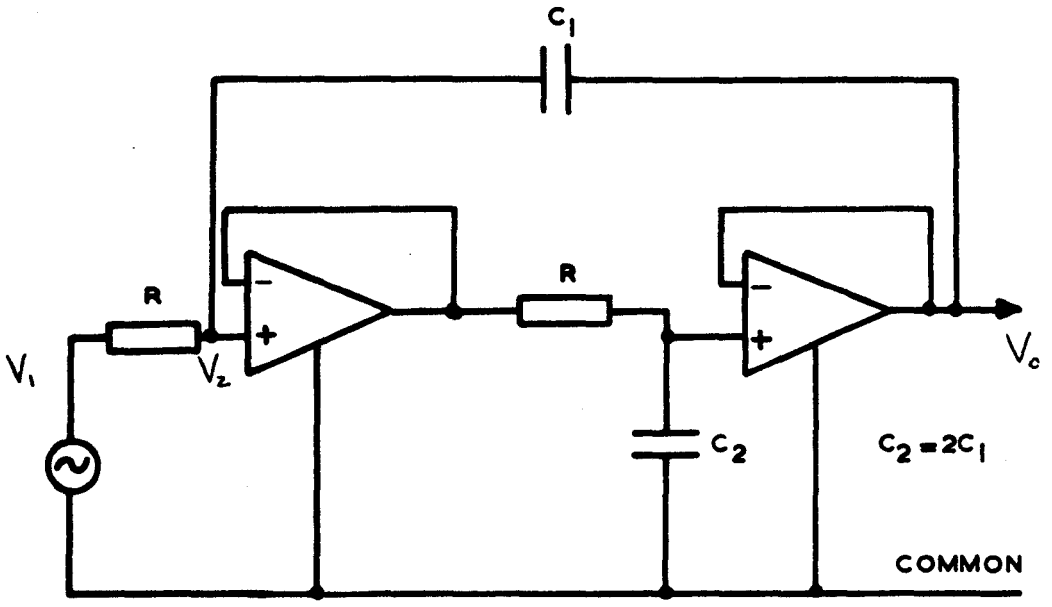

FIG. 3·10 RESYNTHESISED 2nd ORDER BUTTERWORTH

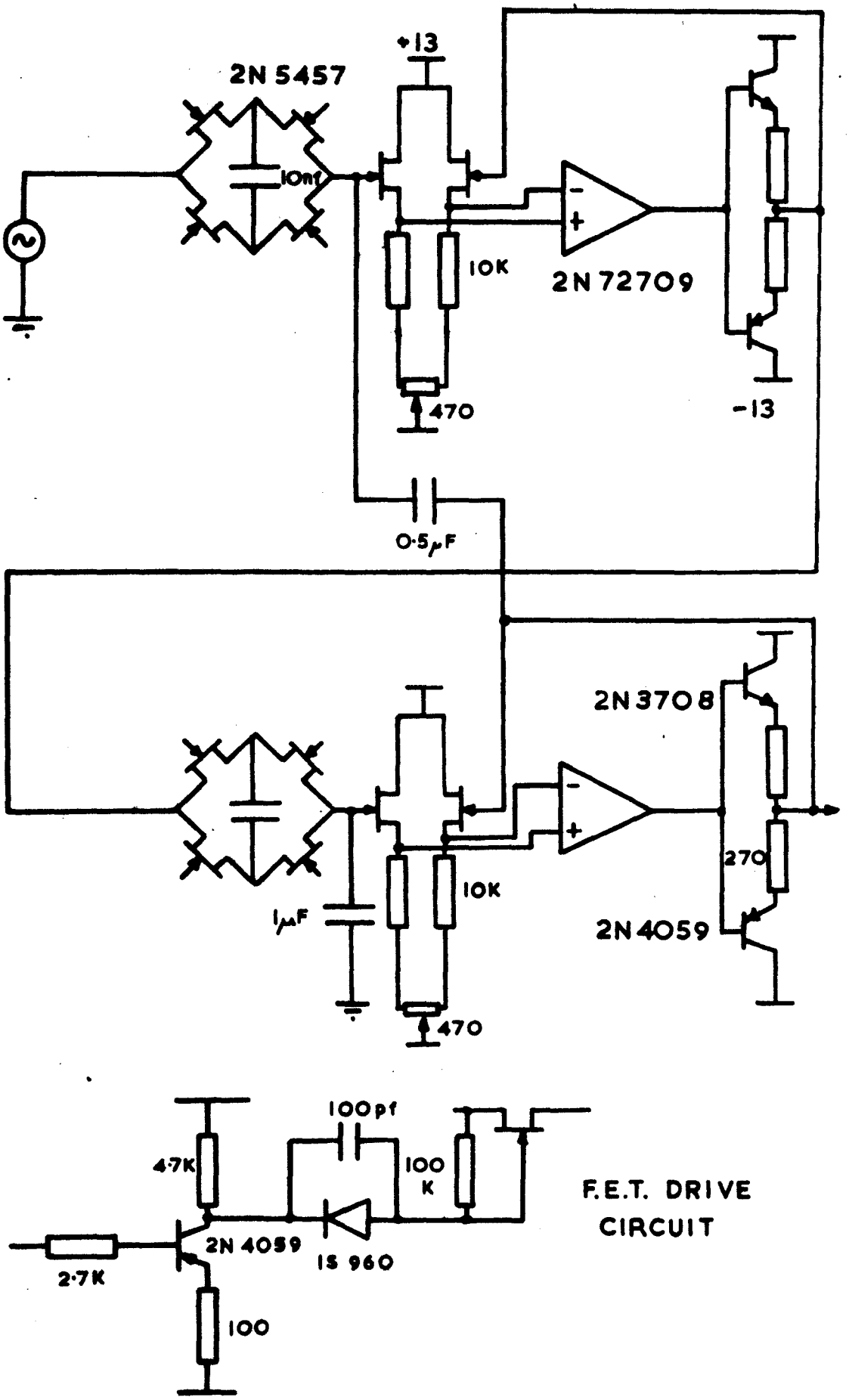

FIG. 3·11 BUTTERWORTH COMMUTATED FILTER

Normalised Frequency	Commutation Frequency 1.01 KHz		Commutation Frequency 101 Hz		Commutation Frequency 10.1Hz	
	Output r.m.s. (V)	Phase Lag°	Output r.m.s. (V)	Phase Lag°	Output r.m.s. (V)	Phase Lag°
0.012	1.96	1	1.96	1	1.96	1
0.023	1.96	2	1.96	2	1.96	2
0.058	1.96	5	1.96	5	1.96	5
0.116	1.95	10	1.96	10	1.96	10
0.232	1.95	20	1.95	20	1.95	20
0.348	1.94	30	1.94	30	1.94	30
0.465	1.91	40	1.91	40	1.91	41
0.580	1.85	51	1.85	51	1.85	52
0.697	1.77	62	1.77	62	1.76	63
0.813	1.65	73	1.65	73	1.64	74
0.930	1.49	83	1.50	83	1.48	84
1.000	1.40	90	1.41	89	1.39	90
1.045	1.34	91	1.34	91	1.33	92
1.160	1.17	99	1.18	99	1.16	100
1.395	0.90	112	0.90	112	0.89	113
2.320	0.34	138	0.34	141	0.34	139
3.490	0.13	147	0.15	152	—	—
4.650	0.07	152	0.09	157	—	—
5.800	0.05	155	0.06	160	0.05	152
8.150	0.02	—	0.02	—	—	—
11.600	0.01	—	0.01	—	0.01	—

TABLE 3.3 EXPERIMENTAL RESPONSE OF SECOND-ORDER CRCF

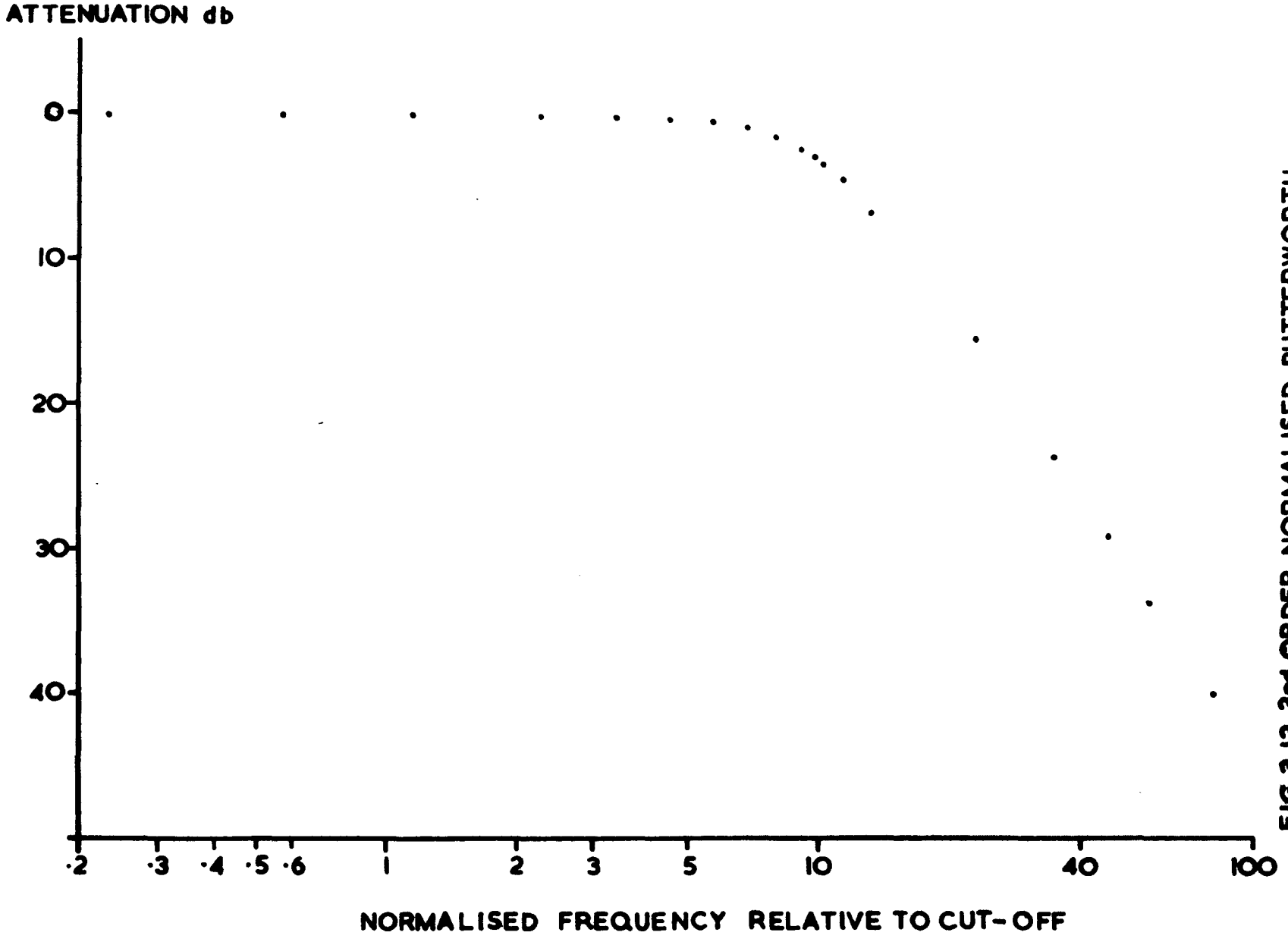

FIG.3.12 2nd ORDER NORMALISED BUTTERWORTH AMPLITUDE PLOT FOR SWITCHED FILTER

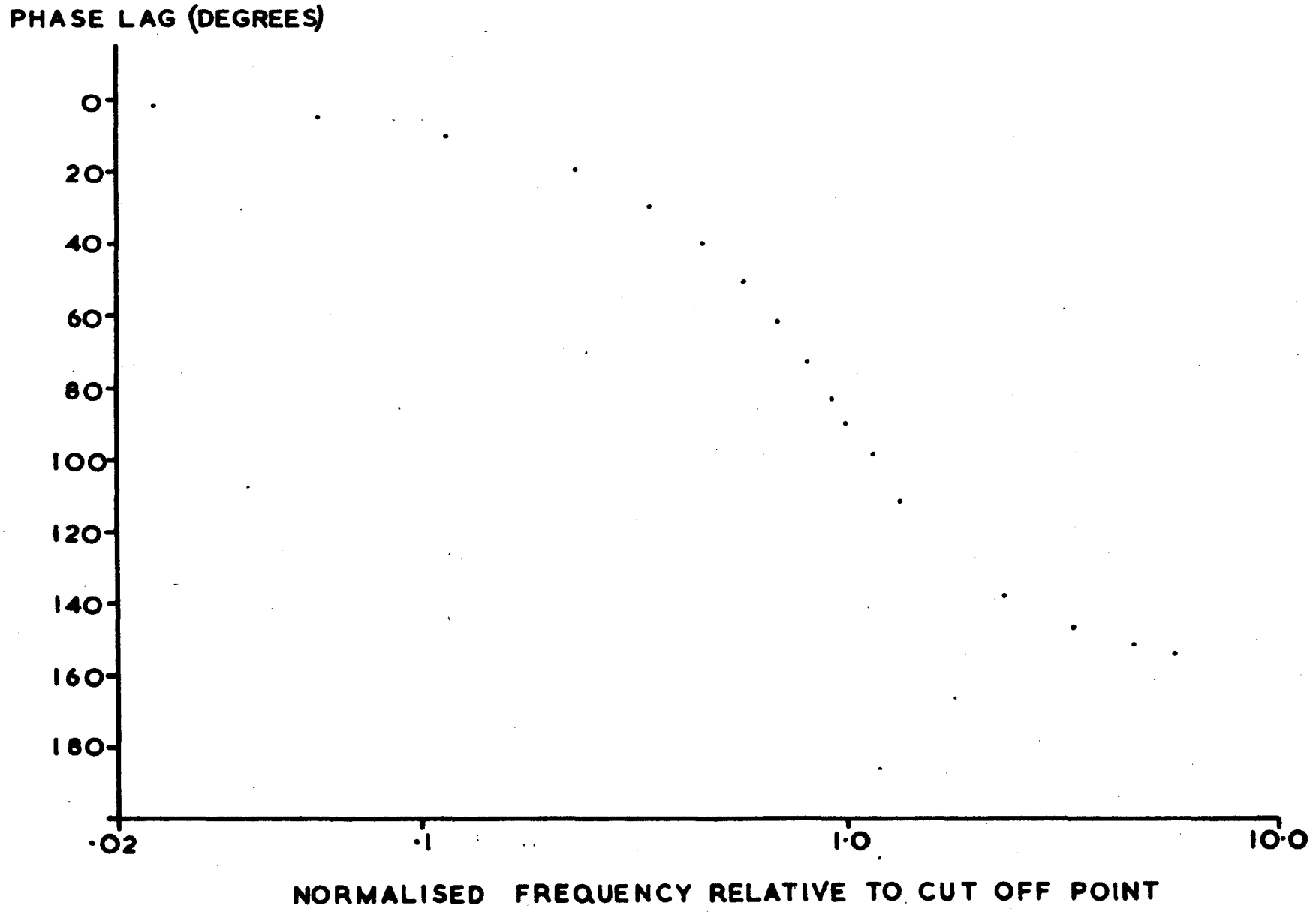

FIG.3·13 PHASE RESPONSE OF 2nd ORDER BUTTERWORTH SWITCHED FILTER.

CHAPTER FOUR

COMPLETE INSTRUMENT ORGANISATION

4.1 Introduction.

In the previous chapter, space was devoted to the novel methods of extracting the data in a suitable form to model the system, following the theoretical ideas developed in Chapter Two. Our attention will now be drawn to the overall format of the instrument's design, which will incorporate use of the designs of the previous chapter, in addition to the complex timing procedures required for the automatic tracking through any one given range of frequencies. In addition, input attenuators, time averaging, signum multiplication and the overall processing and display portions are all detailed.

4.2 Frequency Sweeping.

For operation of the resolver with automatic sweep facilities, a need was established for the generation of accurate clock pulses. Removal of LC/RC oscillators was not completely accomplished, although the swept frequencies were controlled progressively by a binary counter and hence linearly over the range (•01-1999)Hz. Only accurate, repeatable, pulse edges were necessary and this at least removed the usual requirements of stable sinusoids, both in amplitude and phase, as is normal in standard heterodyning techniques.

4.2.1 Digital Techniques.

The binary rate multiplier (BRM) initially seemed to be an ideal choice. This device produces fractional pulse rates when compared to a standard clock reference source. It consists of a divider chain and a control counter. The latter is a gate controller, allowing sufficient pulses through from the divider chain to comprise the required pulse rate and hence, the principle appeared ideal for a variable clock source. A fundamental

disadvantage, however, arises from the asymmetry between the resultant pulse edges. Attempts by Robrock (70) have been made to minimise this feature, using special codes but basically involve extra dividing chains to remove the "jitter." Moshos (71) has indeed shown a maximum asymmetry in any complete cycle of the divide chain to be $\pm\ ^{7}/_{18} + ^{n}/_{6} + (9!2^{n})^{-1}$ where n is the total number of stages in the chain. This maximum error must be considered when the total number of input pulses is not sufficient for the divide chain to fulfil its complete cycle.

One solution appeared to be a BRM operating in a closed-loop with a voltage controlled oscillator (VCO), combined with the allied D/A conversions - a rather cumbersome approach. Inspection of the circuit however, revealed an overall system characterised by a first-order lag. Further, it was most unlikely that a 1% stable VCO could be obtained over the dynamic range •64Hz - 128KHz.

A further attempt to overcome the problem, resulted in the conception of a binary period multiplier. It used exactly the same components as the BRM, minus the differentiating networks. The control counter dialled the gating configuration, to produce one output pulse when the state of the divider chain coincided with that of the control counter. An output train now consisted of an integral number of periods, each symmetrically spaced, the chain being reset at the occurrence of a pulse.

4.2.2 Merits of Digital Techniques.

Since BPM's and BRM's are natural inverse operations, the best resolutions occur in frequency bands at opposite ends of the domain. Pulse rate increments of the BRM are integral multiples of the rate $^{1}/_{2^{n}}$ x reference frequency. This correspondingly yields good resolution at high frequencies, due to the small change and very poor 'Q' factor filters at the low

frequency end of the spectrum. A BPM experiences the reverse process, such that both a MHz initial clock and a reduction in the number of heterodyne weights would be required. In addition, a BPM will produce a non-linear sweep through the frequency domain.

4.2.3 Hybrid Techniques.

Having abandoned purely digital generation of the uniform pulse rates, the next feasible technique seemed to rely upon an oscillator (sinusoidal or relaxation type), whose parameters could be linearly controlled by means of a digital counter. Resistance / capacitance types appeared to be the most promising, using digit variation of the ohmic values, according to some binary coding and decade switching of the capacitors. Blocking oscillators and unijunction relaxation types failed to produce the necessary ·64Hz to 128KHz range. In addition, a linear variation of the astable RC multivibrator (72), using operational amplifiers to produce ramp functions and hence trigger comparators, failed at the upper frequencies, when the amplifier filtered out some of the harmonics of the rectangular waveform.

Hence, a sinusoidal oscillator followed by Schmidt triggering of the output remained - to be satisfied most simply by a Wien bridge configuration. Here, the frequency of oscillation is well known to occur at $(2\pi\sqrt{R_1R_2C_1C_2})^{-1} = (2\pi RC)^{-1}$Hz, when both sides of the bridge are balanced with similar components and is inversely proportional to resistance values. Could this arrangement possibly yield a linear sweep ? Let us assume resistance values to be controlled by a binary coded counter. Consider a single decade. The coded weights 4-2-2-1 are chosen to follow in the order shown (Table 4.1) for a single decade. Interconnections for this feedback counter are less complicated than for conventional BCD and only a single triple-three-input integrated circuit NOR

package is required. In addition, decoding can be performed with a series of similar gates, lending uniformity to the design.

If we consider the counter weights to control the resistance values inversely to the binary weights, it is revealed that $R/4$, $R/2$, $R/2$, R would be required respectively. For example, take the code according to a value of seven times the least significant value. In parallel are placed the values $R/4$, $R/2$, $R = R/7$. Hence the oscillation frequency = $7(2\pi RC)^{-1}$Hz; seven times the fundamental. Therefore, a linear sweep is quite readily attainable, according to a counter, irrespective of the number of decades.

The Wien bridge circuit employed, is shown in Fig (4.1), with range switched values trimmed in practice to allow for parasitic capacitance. The nominal value of C for the highest frequency range is 2•486nF and the resistance values are essentially $\pm$ •2% accurate, controlled by FETS through level translators from the counter. A graph, Fig (4.2), shows the linearity of the sweep in terms of the absolute error at the displayed frequency in the range (1-2000)Hz. With a 6V bulb, a frequency stability of one part in 2×10^{-3} was attainable at normal operating conditions, with the frequency being measured at the output of the Schmidt trigger.

4.3 Automatic Incremental Sweep.

Conventional analysis by heterodyning normally involves a variation of the sinusoidal frequency with time, possibly controlled by a ramp input to a voltage - controlled oscillator. This practice may result in an additional "beating" of the data. Further, fast sweeping to view the approximate response is not satisfactory, since the smoothing involved, eradicates even the beginning of spectral resonances.

With the frequency controlled digitally, it was thought that incremental sweeping would allow a fast sweep facility,

combined with the highlighting of certain good resolved estimates, to obtain an approximate idea of what was happening, before attempting a detailed analysis. Consequently, a 3•2-decade counter, to give 2000 individual steps of frequency, was employed not only to increment in single steps but in blocks of 2, 5, 10, 20, 50, and 100 as well. Range switching, via the decade capacitors in the Wien bridge, allowed this variation in the regions (•01-20, •1-200, 1-2000)Hz, the increments in any one region being in multiples of the slowest frequency. In addition, the sweep could progress either UP or DOWN or be held (HOLD) at any particular frequency, for as long as desired, simply by manipulation of the feedback connections around the complex counter.

4.3.1 Design of the Incremental Sweep Counter.

The multivariable feedback counter was designed using the rules of J - K flip-flops, in which the inputs at the next clock-pulse are a function of the past output variables. Overall minimisation of the logic was conducted by application of Karnaugh maps and finally each functional J - K expressed as a sum of minterms. In Table (4.1), the 4-2-2-1 code is established, as noted previously and both the count sequences for increments of two UP/DOWN given as an example. Tn signifies the state at clock - pulse n and ✖ is an undefined state, equivalent to either 0 or 1; depending on which variate produces the least complex Boolean expression. Figures (4.3,4.4,4.5) yield the complete Boolean composition for the first decade, $(A_1B_1C_1D_1)$, along with the CARRY to the second decade. Decades two, three and binary four are basically of the same construction. For the first decade, the START and INCREMENT facilities are included. These monostables produce pulses of approximately one micro-second duration $\equiv CP_1$.

Finally, it is to be noted that the overall design uses synchronous count within each decade, with ripple-through of the

CARRY. Each decade is decoded using triple-three-input NOR gates and displayed via NIXIE tubes.

4.3.2 Rate of Change of Incremental Sweep.

Having established a method of frequency generation proportional to counter contents and a means of sweeping through the complete spectrum in various steps, the rate of change of the sweep must be developed. From the statistical viewpoint, the degrees of freedom of the resolved estimate depend on both time and frequency averaging. Further, at increased frequencies, one must view a greater number of periods of the heterodyning clock waveform, in order to maintain a constant viewing time per frequency step - in this case at multiples of one second. This is simply achieved using a second 3.2 - decade counter, of design similar to that controlling the Wien bridge, except that it counts the number of pulses fed into the heterodyne circuit unimodally. When this number instantaneously reaches that already dialled on the Wien bridge counter itself, a 13 bit digital comparator produces a single pulse, to reset the former and continue the count again. This idea is closely similar to that conceived for the BPM, except that here, an increased reference frequency leaves the output pulse period constant.

Consequently, a reset pulse occurs once every $^{1}/_{64}, ^{10}/_{64}, ^{100}/_{64}$ seconds, depending upon whether the lowest range frequency is 1, 10^{-1}, 10^{-2}Hz respectively. This occurs independently of the frequencies being examined in that particular range. These normalised pulse periods are easily noted by a third counter of similar unimodal structure and the output, in this instance, compared with a 13 bit code dialled on a thumbwheel switch, indicating averaging time. This code is of course 4-2-2-1. A 3.2 unimodal counter and a 13 BIT comparator are shown in Figs (4.6,7) respectively.

This final stage of comparison again produces reset pulses, which are successively counted in two ripple through counters. The first divides by 64 and the second by 4. Decoding of the final state of the former produces a pulse, whose period corresponds to multiples of either 1,10 or 100 seconds. Division by the latter accomplishes two tasks. It allows a frequency to occur, which will give a radian cut-off to the Butterworth commutated filters in the adaptive loop, corresponding directly to the number dialled in seconds. Secondly, it provides at least four time constants for the said filter to settle. At the very end of this chain, a decoding pulse is generated which, signals the end of averaging, is applied to the INCREMENT control and thus a new frequency is generated, either UP or DOWN, depending on the button previously selected.

After the first divide by two in the ripple-through 64 chain, that output is fed to the averaging filters operating in the time domain. These are first-order equivalents of Fig (3.11). This then, is the frequency which produces the analogue cut-off discussed above, irrespective of the signal frequency being analysed. Hence, the analysis time will always be linked to an integral number of waveform periods and therefore will help to suppress mains interference.

Before proceeding further, all the timing circuitry will be synthesised into a block diagram to aid the understanding of how the frequency generation, sweep variation and averaging time can be intrinsically locked together. In addition, it is easily seen that the START to the Wien bridge sets everything in motion, over one complete range, automatically and is completely self-generating.

4.3.3 Summary of Digital Controller.

All the timing signals required are succintly explained by reference to Fig (4.8). Starting with the Wien bridge control

counter, any combination of :-

1) A specific value of the numerals (1-100),

2) the controls START and UP/DOWN,

3) the RANGE selection for the Wien bridge itself, will initiate a count sequence, whose clock, from then onwards, will be determined by pulses on the INCREMENT COUNTER line. The first state will be level translated through to the Wien bridge, whose combination of resistors will determine the natural frequency of oscillation. A resultant clock, suitable to drive Signetics logic modules is obtained via a Schmidt trigger and used to :-

1) Create a 16 bit test signal arranged as a discrete sinusoid and shown in Fig (4.9) or a 63 bit test signal arranged as a pseudo-random sequence and shown in Fig (4.10).

2) Drive the resolver decoder of Fig (3.3), so operating upon the analogue data present.

3) Be counted in 'S' and compared with the coding initially generated, to produce pulses at $^{1}/_{64}$ of the range period dialled, irrespective of the frequency. These normalised pulses are in a suitable form for similar treatment by 'T' and digital comparison with the coded thumbwheel switch.

It remains to install everything on the universal time scale and this is accomplished with ripple-through counter variants of six and two stages respectively. The former essentially synthesises pulse periods of either one second or multiples thereof. Meanwhile, the averaging filters, themselves, have a radian cut-off at $4\ (n+1)^{-1}$ of the commutating frequency.

Finally, an output pulse from the decoded final state of the $\div 4$, increments the control counter and a new frequency is generated and displayed.

4.4 Analogue Data Reduction.

Previous sections have shown how the difficulty of interlocking

the various operations may be overcome, in order to minimise the operator's interference with the analysis. It now remains to explain the collection and manipulation of the data, in suitable form, to be processed and displayed. A logical method of explanation would follow the sequential layout of the instrument and hence, this procedure will be adopted for the examination of the analogue information paths.

4.4.1 The Attenuators.

These are shown in Fig (4.12). In total, four are required - one for each data point X, E, Y, Z shown in the general schematic of Fig (4.11). X_a, E_a, Z_a (attenuated signals) are obtained via operational amplifiers with FET buffering, since further differencing operations are required. This necessity stems from the viewpoint that, E may not be available directly and this signal must be simulated via Fig (4.13). When E is not available, signals Z_a and X_a' (external link connected) form a difference network, with E_a on open circuit. Conversely, with E_a' present, X_a may be disconnected and Z_a attached to the common, such that the output is E_a.

4.4.2 Signal Amplification.

Since instrument errors are bound to prevail, more consistent results would be obtained by employing some data amplification, such that the analysed signals would be much larger than the inherent instrument errors. These data amplifiers apply only to E_a and Y_a, since zero crossing data is sufficient information from X_a. This will be explained further. Previous analysis (Chapter 2.3.1) revealed that both E and Y required multiplication by X before an unbiased estimate of the forward path transfer function could be obtained. Akaike (18) mentioned that a less stringent requirement for removing bias, resulted from using a signal which was only correlated with X, e.g. the signal obtained

by hard limiting X. This device produces values of $\pm$ 1, depending on whether the signal applied to it is greater or less than zero. Analysis of a hard limiter was primarily carried out by Lowson and Uhlenbeck (73), to produce a correlation function of the output related to the input Gaussian signal, by an arc sine law,i.e.

$$C(\tau)_{\pm 1} = \frac{2}{\pi} \sin^{-1} \frac{C(\tau)}{C(0)}$$

whose variance is unity. This may be expressed as a power series in $\rho(\tau)$, the normalised correlation coefficient for the input signal.

$$\therefore C(\tau)_{\pm 1} = \frac{2}{\pi}\left[\rho + \frac{1}{2}\rho^3/3 + \frac{1.3}{2.4}\rho^5/5 + \cdots\right]$$

Application of this technique, removes at least eight true multipliers from the instrumentation, saving both cost and accuracy. It results in a system of trivial multipliers. Consequently, amplification of signal X_a need be accomplished without knowledge of its accuracy and can be viewed in Fig (4.14) where approximate gains of (0,30 and 60)dB are available, by means of a push-button switch on the front panel.

Data channels E_a and Y_a require controlled gain via Burr-Brown instrumentation amplifiers (3088/16), which have been set-up better than 1% each to each.

4.4.3 Signal Filtering.

Data is heterodyned and filtered using the cicuits of Chapter Three. Six channels result from the three resolvers, four of which (E,Y) are each passed through a cascaded pair of commutated second-order Butterworth filters. The two resolved X channels are passed through single commutated filters of the same structure, the outputs of which are detected by the hard limiter previously discussed. Each of the ten filters is controlled simultaneously, by means of a thumbwheel switch on the front panel. This enters

fixed resistance values into an astable circuit, according to a thumbwheel combination - coded 4,2,2,1 - and similar in principle of operation to the Wien bridge. A resultant rectangular waveform is produced, whose frequency is proportional to the dialled cut-off point in the range (·01 - 9.99)Hz. The circuit is illustrated in Fig (4.15).

An inherent disadvantage of circuits employing any form of modulation which is not strictly sinusoidal, results from the mixing of certain portions of the signal content with harmonics of the modulation frequency, to result in an unwanted aliased component. The commutated filters, so described, are no exception. Prefiltering of the data can be carried out with second-order Butterworth controlled - sources, whose resistance values are switched to produce cut-off points at (15, 1·5, ·15)Hz - Fig (4.16).

In addition, further signal gain may be required if a wide-band random signal is analysed in small bandwidths. Recovery of the signal is possible with an a.c. coupled amplifier of gain 15x and cut-off ·03Hz. This will block d.c. millivolt shifts, which would obviously bias the output, when using a non-sinusoidal test signal. The configuration is shown in Fig (4.17). In effect, it will be observed that the composite amplifier is really a first-order band-pass structure, which blocks d.c. components and removes those above 25Hz, as a precaution against mains interference. The mid-band flat gain response is the section analysed by the commutated filters. In the instance of a deterministic sinusoidal test signal, this amplification card may be replaced by a junction card, which contains only copper track and no components.

4.4.4 Signum Multiplication.

In section (4.4.2), it was explained that a limited form of multiplication, would suit the requirements for an unbiased estimate of frequency response. This is required immediately, after all

filtering operations have been accomplished. A total of eight multipliers are manipulated by the filter signals of the resolved X input, re-arranged as a rectangular sequence of amplitude $\pm$ 1. This is easily accomplished by means of an active detector operating upon an FET switch - Fig (4.18). The output - a function of E or Y - will be of the correct polarity, inverting either E or Y or both if X is negative and vice versa.

4.5 Analogue Data Processing.

The data, so gathered by the above circuitry, is in a suitable form, after summation of multiplicands has been performed on the outputs of the signum multipliers. A block diagram in Fig (4.19) will aid the understanding. From the outputs, E_c^1, E_s^1, Y_c^1, Y_s^1, it is to be understood that they are the real and imaginary vectors of the resultant multiplication by SGNX. The complete expressions i.e. $Y_c^1 = x_c y_c - x_s y_s$, $E_s^1 = x_c e_s + x_s e_c$ etc were derived in Chapter (2.3.1).

It remains to organise the adaptive loop to solve the imposed differential equation and explain the display facilities. The block diagram of Fig (4.20) is fairly self-explanatory, in showing its closed-loop nature. Variations in the polarity at certain points results from using operational amplifiers. Provided that the polarity of the loop error (ε_c,ε_s) is in the same sense as the signals being compared, other changes make no difference to the convergance in the mean of $\hat{U}_m$, $\hat{V}_m$.

Multiplication of ε_m and E^1 is again accomplished with SGN multipliers. This only results in a change of the absolute magnitude of the time averaged signal at any moment, so removing the need for true multiplication. Motorola MC 1595L multipliers are however required for an analogue comparison of Y^1 with $\hat{U}_m \times E^1$ and $\hat{V}_m \times E^1$. Inherently, an attenuation of 10 results but the addition of a closely controlled gain of - 2, allows a full-scale

deflection of five volts to be equivalent to unity gain, for the real and imaginary parts of the transfer function.

The commutated averaging filters, described previously, are preceded by true integrators, controlled, in decade steps, by the thumbwheel switch on the front panel. This is shown in Fig (4.21). As the range is changed, so must be these integrator time constants, since it will be remembered that the time scale increases automatically, by a factor of 10, from the previous higher range. This facility is easily adopted by pressing the buttons indicated. A shift register action occurs, such that, the lowest decade on the thumbwheel switch now sees an integrator time constant ten times larger than the previous one.

The output display is via a sample and hold device Fig (4.22), to a pen recorder energised when the next INCREMENT COUNTER pulse comes along.

4.6 General Layout.

Pictures of the instrument and cards are shown in Figs 4. (23,24,25). A racking system has been adopted with plug-in cards. Most of the analogue variants contain double-sided track, unused track being connected to the signal common. Masks were made for each card and the components assembled as shown in the photographs. The leads to the common were kept as short as possible and the result for 50 cards, reveals about 1mV maximum deviation between the common to each card. The digital circuits were linked by discrete wiring, to accommodate a maximum card packing density of 17 fourteen-pin packages on a board approximately 7" x 5".

4	2	2	1
D	C	B	A
0	0	0	0
0	0	0	1
0	0	1	0
0	0	1	1
0	1	1	0
0	1	1	1
1	1	0	0
1	1	0	1
1	1	1	0
1	1	1	1

SINGLE DECADE

Tn			
D	C	B	A
0	0	0	0
0	0	0	1
0	0	1	0
0	1	1	0
1	1	0	0
1	1	0	1
1	1	1	0

Ja=0; Ka=1.

Tn 1				Ja	Ka	Jb	Kb	Jc	Kc	Jd	Kd
D	C	B	A								
0	0	1	0	0	X	1	X	0	X	0	X
0	1	1	0	0	X	X	0	1	X	0	X
1	1	0	0	0	X	X	1	X	0	1	X
1	1	1	0	0	X	1	X	X	0	X	1
0	0	0	0	0	X	X	1	X	1	X	1

Jb=1; Kb=C. Jc=B; Kc=B&D. Jd=C; Kd=B. Carry Over=B&D

INCREMENTS OF TWO-UP

Tn			
D	C	B	A
0	0	0	0
1	1	1	0
1	1	0	0
0	1	1	0
0	0	1	0

Ja=0; Ka=1.

Tn 1				Ja	Ka	Jb	Kb	Jc	Kc	Jd	Kd
D	C	B	A								
1	1	1	0	0	X	1	X	1	X	1	X
1	1	0	0	0	X	X	1	X	0	X	0
0	1	1	0	0	X	1	X	X	0	X	1
0	0	1	0	0	X	X	0	X	1	0	X
0	0	0	0	0	X	X	1	0	X	0	X

Jb=1; Kb=$\bar{C}$+D. Jc=$\bar{B}$; Kc=$\bar{D}$ Jd=$\bar{B}$; Kd=$\bar{B}$. Carry Over=$\bar{B}$ & $\bar{D}$

INCREMENTS OF TWO-DOWN

TABLE 4.1

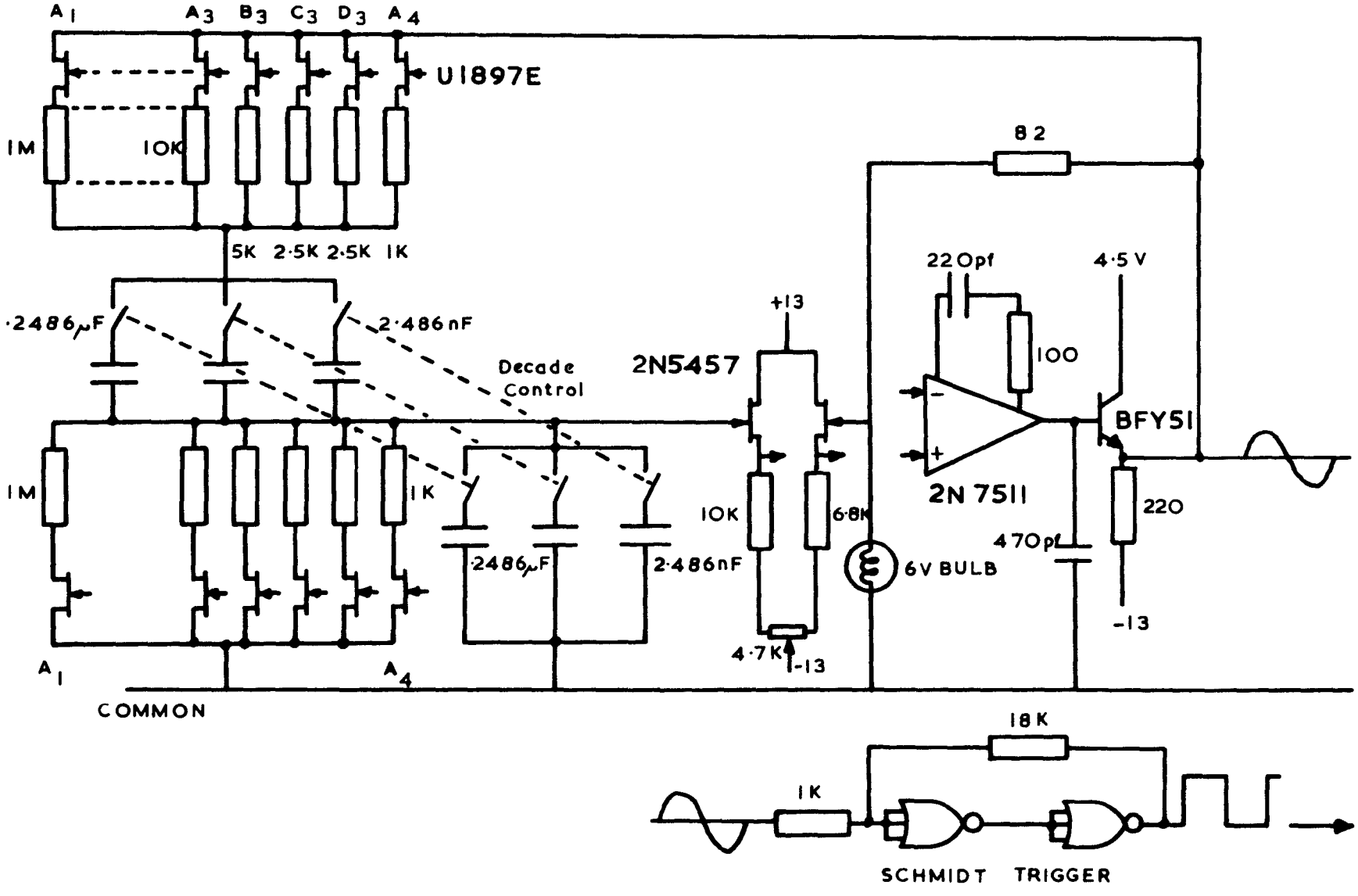

FIG.4·1 WIEN BRIDGE OSCILLATOR

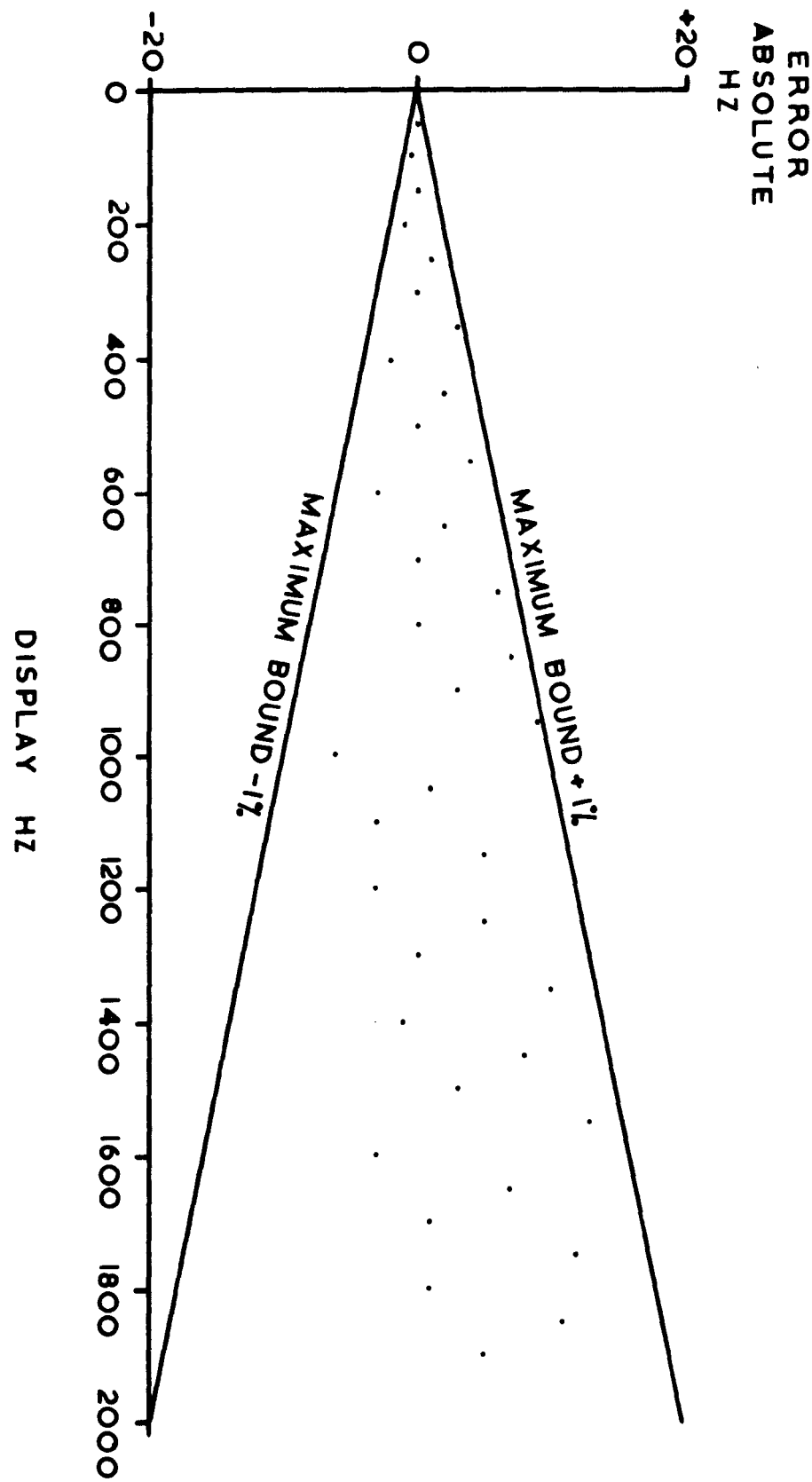

FIG. 4·2 WIEN BRIDGE LINEARITY

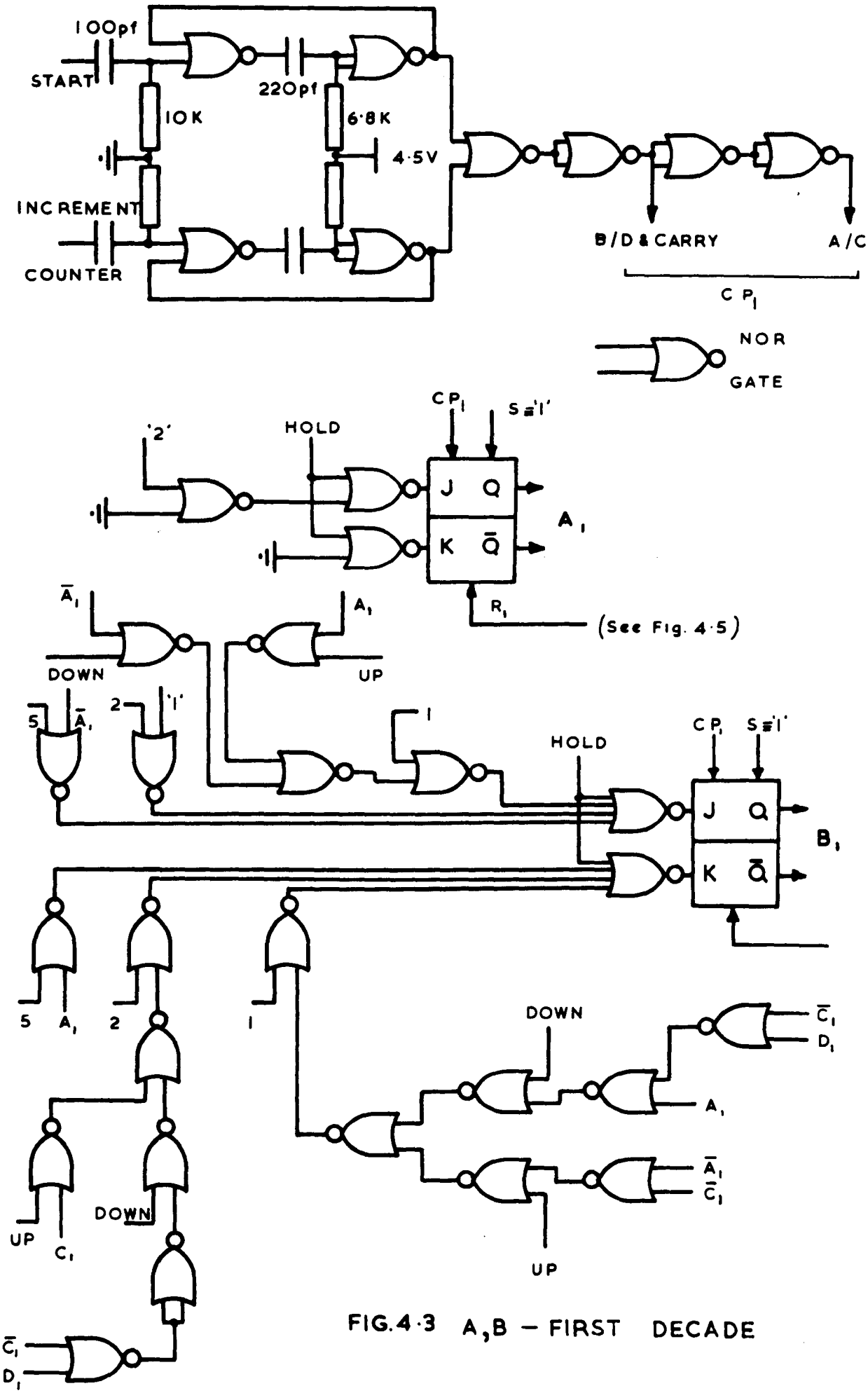

FIG. 4·3 A, B – FIRST DECADE

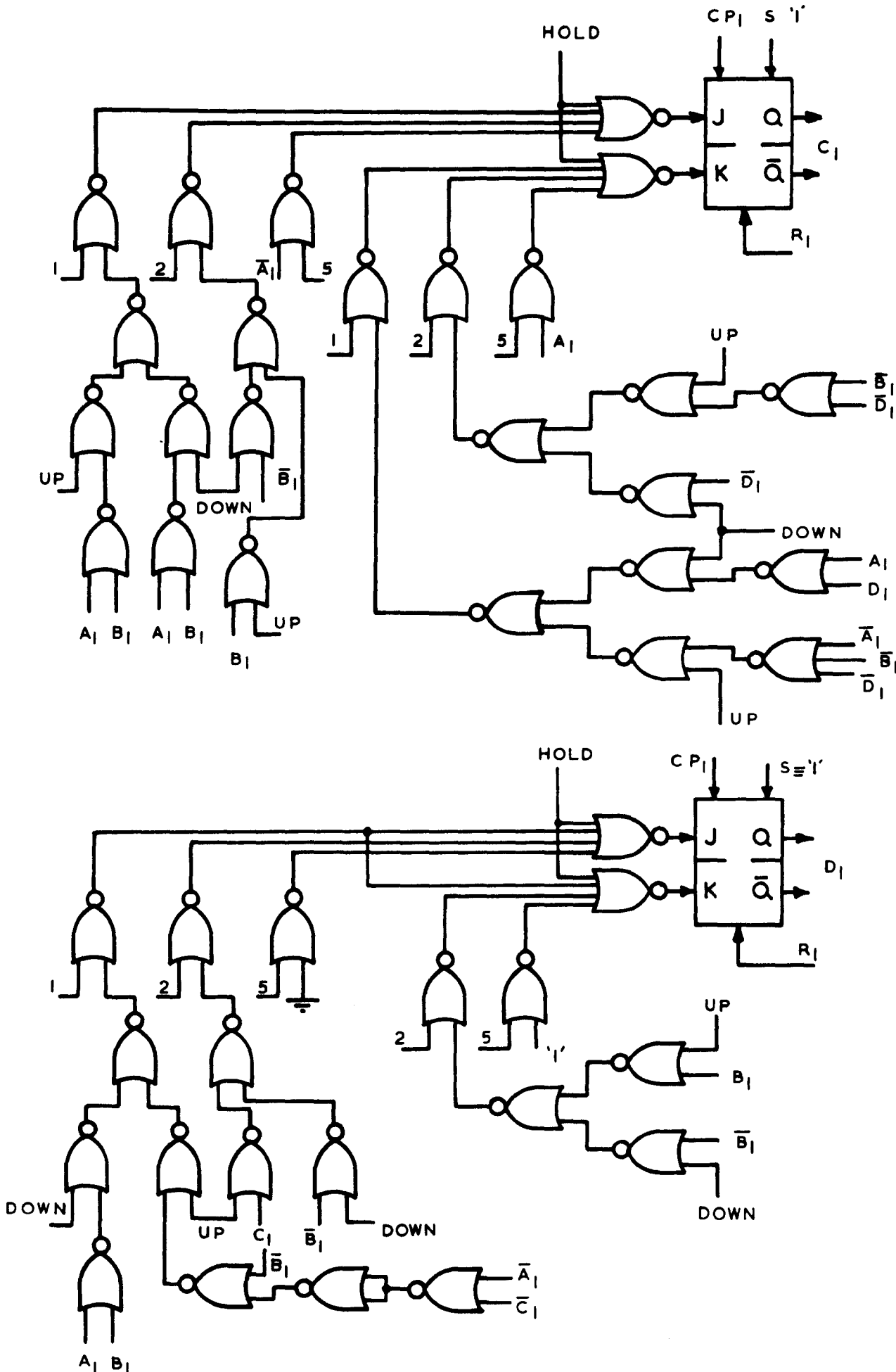

FIG. 4·4 C, D – FIRST DECADE

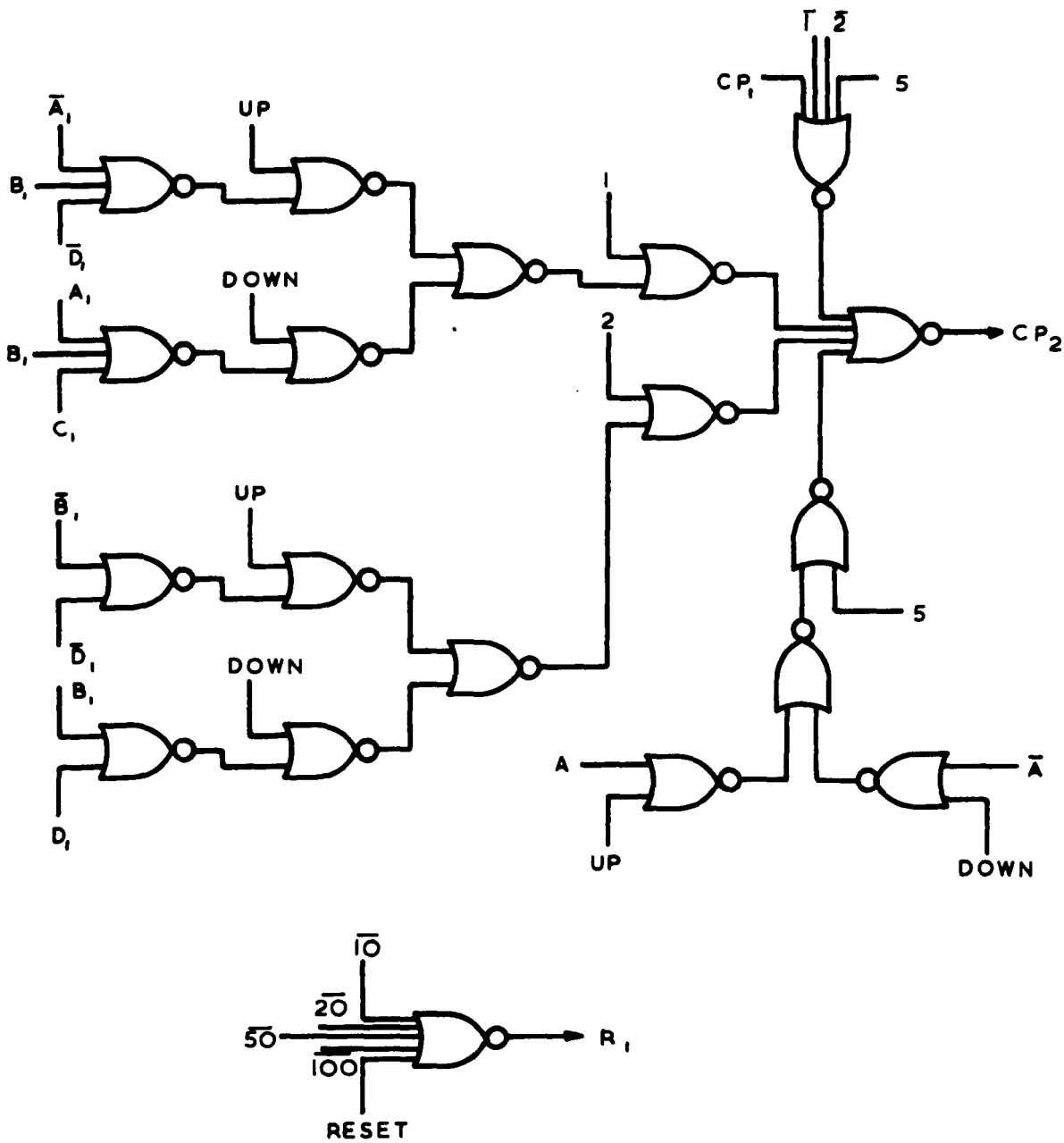

FIG.4·5 CARRY TO DECADE TWO

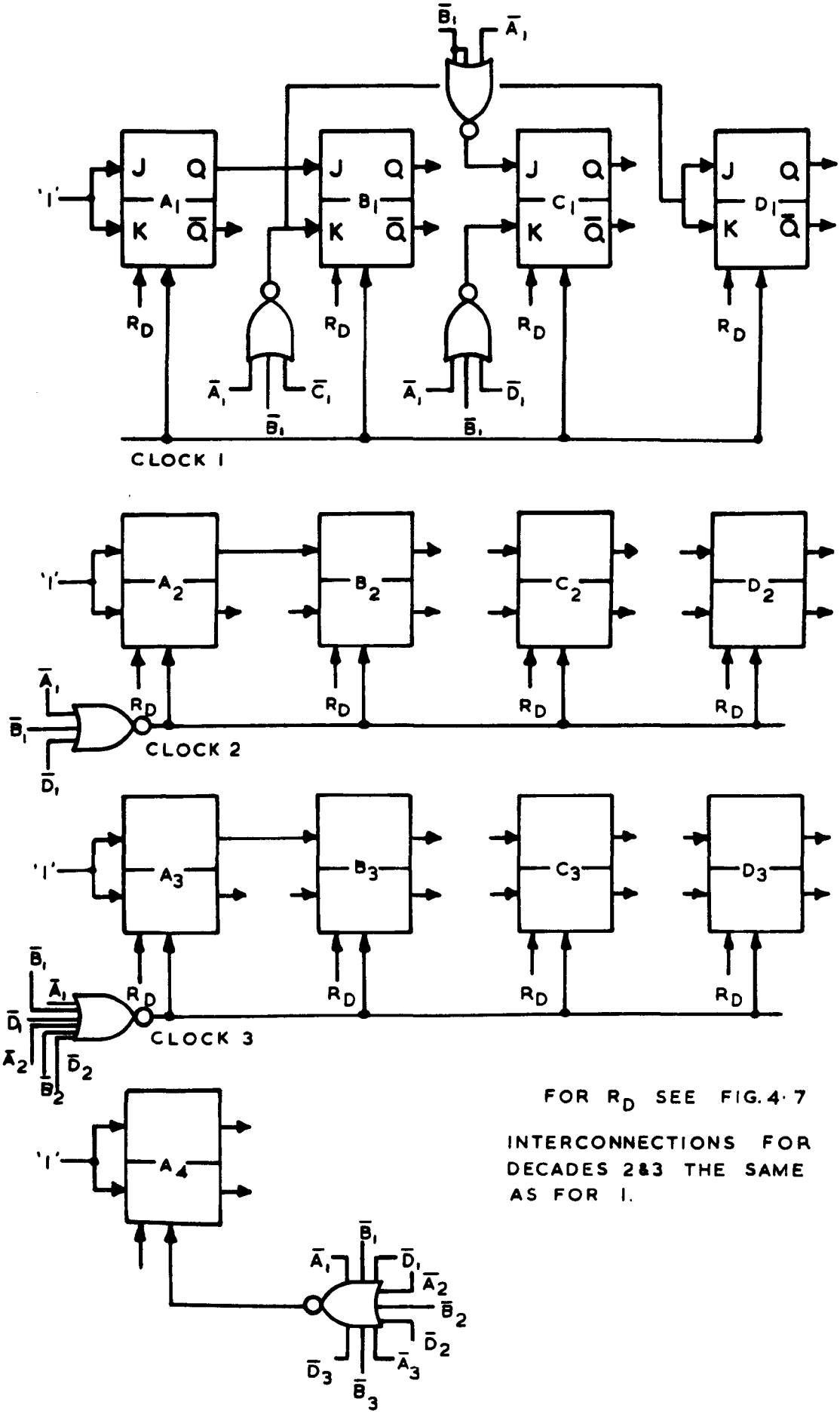

FIG.4·6 COUNTER (0–1999)

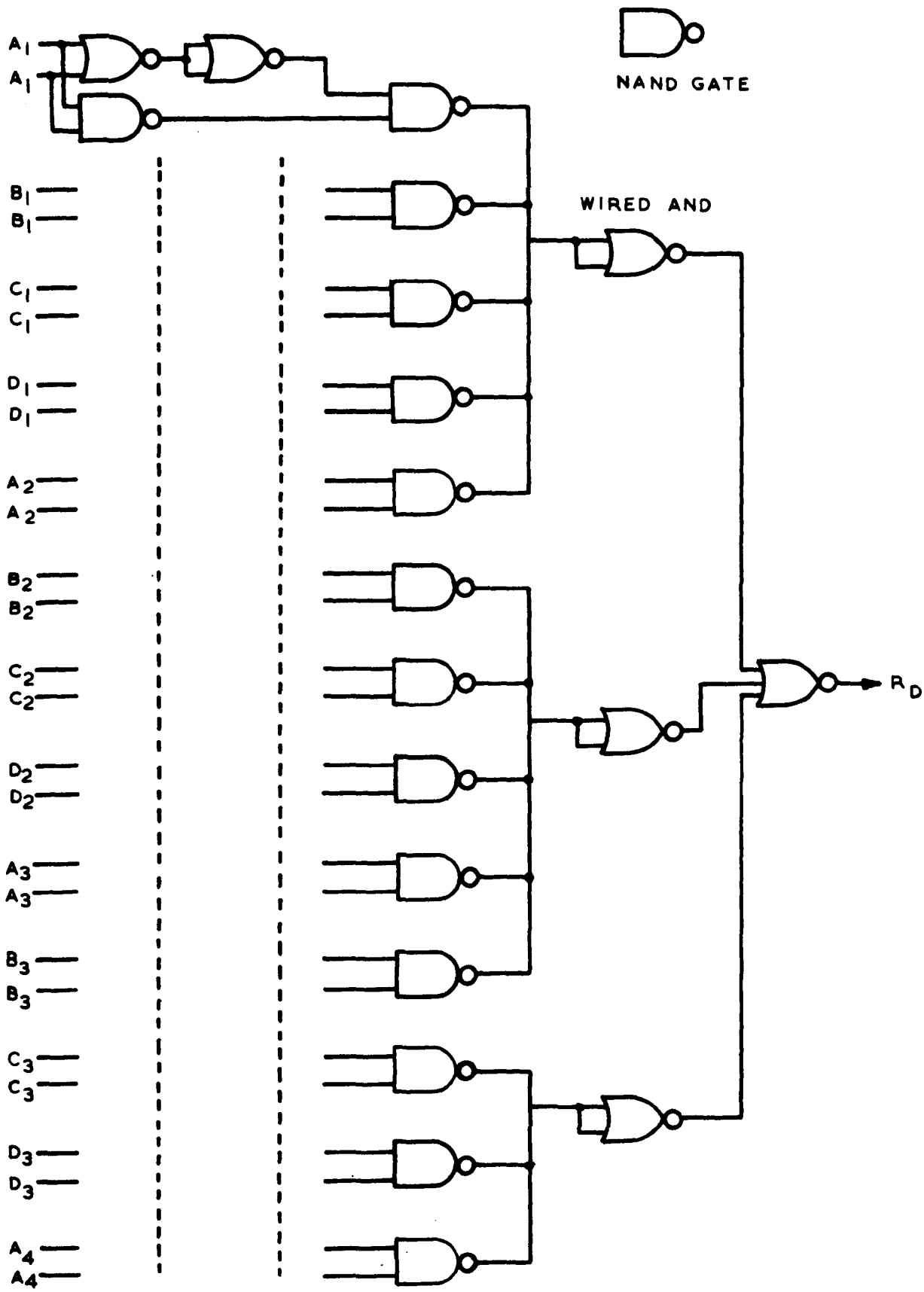

FIG. 4·7 13 BIT DIGITAL COMPARATOR

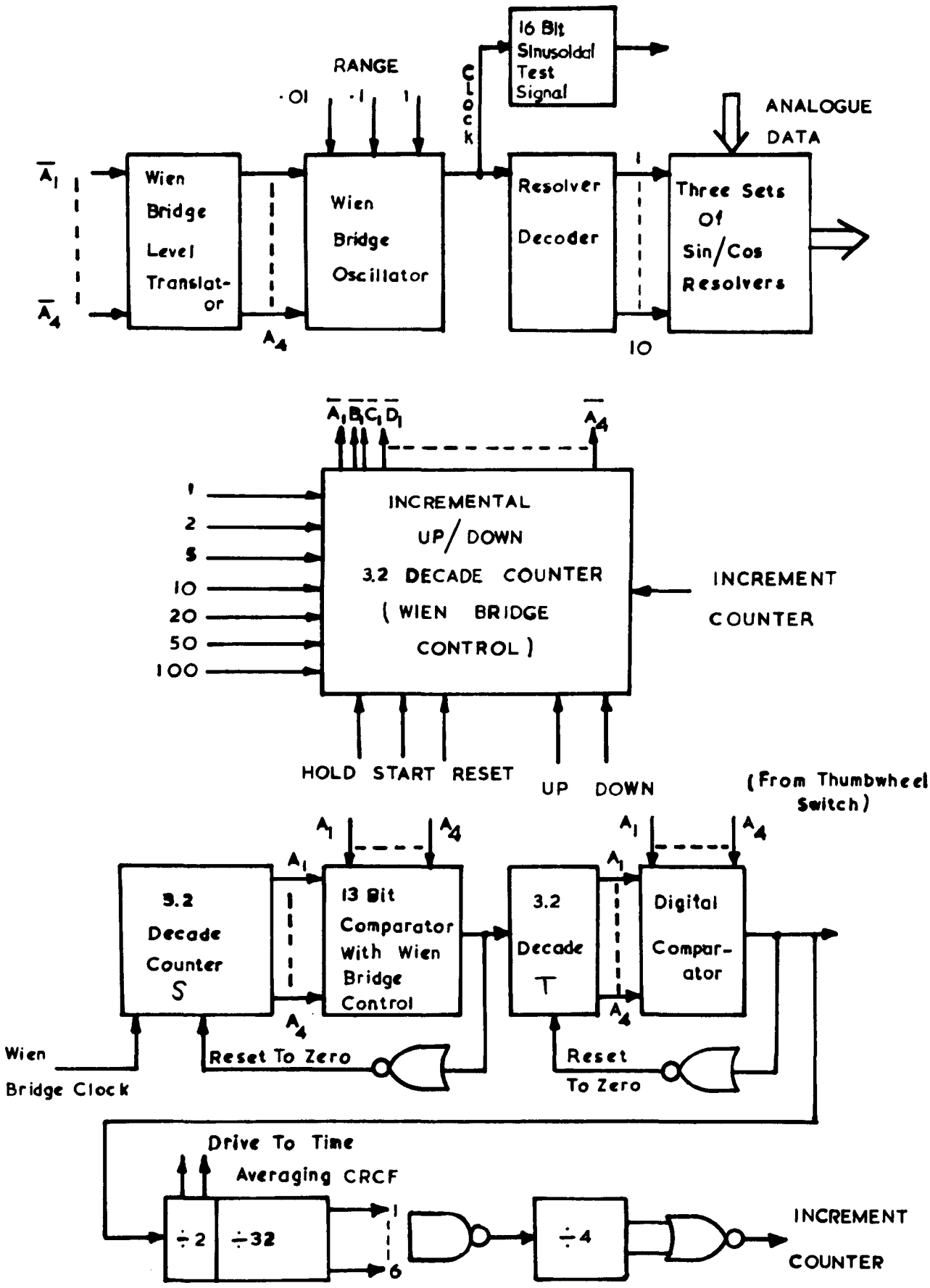

FIG. 4.8 BLOCK DIAGRAM OF DIGITAL CONTROLLER

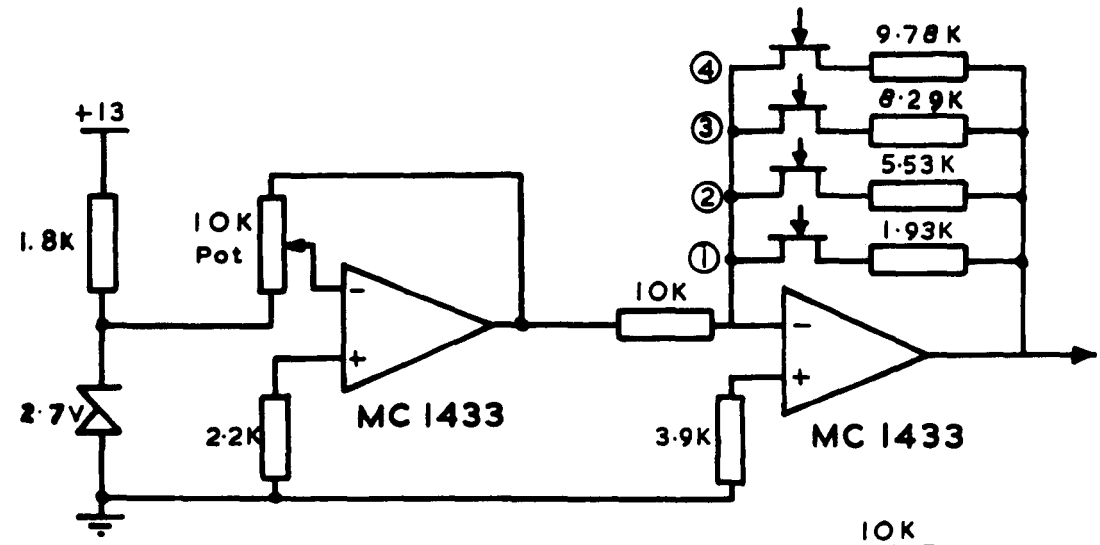

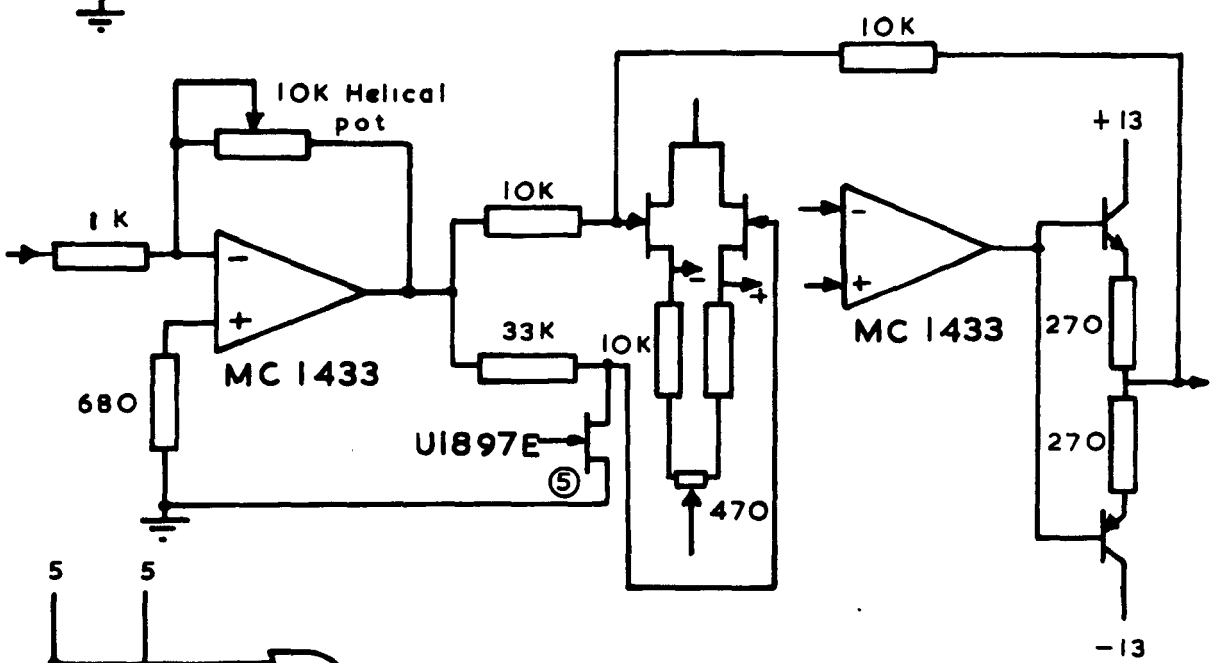

SEE FIG.3·3 FOR 3,4,5 e.t.c.

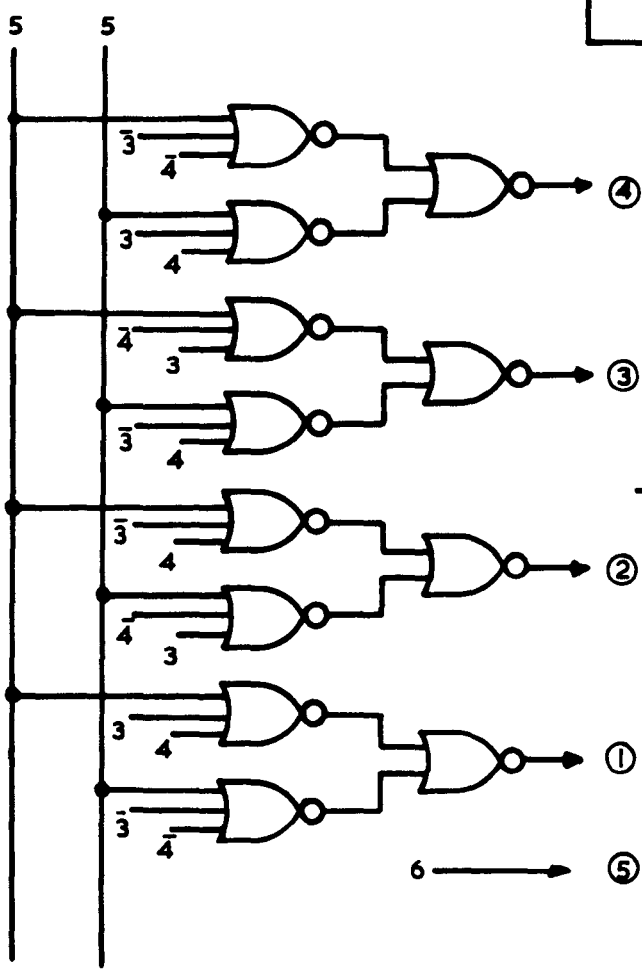

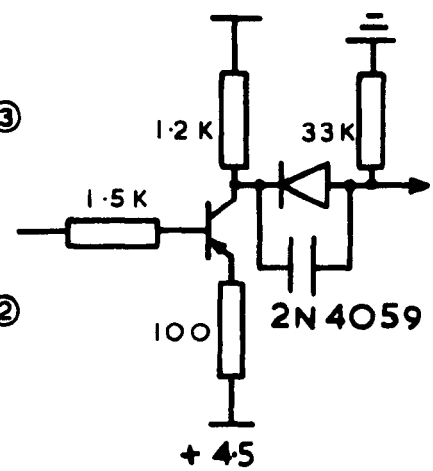

FIG.4·9
16 BIT SINUSOIDAL TEST SEQUENCE

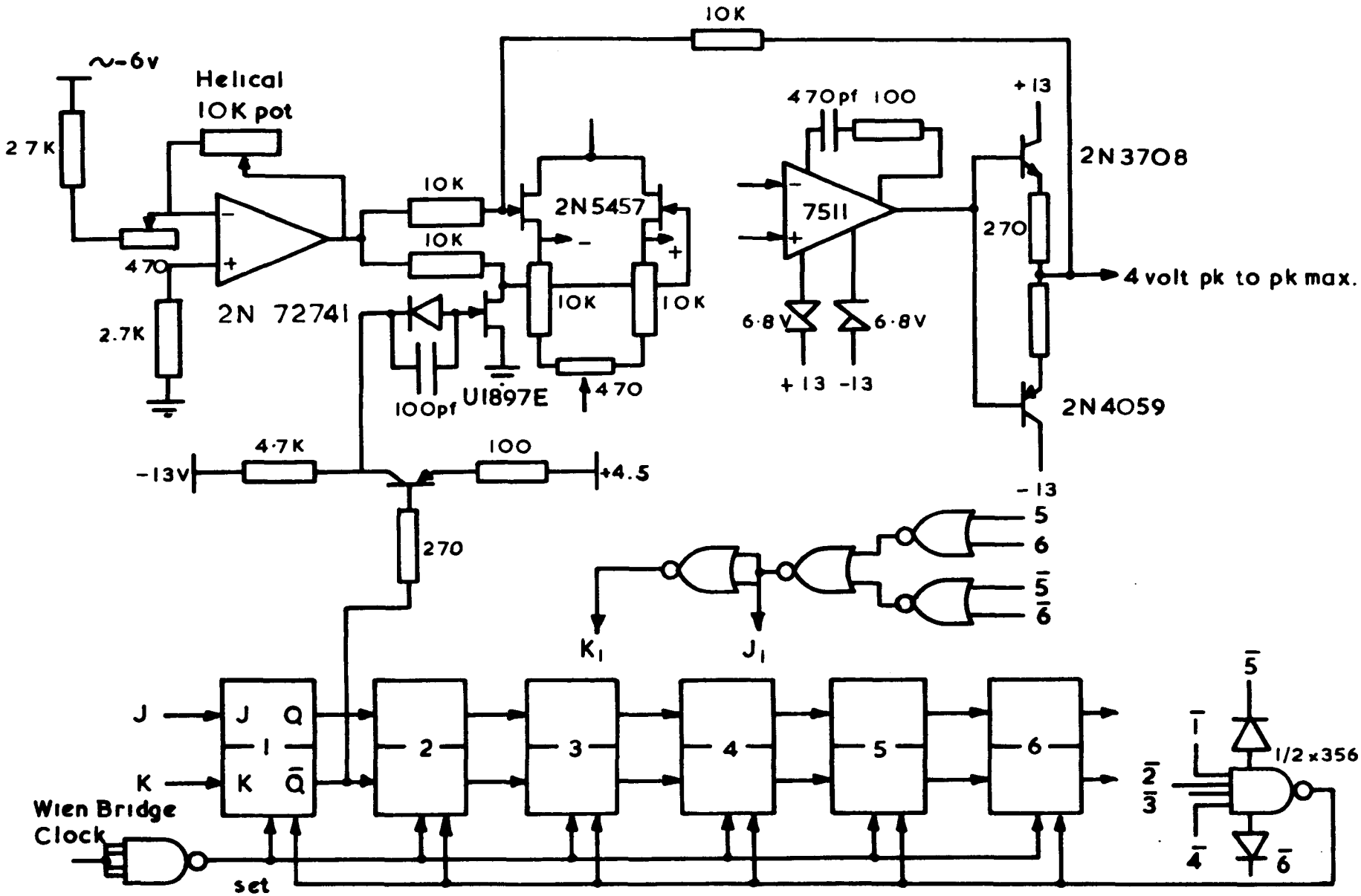

FIG. 4·10 63 BIT PSEUDO RANDOM TEST SEQUENCE

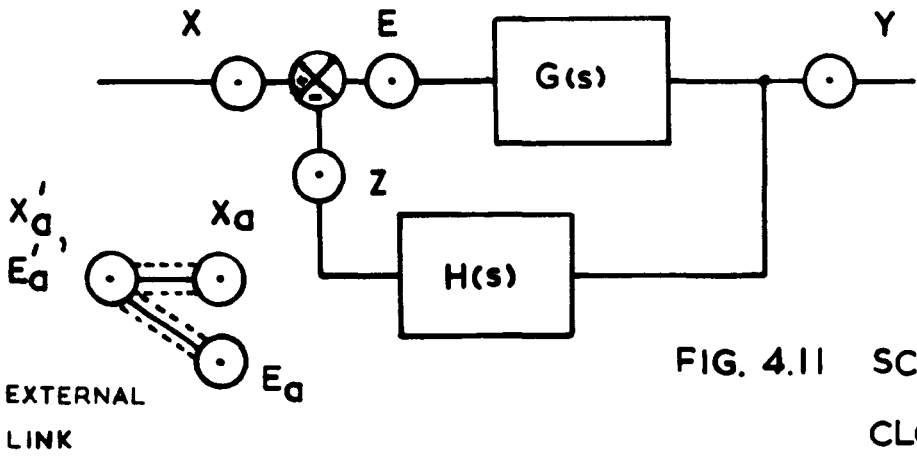

FIG. 4.11 SCHEMATIC OF CLOSED LOOP

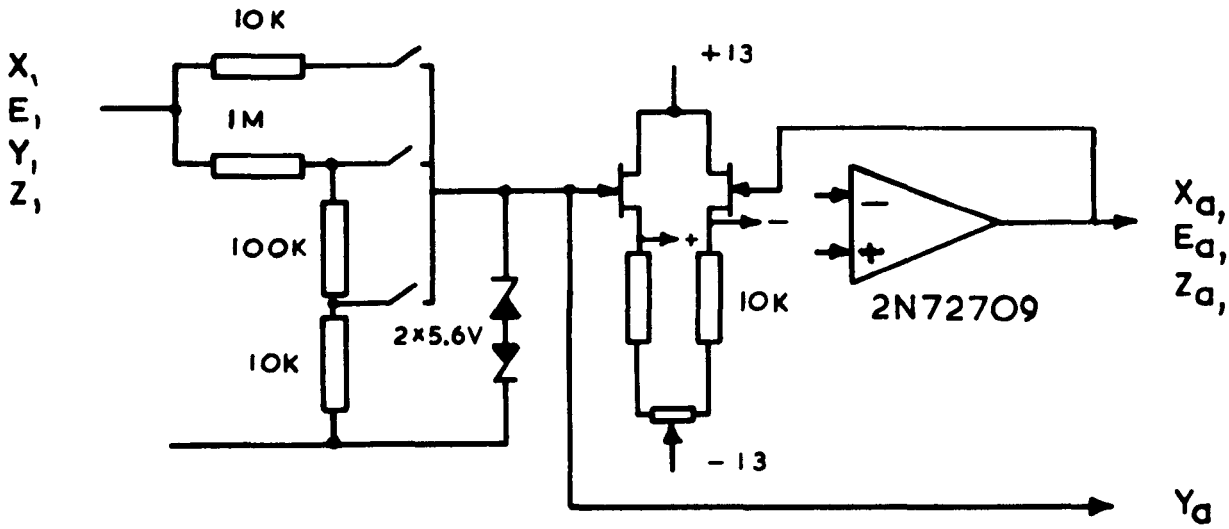

FIG. 4.12 ATTENUATOR

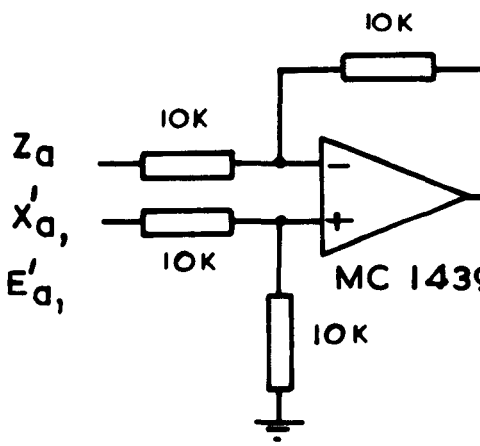

FIG. 4.13
ERROR FORMULATION

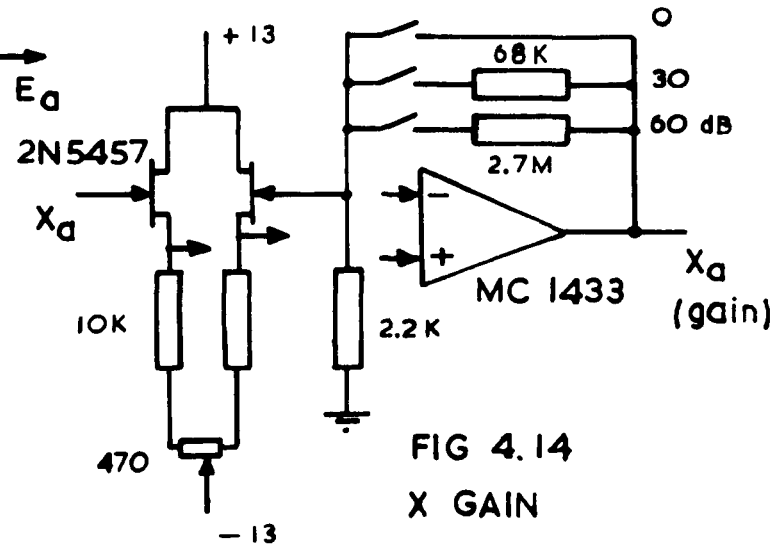

FIG 4.14
X GAIN

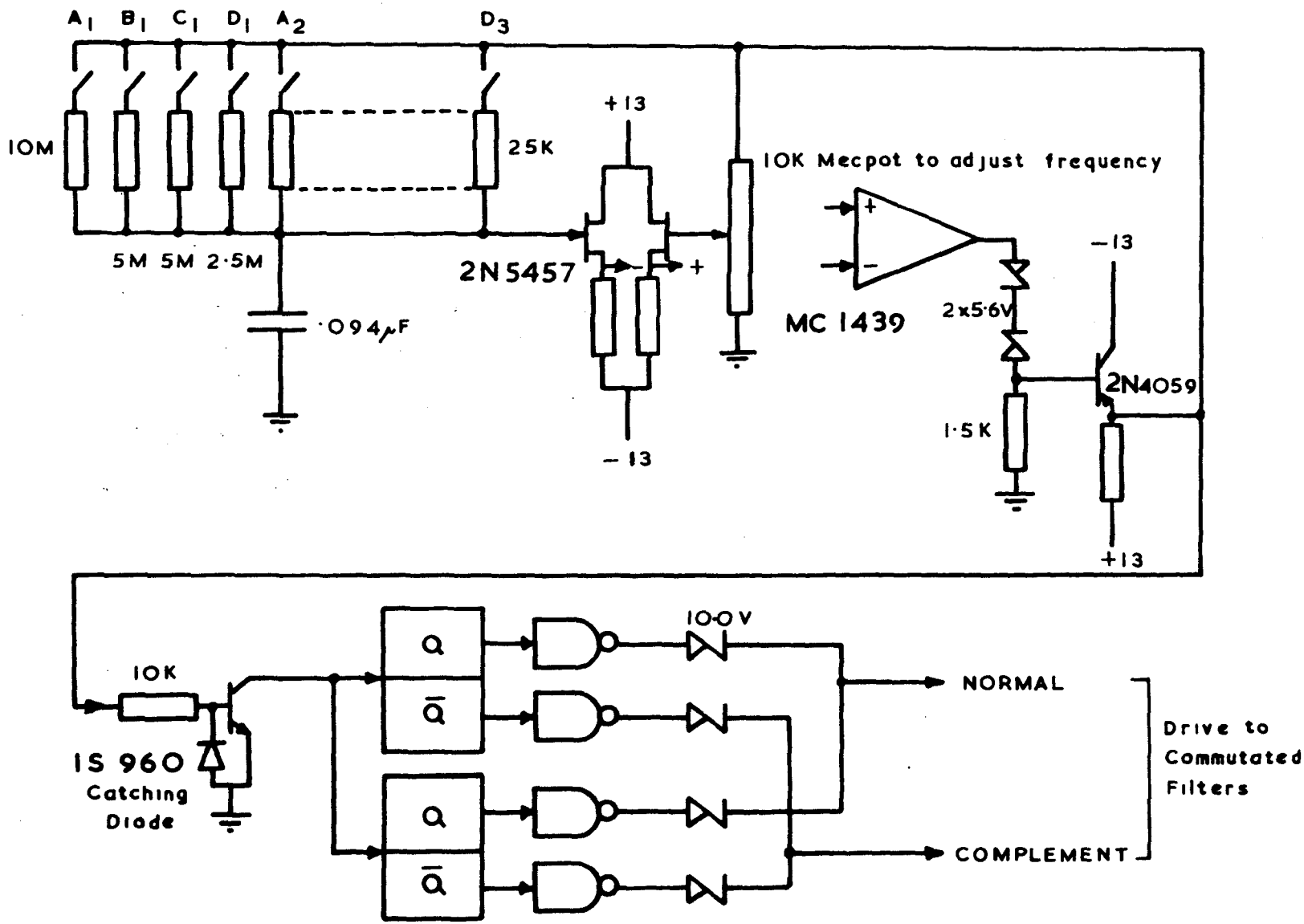

FIG.4·15 COMMUTATED FILTER GENERATOR

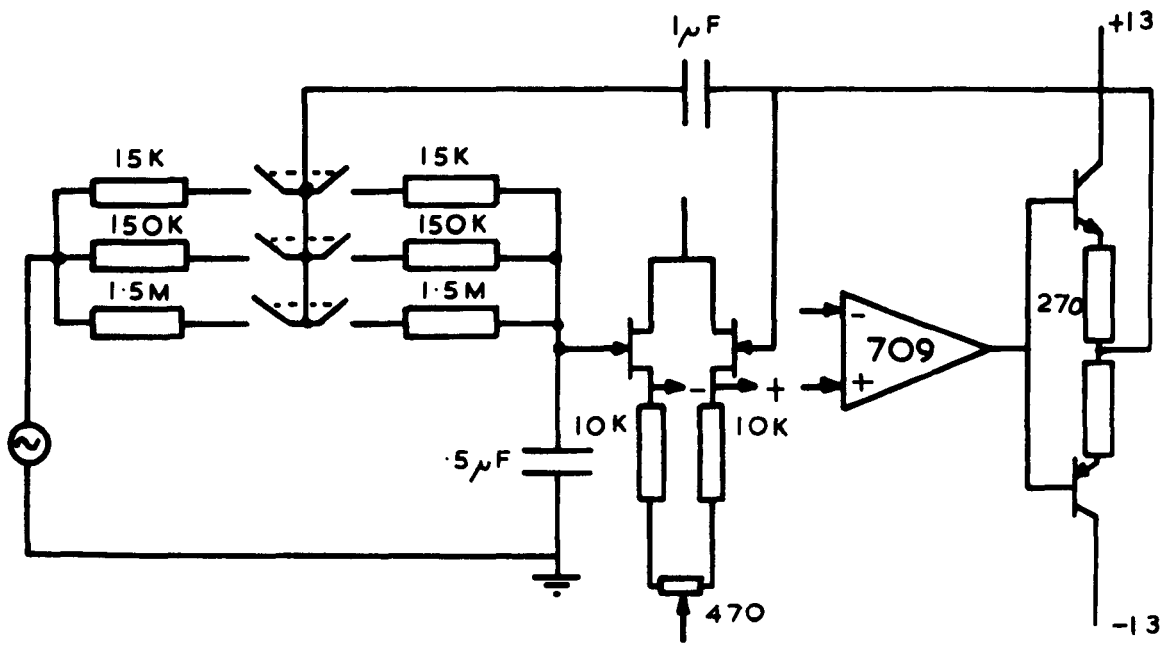

FIG.4·16 GUARD FILTERS (2nd ORDER BUTTERWORTH)

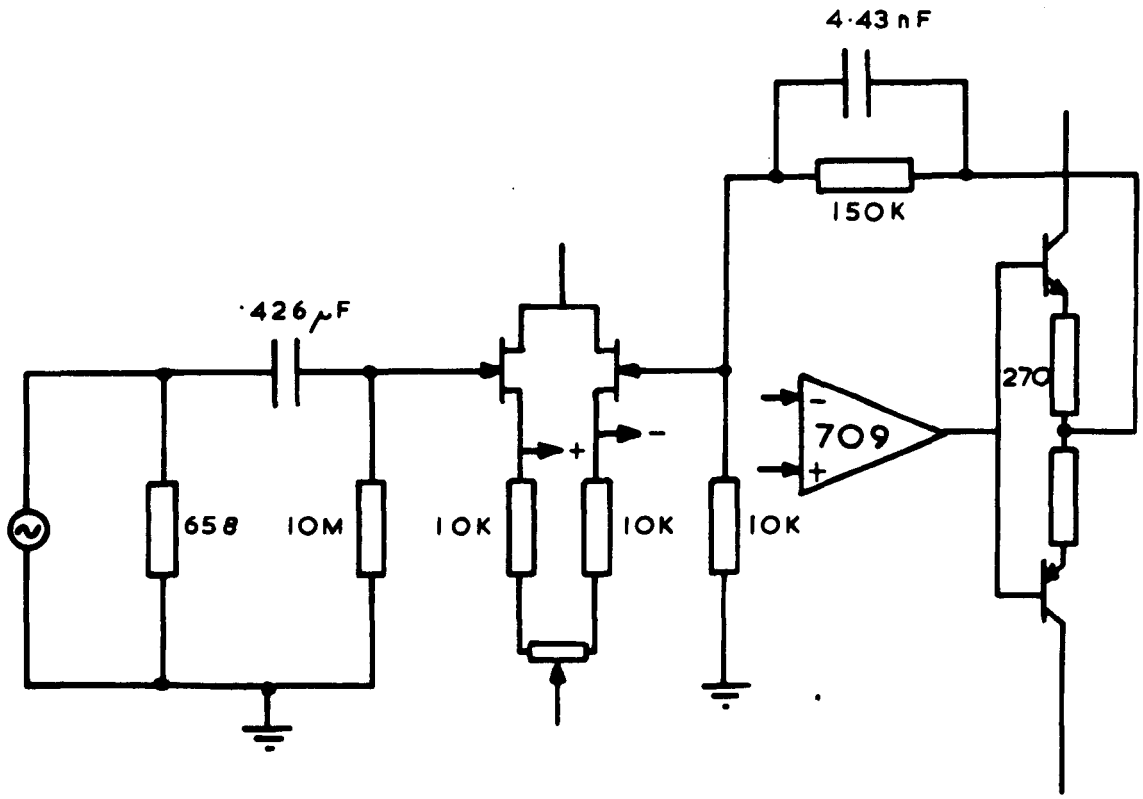

FIG. 4·17 A.C. AMPLIFIER

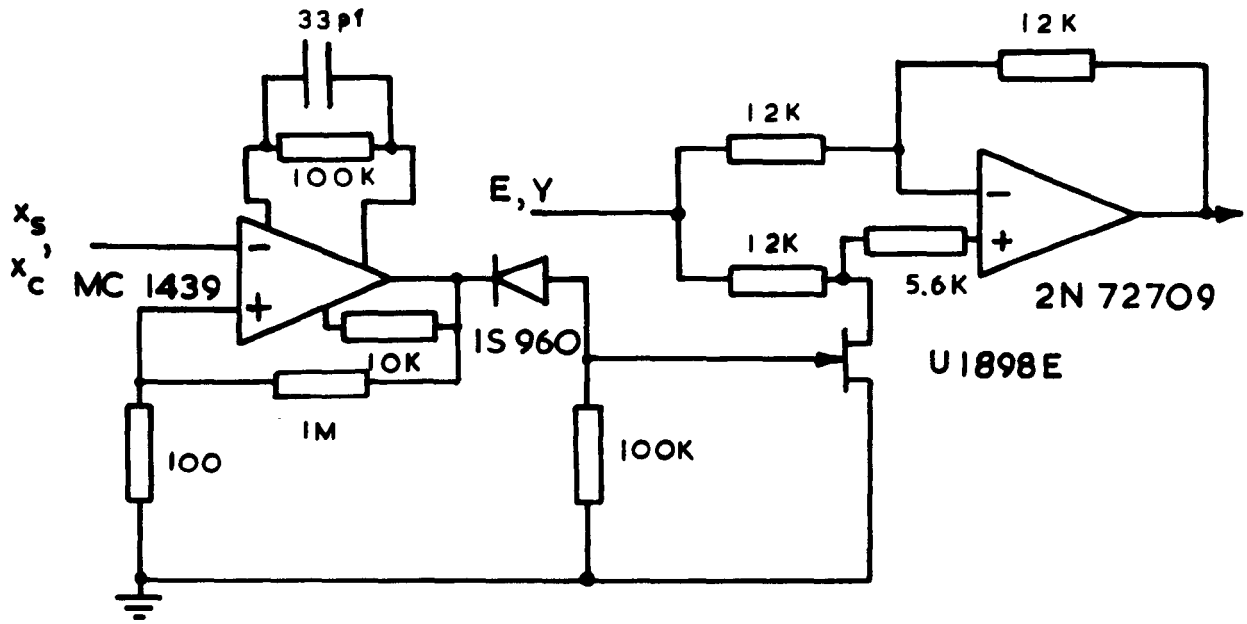

FIG. 4.18 SIGNUM MULTIPLIER

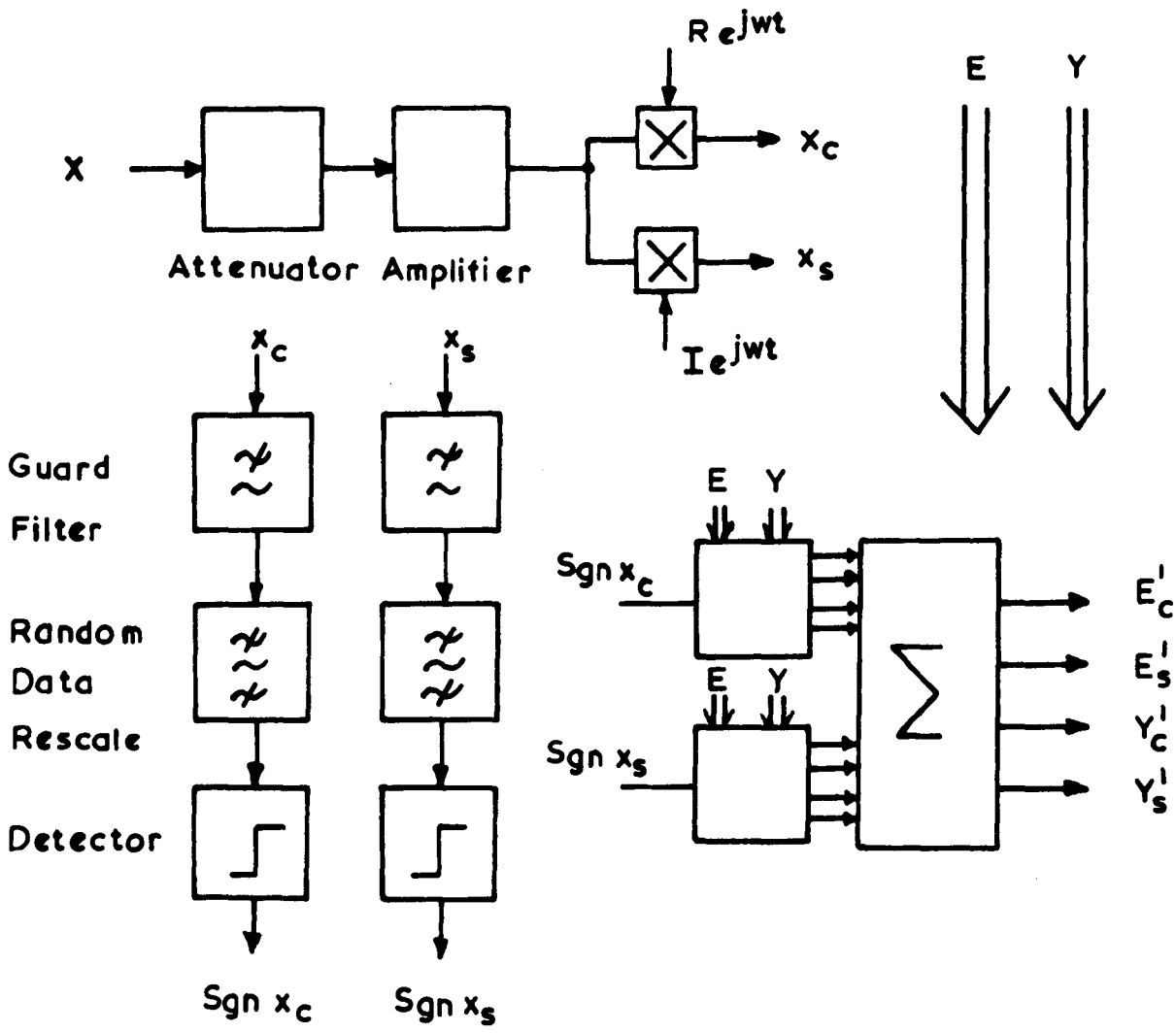

FIG. 4.19 DATA REDUCTION BLOCK DIAGRAM

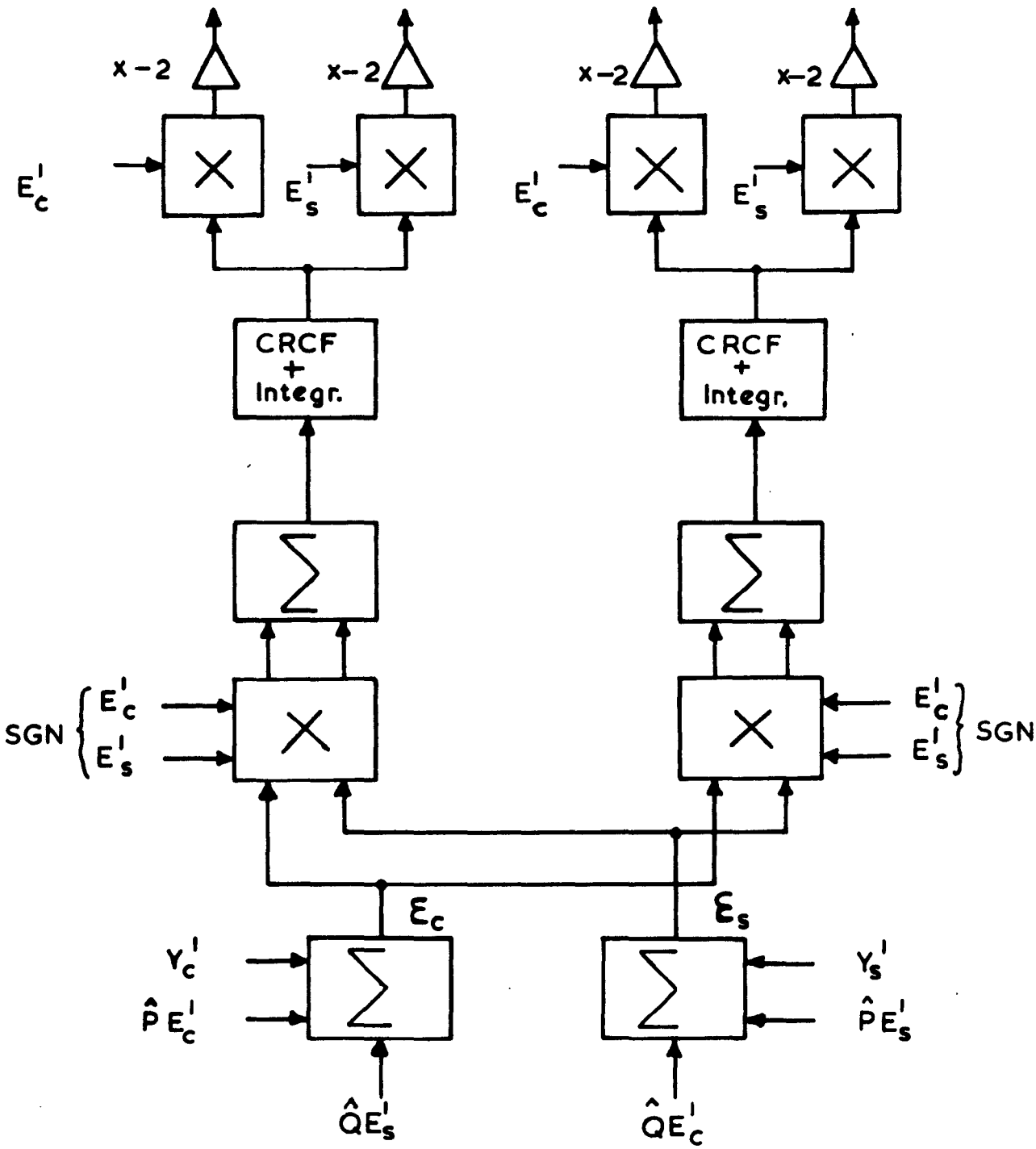

FIG. 4.20 BLOCK DIAGRAM OF ADAPTIVE LOOP

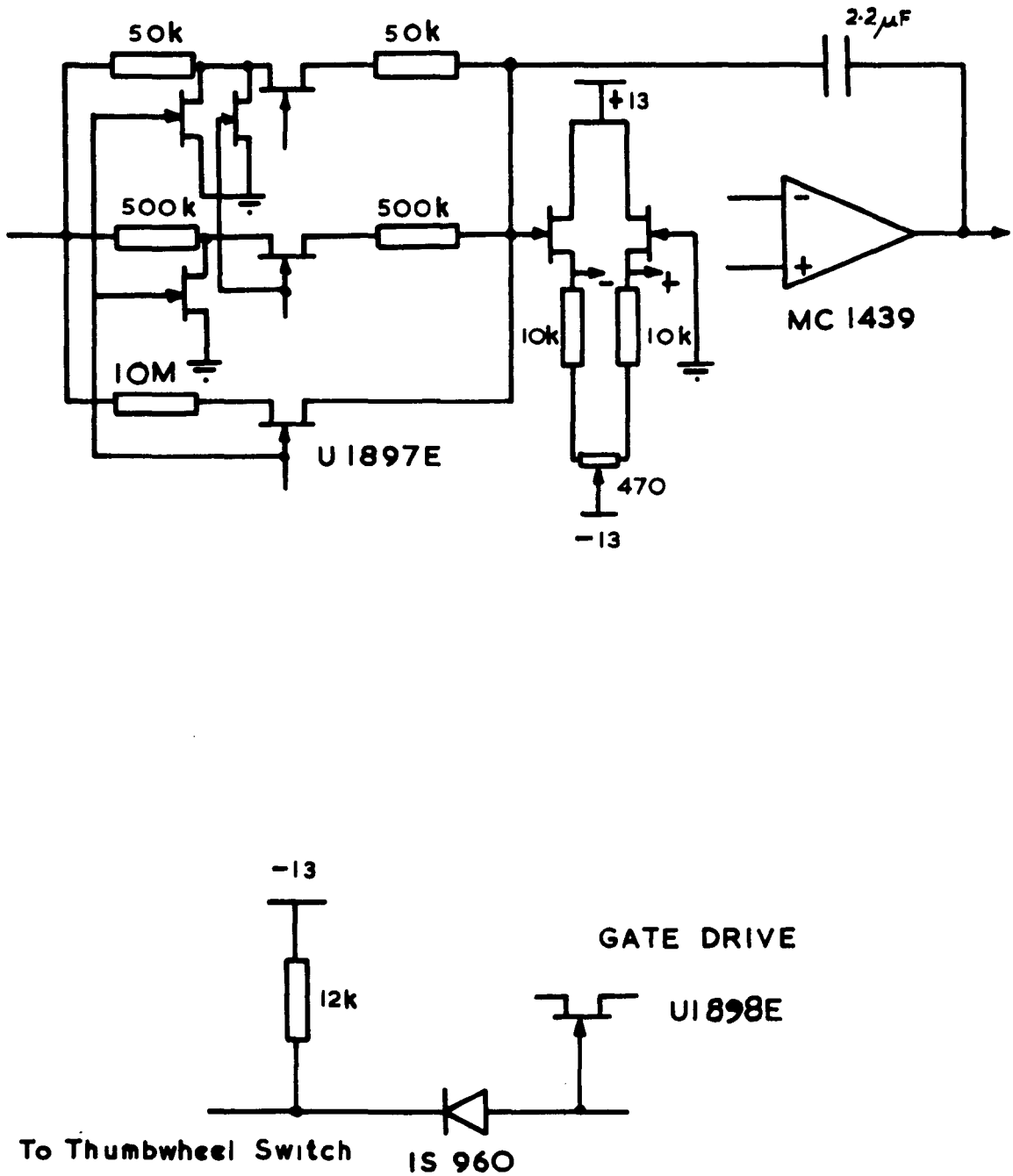

FIG. 4·21 INTEGRATOR

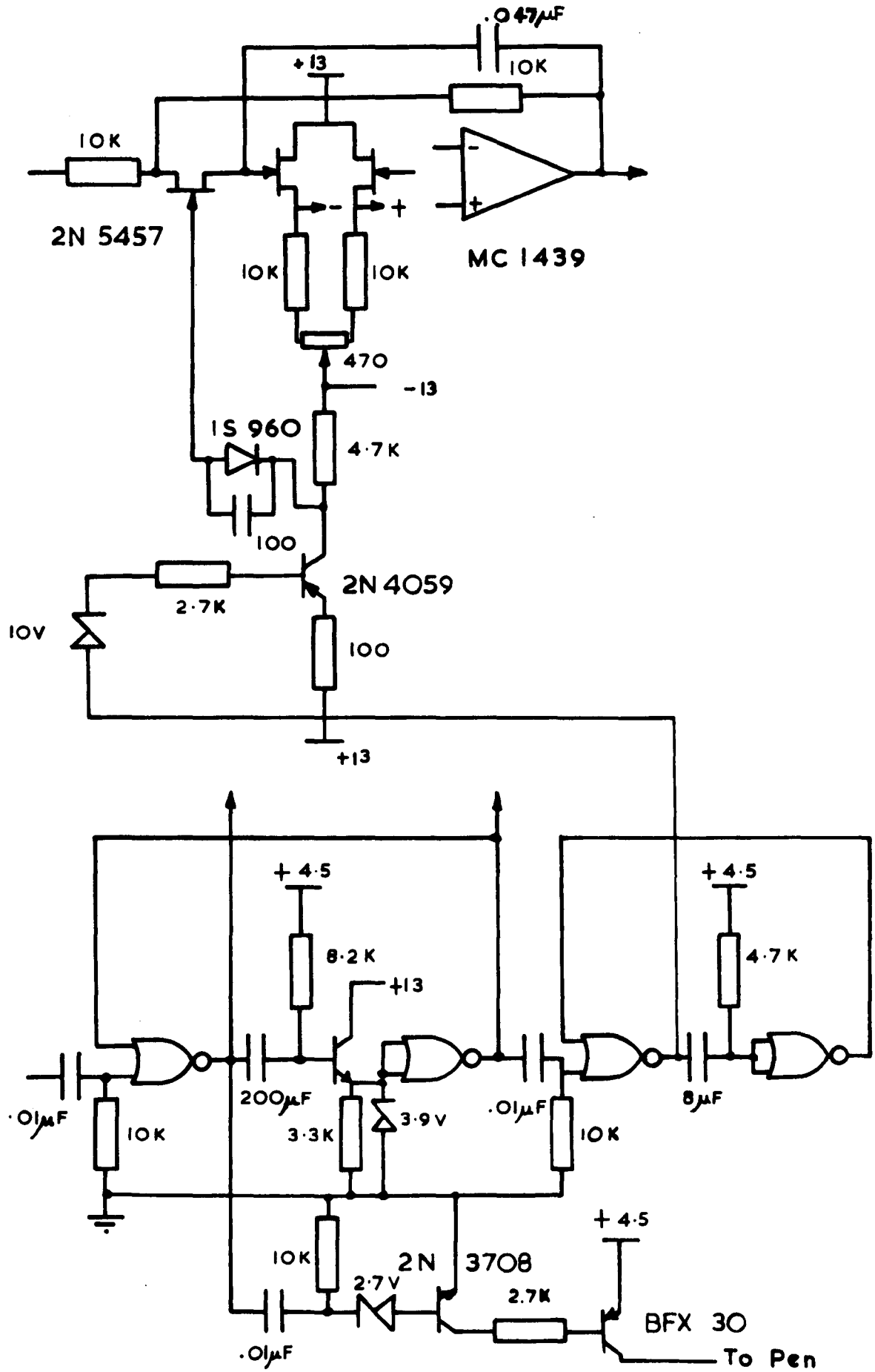

FIG. 4·22 SAMPLE AND HOLD DISPLAY

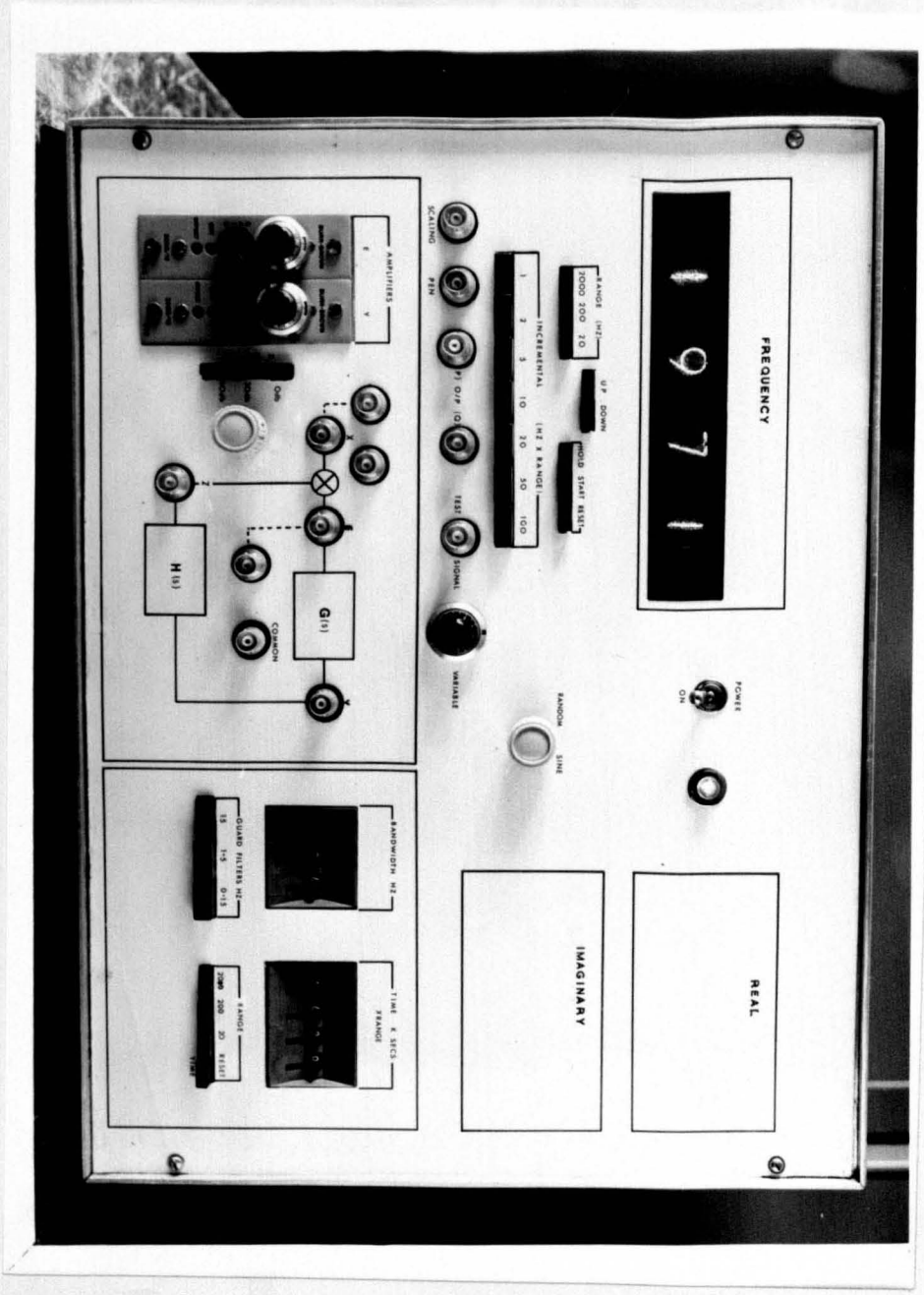

FIG. 4. 23 FRONT VIEW OF INSTRUMENT

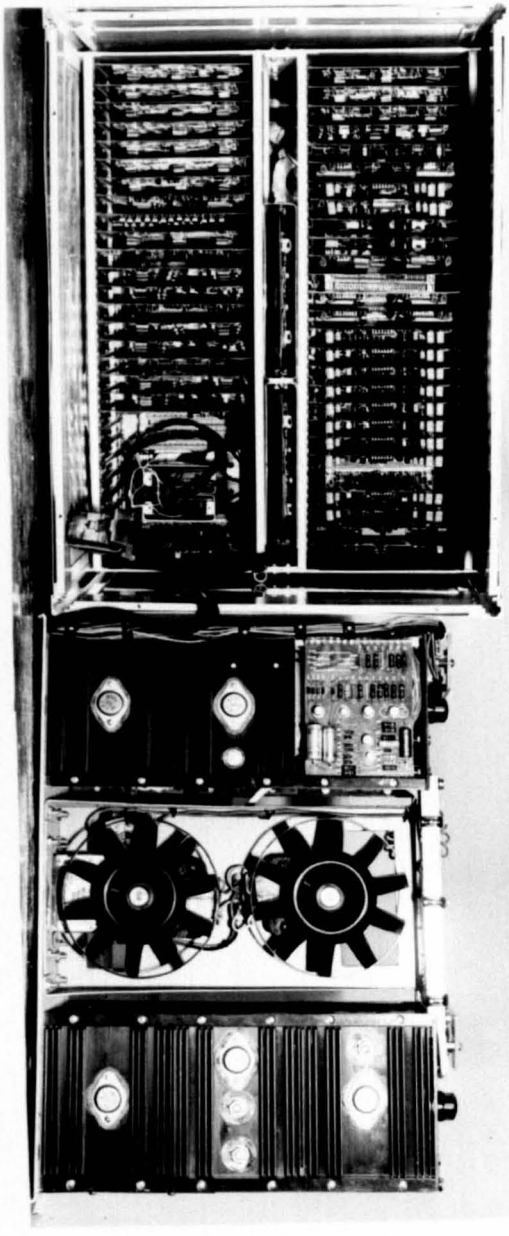

FIG. 4.24 REAR VIEW OF INSTRUMENT

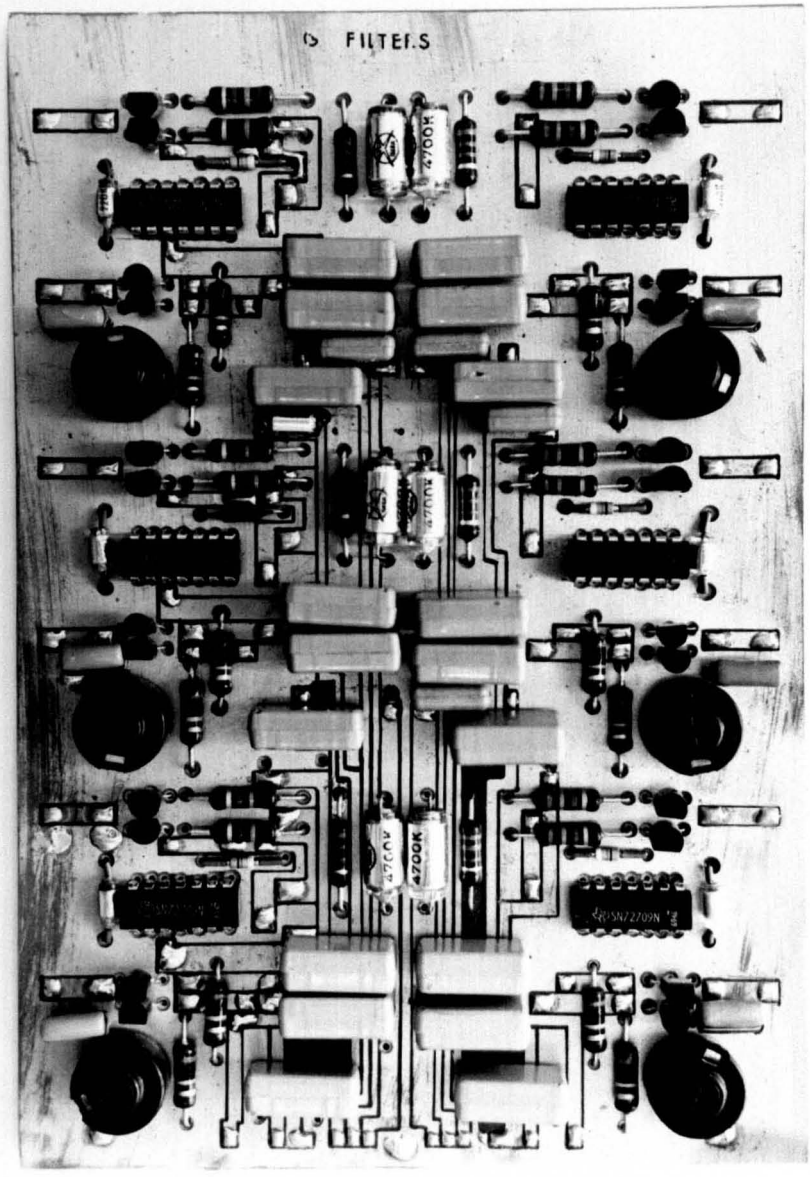

FIG. 4.25 A TYPICAL PRINTED BOARD

CHAPTER FIVE

PERFORMANCE OF THE INSTRUMENT

5.1 Introduction.

This chapter will deal both with an assessment of the characteristics of the adaptive loop and of the instrument's performance when deterministic and random signals are available. From experiments with these signals, the results will show that a powerful on-line analysis technique has been developed to produce valid estimates for the forward path transfer function, in the presence of noise sources arising in the inner loop. The various experiments used both simulated networks and real systems, such as represented by the performance of a motor vehicle when road tested.

Finally, practical sources of error are discussed for the various points of the analysis chain.

5.2 Transient Behaviour of the Adaptive Loop.

Equations (2.51, 2.53) when averaged and transformed, have revealed that the settling times of the appropriate adaptive loops are inversely proportional to the stimulating input signal cross-powers. An obvious disadvantage must thus accrue, unless one is prepared to monitor, continuously, the necessary signal levels, to ensure lack of bias through incorrect frequency sweeping - another case of operator interference. However, in Chapter (4.3.3), it was revealed that a CRCF was inserted into the adaptive loop as part of the averaging circuitry and the purpose of this section is to reveal the inadequacies in using a simple integrator.

5.2.1 Use of a Single First-Order CRCF.

In general, we shall study the situation affecting the step response of the real part of the model and in addition, assume

$\bar{\hat{U}}_m(0)$ and its derivatives are all zero. This will, in any case, be realistic for at least one particular point in the frequency domain.

By substituting a first-order lag network for the integrator in (2.67) we have :-

$$\bar{\hat{U}}_m(s) = \left[S_{yx} S_{xe} w_e^2 - \bar{\hat{U}}_m(s) S_{ex} S_{xe} w_e^2 \right] \frac{A}{sT_n + 1} \qquad (5.1)$$

where A corresponds to real gain

T_n is the time constant of the first-order lag

w_e is the "equivalent bandwidth" assumed identical for each channel.

$$\therefore \bar{\hat{U}}_m(s) \left[s T_n + 1 + A S_{ex} S_{xe} w_e^2 \right] = A S_{yx} S_{xe} w_e^2 \qquad (5.2)$$

Equation (5.2) may be re-arranged in terms of $\bar{\hat{U}}_m(s)$. In particular, when an applied step change occurs in the output cross-power, we have

$$\bar{\hat{U}}_m(s) = \frac{A S_{yx} S_{xe} w_e^2}{s T_n \left(s + \frac{A S_{ex} S_{xe} w_e^2 + 1}{T_n} \right)} \qquad (5.3)$$

In terms of partial fractions, (5.3) may be re-assembled as :-

$$\bar{\hat{U}}_m(s) = \frac{A S_{yx} S_{xe} w_e^2}{A S_{ex} S_{xe} w_e^2 + 1} \left[\frac{1}{s} - \frac{1}{\left(s + \frac{A S_{ex} S_{xe} w_e^2 + 1}{T_n} \right)} \right] \qquad (5.4)$$

The steady-state gain expression has a denominator inflated by a term equal to $1/A$. The resultant bias, below the true value, is readily apparent from equation (5.4) to be solely dependent upon the error / input cross-powers to the adaptive loop. This bias cannot be assessed from knowledge of A alone.

Proceeding further with (5.4), the complete solution,

including the transient term, is obtained by inverse transformation. Therefore,

$$\hat{\bar{U}}_m(w_o,t) = \frac{\alpha}{\beta}\left[1 - (\exp -\beta t\, T_n^{-1})\right] \qquad (5.5)$$

where $\alpha = A\, S_{yx}\, S_{xe}\, w_e^2$

$$\beta = A\, S_{ex}\, S_{xe}\, w_e^2 + 1$$

Examination of β produces the conclusion that, the time constant of adaptation can never be greater than T_n. Unfortunately therefore, although the speed of adaptation of the loop will increase with the applied input signal power, the variance of the resultant estimate can still not be arrived at, without monitoring the signal level (25).

5.2.2 First-Order CRCF and Integrator.

From equation (5.4), the bias term could be simply removed by letting $^1/A$ tend to zero. A true integrator would appear ideal. Equation (5.1) now becomes :-

$$\hat{\bar{U}}_m(s) = \left[S_{yx}\, S_{xe}\, w_e^2 - \hat{\bar{U}}_m(s)\, S_{ex}\, S_{xe}\, w_e^2\right] \frac{1}{s\, T_f(s\, T_n+1)} \qquad (5.6)$$

where T_f is the time constant of integration.

Hence, looking again at the step response :-

$$\hat{\bar{U}}_m(s) = \frac{S_{yx}\, S_{xe}\, w_e^2}{s\, T_f T_n\left(s^2 + \frac{s}{T_n} + \frac{S_{ex}\, S_{xe}\, w_e^2}{T_n T_f}\right)} \qquad (5.7)$$

Inspection of the characteristic function, by means of a Routh array (74), reveals that the loop is intrinsically stable. Use of partial fractions simplifies (5.7) to

$$\hat{\bar{U}}_m(s) = \frac{S_{yx}\, S_{xe}\, w_e^2}{S_{ex}\, S_{xe}\, w_e^2}\left[\frac{1}{s} - \frac{s + (T_n)^{-1}}{(s+\frac{1}{2T_n})^2 + \frac{S_{ex}\, S_{xe}\, w_e^2}{T_n T_f} - \frac{1}{4T_n^2}}\right] \quad (5.8)$$

and the complete time solution may now be expressed as :-

$$\hat{\bar{U}}_m(w_o,t) = \frac{S_{yx} S_{xe} w_e^2}{S_{ex} S_{xe} w_e^2}\left[1 - \exp{-at}\left\{\cos\left(ab - \frac{a^2}{4}\right)^{\frac{1}{2}} t + \frac{a \sin(ab - \frac{a^2}{4})^{\frac{1}{2}} t}{2(ab - \frac{a^2}{4})^{\frac{1}{2}}}\right\}\right] \quad (5.9)$$

where $a = (T_n)^{-1}$

$$b = S_{ex}\, S_{xe}\, w_e^2\, (T_f)^{-1}$$

Obviously, (5.9) leaves an unbiased steady-state estimate of the desired result but more important, is the fact that, the convergence of the solution depends entirely upon T_n, without complications of signal power. A first-order CRCF, with an integrator, is therefore very satisfactory. For compactness, equation (5.9) may have its oscillatory features expressed as $\cos(w_c t + \phi)$ where $w_c = (ab - a^2/4)^{-1}$

$$\phi = \tan^{-1} \frac{a}{2} (ab - \frac{a^2}{4})^{-\frac{1}{2}}$$

5.2.3 Second-Order CRCF.

Following the previously outlined techniques, it would be possible to insert a second-order CRCF, identical to that devised in Chapter Three. However, it suffices to state that with a real gain of A, similar bias terms result, when compared to (5.4). These may again be removed with the addition of a true integrator, to yield a convergent loop response, dependent upon $w_n/\sqrt{2}$, where w_n is the radian cut-off of the Butterworth CRCF. However, the compounded third-order characteristic function is not universally stable, for the time constants envisaged in Fig. (4.21).

Therefore, the adaptive loop is arranged, as devised in

section (5.2.2), such that the first-order CRCF contains capacitors whose ratio is 66:1. For each number dialled on the thumbwheel marked "Averaging Time", a time constant is inserted into the loop, equivalent to that number in seconds. Automatically, the loop is arranged to hold the data for four time constants, before proceeding to the next analysis point.

5.3 Experimental Results.

A practical assessment of the instrument could be deduced by a comparison with the response of a commercial TFA. This cannot be complete, otherwise the present research would have been redundant! However, by employing an established instrument - such as the Solartron JM1600 - accurate sine-wave analysis should yield a robust estimate of the network to be examined. For the stepped sinusoidal option of the new instrument, point by point comparison with this robust estimate can be taken directly as a measure of the instrument's performance. Otherwise, with random excitation, the robust estimate should correspond to the mean locus of the Nyquist plot.

The closed-loop network to be examined, is the result of combining an integrator in the forward loop with unity gain feedback, to give an overall performance equivalent to a first-order lag - Fig.(5.1). To provide answers from the commercial instrument, using a sufficiently wide range of frequencies, a time constant of 10^{-2} seconds was adopted for the network. Should the new TFA yield a good performance with the random data option, it will have established a technique for powerful on-line identification. This is simply because :-

1) All forward paths must at present be observed off-line if correlated error signals exist.
2) Integrators off-line will drift and hence known local feedback is required before an estimate can be taken.

5.3.1 Experiments with Commercial TFA.

A sinusoidal test signal of 1 volt r.m.s. was selected and the network swept with frequencies in the range (1-110)Hz. Throughout, the analysis had to be performed relative to a fixed number of periods of the waveform. Accordingly, this was arranged such that the averaging time was always in excess of one second per point.

Fig.(5.2) illustrates the Nyquist representation of the overall transfer function. No corrupting noise has been inserted. Points not marked, can easily be estimated from the knowledge that, their differences are identical to any two preceding marked points. Full-scale display represents a magnitude of 1 ≡ 5 volts. It will be observed, that a noticeable variance has crept into the results at small signal levels, although the mean shape is readily identifiable.

Using the same signal levels and frequencies of interest, another series of results was taken at the error point. Manually dividing the output by the error, at corresponding points in the frequency domain, resulted in the diagram of Fig. (5.3). It verifies the known fact that an integrator was being viewed, whose time constant was approximately $(2\pi.16)^{-1}$ seconds. However, the most interesting observation stems from the deviation of the plot from a straight line. From the scaling used, it appears to be no less than 4% and illustrates the problems of dividing one estimate by another, especially if errors exist separately in the numerator and denominator.

5.3.2 Deterministic Experiments with New TFA.

The experiments of section (5.3.1) were repeated using the new instrument and the results are depicted in Figs.(5.4),(5.5). The stepped sinusoidal option was used with an amplitude of

1 volt r.m.s. For an averaging time of two seconds per point and bandwidth 1 Hz, two point estimates were required for each response. Hence, the signals entered the instrument through X and Y, with Z attached to the common. As the frequency was swept downwards, it was easy to foretell when a change of increment control was required. Three different increments - (100,5 and 1)Hz - were selected to give accurately resolved plots. It suffices to state that the plots show excellent agreement with the Solartron equipment and especially for the integrator response, appear much more smooth. At 1Hz, in Fig (5.4.), a bias is observed, which confirms the previous theory that the analyser bandwidth should preferably never exceed one half of the analysed frequency.

Fig.(5.6) shows the closed-loop response of the network when subjected to the internally generated pseudo-random sequence. This was arranged to be 1 volt peak to peak.

Connections were made to the points E and Y, with X on open circuit and the external link connected to E. Alternatively, the inputs could have been to X and Y with E on open circuit - Fig.(4.13). Again the network was swept downwards in frequency from (400 to 1)Hz in the increments noted on the diagram.

During the sweep, with the front panel switch on "sine", the scaling point - real filtered portion of E - was observed. The signal level here was too small to give satisfactory results. Had the front panel rotary switch been set to "random", an internal a.c. gain of 15x would have appeared in each channel - Fig.(4.17). However, for the limited 63 BIT internal P.R.B.S. generator at low analysed frequencies (below 10Hz), much of the signal exists around d.c. and is effectively blocked by the a.c. amplifier. Satisfactory scaling - r.m.s. greater than 500mV - could only be achieved by returning the rotary switch to "sine" and setting the Burr-Brown data amplifiers to a gain of 10x.

With this scaling in operation, increments of 5Hz, resolved within 2Hz bandwidth, produced satisfactory results with 3 seconds averaging time. Below 20Hz, however, the estimates - observed on panel meters finally to fit in the indicated windows in Fig (4.23) - were not stable, unless an averaging time of 10 seconds was selected. To keep any unwanted bias terms to a minimum, a filter bandwidth of 1 Hz was also dialled.

From Fig (5.6), very good agreement is seen when compared to the two previous plots, with a predictable bias at 1 Hz. The origin is unfortunately fractionally to the left of its true position. This is again a failing of the internal P.R.B.S. generator which now has many of its frequency components outside the 9.99Hz maximum bandwidth for heterodyned frequencies greater than 300Hz. Had the curve been continued by hand from 100Hz, an even better representation of the response would have been obtained.

5.3.3 Random Data Experiments with New TFA.

The final "acid" tests for discovering the instrument's true capabilities will require signals which are as random as possible and not linked in any way to an internal clock reference. These tests will again be performed using the simple network of Fig.(5.1). However, it is proposed to insert additive noise into the inner loop and this is done by placing a unity gain adder into the circuit - Fig.(5.7).

A multilevel signal was taken from a Solartron P.R.B.S. generator (JM1861) and passed through a Butterworth filter with a cut-off at 1.5KHz. This was to be the test signal of about 1 volt r.m.s. and shown in Fig. (5.8). An additive Gaussian noise of one volt r.m.s. was obtained from an independent Hewlett-Packard noise generator, again cutting off at 1.5 KHz. This is also shown in Fig. (5.8) and the experiment was aimed to identify the forward

path transfer function.

Signals from X_n, E_n, Y_n of Fig.(5.7) were taken to corresponding points on the instrument with the rotary switch on "random". With both Burr Brown amplifiers set to a gain of unity and the bandwidth at 7Hz, ample signal amplitude was observed at the scaling point. The forward path response was plotted with this signal/noise ratio of 1:1 and the result is depicted in Fig.(5.9). This shows that an unbiased estimate of the integrator response has been obtained with a remarkably low variance, using an averaging time of 10 seconds per point. However, the unbiased value was not totally unexpected, since the noise source was effectively placed in the feedback loop, as far as the network output was concerned.

A further experiment was conducted, with this network having an additive noise source of 200 mV r.m.s. However, for the same input signal of 1 volt r.m.s., it was intended to feed the signal content of Z_n into the Y position of the instrument, all other entries to the instrument being as for the previous experiment. The noise source was now effectively in the forward path and only cross-spectral densities, using three records, could possibly remove the bias of the estimate. A bandwidth of 7Hz and averaging time of 10 seconds was used to resolve the data. No extra amplification of the signals was used, apart from the internal gain due to the rotary switch being in the "random" position. The results achieved are plotted in Fig.(5.10), where it is observed that a definite variance exists but an effectively unbiased result for the forward path has been obtained.

5.3.4 Experiments on Real Systems.

Finally, it was decided that some experiments should be conducted on real operating systems, which would be far from

working under the ideal conditions of a simulation.

An engine test rig (75) was available. This consisted of a Hillman Hunter engine which could be computer controlled. Accordingly, much electronic equipment to monitor and transmit data, concerning the engine's performance, was available whilst the engine was running. Since the signals from the transducers, which measure engine speed and fuel flow, were known to be heavily corrupted by noise, it was decided to excite the engine around some mean speed, using the TFA's sinusoidal option.

Experiments were conducted to find the Torque/Throttle, Fuel-Flow/Throttle and Torque/Fuel-Flow transfer functions, the latter being made from transducer signals which were both very "noisy". The various signals from the transducers and the throttle excitation are shown in Figs.(5.11,5.13). Corresponding transfer functions are shown in Figs.(5.12,5.14,5.15) with the appropriate instrument settings. It is observed that each plot indicates the presence of a high-order system with some very sharp resonances. These would have to be resolved to ·1Hz, in certain cases, to determine their exact **Q** - factors, if required.

Throughout the experiments, the engine was excited around a mean speed of 2300 r.p.m. and perturbed by a stepped sinusoid of 400mV peak - to - peak. This value tended to swing the engine speed by $\pm$ 100r.p.m. For two-point measurements, entry was made to E, Y on the instrument's front panel and to X,E,Y for the three-point estimates of Torque/Fuel-Flow response. Since the transducer signals had a significant d.c. content, intermediary high-pass filters, which had a cut-off at ·2Hz, were used. This accounts for the phase lead, at low frequencies, which is prominent in two of the plots.

Satisfactory amplitude scaling was achieved by using 5x and 10x options on the Burr-Brown amplifiers. These were juggled with in order that neither meter indicated a magnitude greater than five volts,

since the multipliers would tend to lose accuracy. Accordingly, in Fig.(5.15), gain adjustments had further to be made around 3Hz and below, due to the transfer function having a component greater than 1 ≙ five volts.

A further similar system of interest was a Singer Vogue, instrumented to record torque and throttle position, via a tape recorder, when the car was out on the road. The vehicle was set to run at approximately a mean speed of 35m.p.h., in third gear and the driver requested to randomly pump the accelerator pedal, such that the car "kangarooed" along the road. A portion of the relevent waveforms on the joint record - itself lasting $2\frac{1}{2}$ minutes - is shown in Fig.(5.16) and the estimated transfer function in Fig.(5.17).

The data was processed at four times the recording speed and therefore, all frequencies and bandwidths in Fig.(5.17) should be divided by four to obtain the true values. Averaging time was set at 20 seconds per point, with a bandwidth of 6Hz. A delay between the throttle and fuel-flow is seen in Fig.(5.17) to correspond to the visual delay of Fig.(5.16). However, above 5Hz - true frequency - it was observed that little signal was available, presumably due to the comparatively slow response of the driver's foot. In addition the signals were processed through the "random" channel with its a.c. gain of 15x. The amplitudes of the analysed waveforms were further enhanced by gains of 5x and $2\frac{1}{2}$x on E and Y respectively, after having first passed through high-pass filters at •2Hz.

Even allowing for this large scaling, a consistent plot was obtained, to show that valuable information was available - once the data had been properly conditioned to the instrument. Resolution of the data was •25Hz (true) and there did not appear to be any sharp resonances. Estimates below 6Hz were not taken with a bandwidth of 6Hz, since they would have been invariably biased.

5.4 Instrument Errors.

Preceding sections have illustrated that the new TFA will produce viable plots of transfer functions, irrespective of whether the available data is deterministic or random. In addition, simulated networks or complex engineering systems may be investigated. This section will study critical points in the instrument, which may give rise to errors affecting the overall accuracy of the plots.

5.4.1 Commutating Filters.

The results produced in Table (3.3) are at variance with the theoretical values of 9Hz and 2 volts r.m.s. for the cut-off frequency and pass-band amplitude respectively, when the commutating frequency is 1°01KHz. It is intended that this section should provide some explanation and at the same time, reveal a further insight into the mechanisation of a CRCF.

Failure of the second-order CRCF to reach the theoretical values, depends solely on the momentary loading of the switching capacitor by the bridge impedances, at the instant of commutation. This capacitor will see two parallel paths during this instant, each containing two switches, one of which is turning ON, the other OFF. A race hazard arises, such that the OFF-ON transition acts faster to produce a sum resistance, which is temporarily much lower than the OFF condition. A slight discharge of the commutated network will occur, until the ON-OFF transition restores the balance condition of high sum resistance. Slowing down the leading edges of the gate drive to the FETS, resulted in an output level only $-\frac{1}{2}\%$ from the maximum but there was no way by which the turn OFF time could beat the turn ON. The only way that this could be rectified, would be to introduce a fixed delay, to ensure that the ON-OFF condition had reached its steady state, before the opposite transition had taken place.

The second and more serious error at low switching rates, arises from the semiconductor leakage currents charging the capacitors. Current from the buffer circuitry will see two capacitors in parallel. A drift voltage will occur, until the commutated capacitor reverses direction and discharges the combination. However, the reaction is very minor when compared to the leakage current from the switching FETS, which see the smaller capacitor as a series circuit. Drift voltages of some tens of millivolts will result for cut-off frequencies at ·01Hz, although the a.c. performance will remain very adequate. It is for this reason that low leakage devices are essential for extremely low cut-off filters.

Let us assume that, during the instant of commutation, a dynamic resistance of the bridge switches will exist such that, the impedance across the capacitor is no longer the OFF impedance of the FET. This capacitance will then discharge momentarily, under an effective time constant depending on the bridge resistances, during transition. The speed of transition will determine the loss of stored charge.

First of all, let us consider the effect upon the switched capacitor, as this will be more pronounced than on the sink capacitor. Let the stored voltage on the switched capacitor fall to $(1-\alpha)$ of its original value, due to dynamic switch loading. After commutation, the remaining stored charges will balance as before. Now equation (3.44) may be modified to read as follows :-

$$V_1(T_2) = \frac{n}{n+1} V(T_1) + \frac{1}{n+1} v(T_1)(1-\alpha) = - v_1(T_2) \qquad (5.10)$$

$$\text{Also } v_{css}(T_2) = - \frac{nA}{n+1} - v_1(T_2) \qquad (5.11)$$

$$\therefore \quad v_{css}(T_2) = - \frac{nA}{n+1} + \frac{n}{n+1} V(T_1) + \frac{1}{n+1} v(T_1)(1-\alpha) \qquad (5.12)$$

Likewise,

$$v_{css}(T + T_1) = \frac{nA}{n+1} - v_1(T + T_1)(1-\alpha) \tag{5.13}$$

$$v_{css}(2T) = -\frac{nA}{n+1} - v_1(2T)(1-\alpha) \tag{5.14}$$

Following the conventions of (3.50), we have :-

$$v_{css}(T_1) = bA \tag{5.15}$$

$$V_{ss}(T_1) = A(1 - b) \tag{5.16}$$

$$\begin{aligned} v_{css}(T_2) &= -bA + bA(1-b)+(1-b)(1-\alpha)bA \\ &= bA\left[-b+(1-b)(1-\alpha)\right] \\ \therefore\ v_{ss}(T_2) &= bA\left[(b-1)(1-\alpha)+b\right] \end{aligned}$$

The abbreviations may be applied to 5.13) to give ;-

$$\begin{aligned} v_{css}(T + T_1) &= bA - bA\left[1-b\left\{(b-1)(1-\alpha)+b\right\}\right] \\ &\quad -(1-b)(1-\alpha)bA\left[(b-1)(1-\alpha)+b\right] \\ &= bA\left[(b-1)(1-\alpha)+b\right]\left[b-(1-b)(1-\alpha)\right] \end{aligned} \tag{5.17}$$

Repeating the above for (5.14) and generalising for the k^{th} period we may say :-

$$v_{ss}(kT) = Ab\left[(b-1)(1-\alpha) +b\right]^{2k} \tag{5.18}$$

$$V_{ss}(kT) = Ab\left[1 - b\left\{(b-1)(1-\alpha)+b\right\}^{2k}\right] \tag{5.19}$$

Hence,

$$v_{ss}(kT+T_1) - v_{ss}(kT) = Ab\left[(b-1)(1-\alpha)+b\right]^{2k}\left[(b-1)(1-\alpha)+b-1\right] \tag{5.20}$$

Dividing (5.20) by the expression for $v_{ss}(kT)$ gives

$$\begin{aligned} \frac{v_{ss}(kT+T_1) - v_{ss}(kT)}{v_{ss}(kT)} &= (b-1)(1-\alpha) + b-1 \\ &= (b-1)(2-\alpha) \\ &= -\frac{2(1-\alpha/2)}{n+1} \end{aligned} \tag{5.21}$$

A time constant has again been re-synthesised - compare (3.54) -

such that a lower cut-off frequency may be obtained by using a dynamically slower switch. This theoretical expression ties in with the observations of Chapter Three. It is worthwhile to notice that when $\alpha = 1$, the cut-off point will not tend to zero but remain fixed at one-half of the maximum.

Further, if we consider a $(1 - \beta)$ fall in the voltage stored on the sink capacitor and proceed similarly to equation (5.10), it will be observed that a loss of output signal results, proportional to β.

5.4.2 True Multipliers.

Section (4.5) mentioned that the four quadrant true multipliers used were Motorola 1595L. These were found to give a good performance on the bench set-up experiments, especially with grounded plane double-sided printed boards. Unfortunately, when placed inside the instrument, a considerable offset of the order of 300mV was self generated on each output, which could only emanate from some parascitic coupling between the other cards. Yet, when removed from their location and inserted via extension cards, the same bench set-up performance was obtained. One simple answer was to allow for the offset but this was precluded, in situ, due to the compact nature of the instrument lay-out.

The action of these multipliers depends upon a non-linear relationship between voltages and currents of matched long-tail pairs of transistors. Therefore, with a following operational amplifier operating in differential mode, a gain of 70 was required (manufacturer's data sheet), such that a slight offset on one channel, not common to both, would be greatly amplified at the output. Very good performance curves were therefore taken with these multipliers connected via extension boards but the situation proved to be of little use when the boards were fully integrated into the system. A single-ended action was thus required, if

possible, preferably with full negative feedback. Consequently, a novel four quadrant low-frequency multiplier was devised, as shown in Fig.(5.18). Its multiplying capabilities were well within 1% of its full-scale inputs of $\pm$ 5V and in addition, the multiplications were both consistent, repeatable and tolerant of minor changes in the stabilised power supply. The action of the device is explained as follows :-

A reference signal of magnitude 10.00 volts is set up via a zener diode and amplifying circuit. Its polarity is inverse to the voltage A, one of the multiplying signals. When this reference voltage is applied to a negative integrator, a linear ramp ensues, with the shunt FET switched OFF. This ramp is compared with A, such that the output from the comparator will switch ON the FET to discharge the capacitor when the two voltages coincide. The discharge period is determined by the monostable circuit of (100pF, 1.5 KΩ, 47 KΩ). Hence, the output of the integrator must be a periodic ramp, whose envelope follows sampled values of A, the rate of sampling depending upon the integrator constant and the amplitude of A. The sampling bandwidth is further determined by the frequency response of the operational amplifiers, 2N72741.

Meanwhile, a signal B, whose polarity to a second integrator again depends upon the signal A, produces a repetitive ramp function at the output, whose amplitude depends on both B and the ramp duration of signal A. Hence, from the integrator related to A,

$$\text{Vout} = \frac{V_{ref}\,t}{RC} \qquad (5.22)$$

whose maximum level is A.

$$\therefore\ t = \frac{ARC}{V_{ref}} \qquad (5.23)$$

Secondly, for the integrator related to B

$$\text{Vout} = \frac{Bt}{RC} \qquad (5.24)$$

But both integrations start at the same time and have equal durations. Therefore time is common to both. Eliminating this variable and assuming identical time constants, it can now be shown that the output peak = $(AB)(V_{ref})^{-1}$.

This result in itself is not completely original, since one other method has used a simple combination of RC first-order networks (76) to give a peak output product for two quadrants. Removal of the ramp waveforms requires a sample and hold device, which must incorporate circuitry to forecast the termination of the ramp, so that the peak and only the peak value will be held. This adds more complications to the circuitry.

The advantage of true integrators lies in the provision for the d.c. content of the repetitive ramp function to be equal to the desired product. By simple geometry, the average value of the ramp function is equal to one half the height. Therefore a simple gain of two will compensate for the factor of one half. This gain may also incorporate a low-pass filter circuit to remove the ripple in the output. A band - limited frequency response results from using 2N72741's but other operational amplifiers could be used to advantage.

The above discussed method, relating the product to the average value of the waveform, could only be used with RC lag networks, when the output is operating over a region with a constant gradient i.e. with a low-level input signal. Otherwise, the area under an exponential curve is no longer directly proportional to the input signal level. It was with these multipliers that the results produced in the various Figs.(5.4 - 5.17) have been obtained.

5.4.3. Other Errors.

Finally, other errors will be pointed out which affect the overall accuracy. If we start at the entry to the instrument, the

important channels - E,Y - for amplitude information have been observed to stay locked together, within ± 1% of the full scale voltage of five volts, when the same signal is applied to each. This is valid to the end of the filtering procedures. Subsequently, a number of small errors occur, due to the offsets, in the operational amplifiers used for addition and subtraction of the various signals. This is particularly relevent to the signum multipliers, which feed to the adaptive loop, since their alternate operations, of inversion and common mode, present asymmetrical resistances to the separate amplifier bias currents. Variations in offset up to 5mV tend to prevail. Within the closed loop of the adaptive circuitry, negligible errors will occur due to the high gain of the integrators used. Consequently, if one uses signals of the order of one volt peak, at the input to the instrument, allowing for any scaling by amplifiers, a typical accuracy of the output plot should be better than ± 2%. The application of higher signal levels will improve this accuracy, since the inherent offsets will be small in comparison.

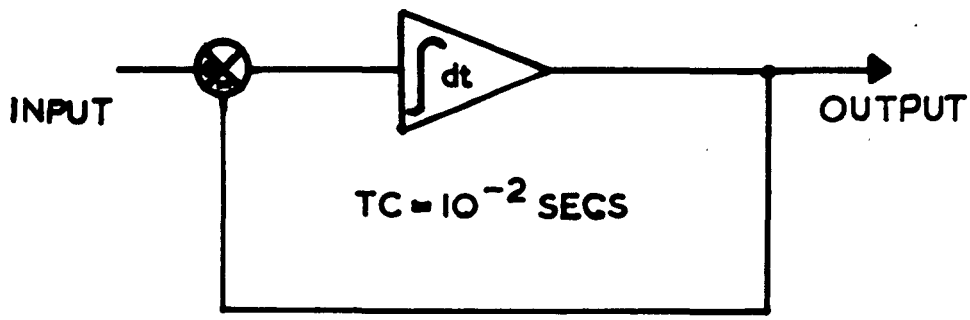

FIG. 5.1 EXPERIMENTAL NETWORK

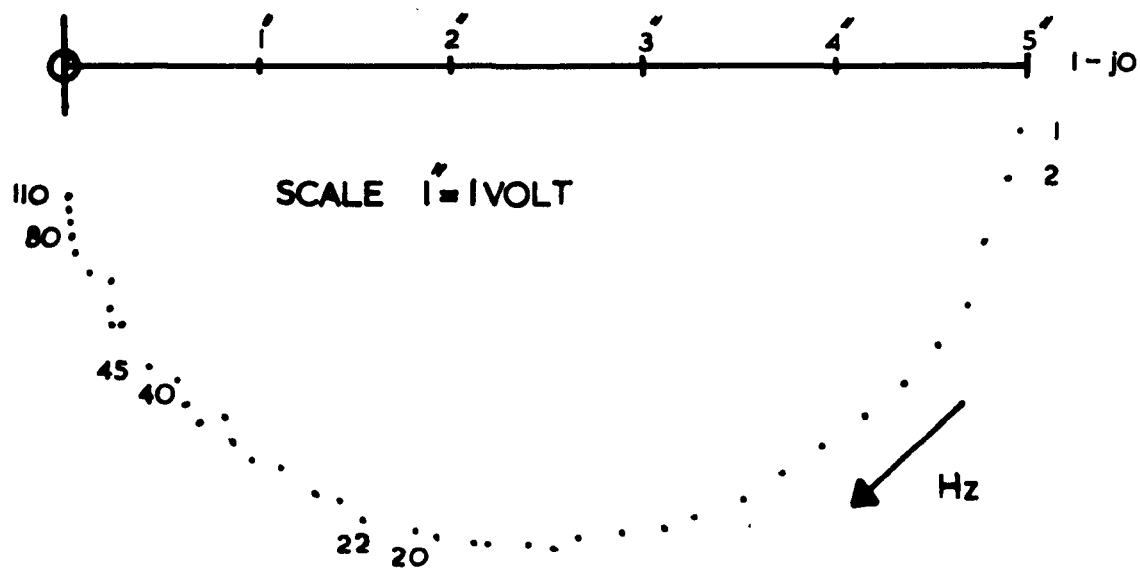

FIG. 5.2 OVERALL RESPONSE USING COMMERCIAL TFA

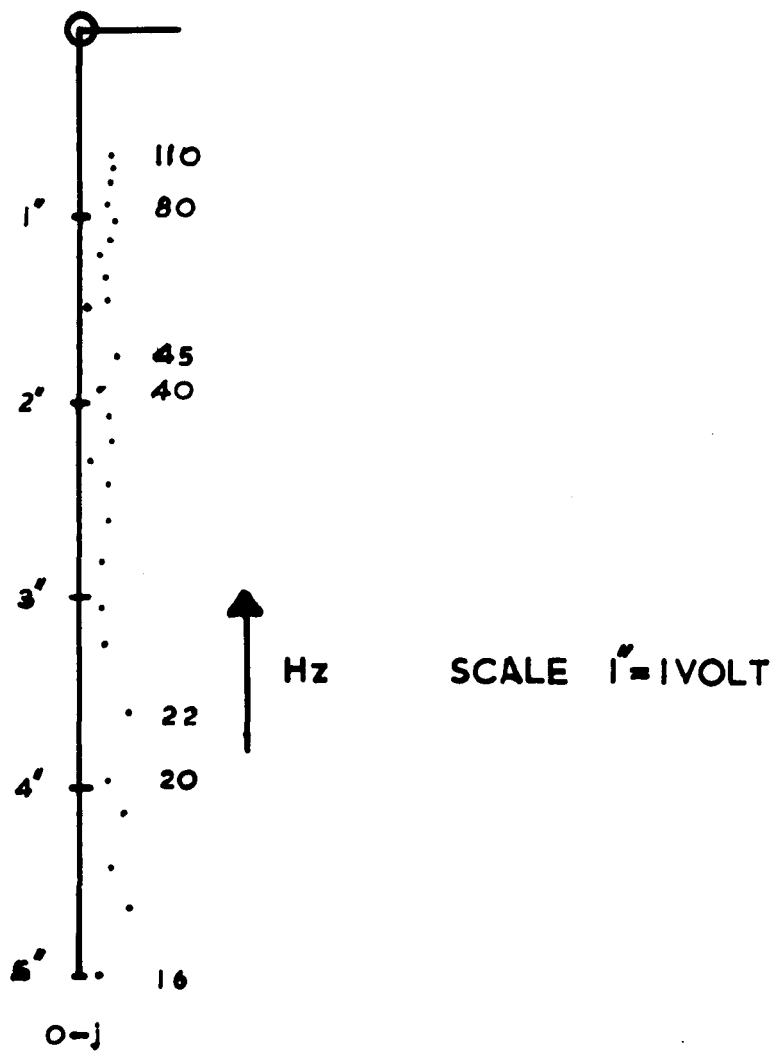

FIG. 5.3 NYQUIST PLOT OF FORWARD PATH USING COMMERCIAL TFA

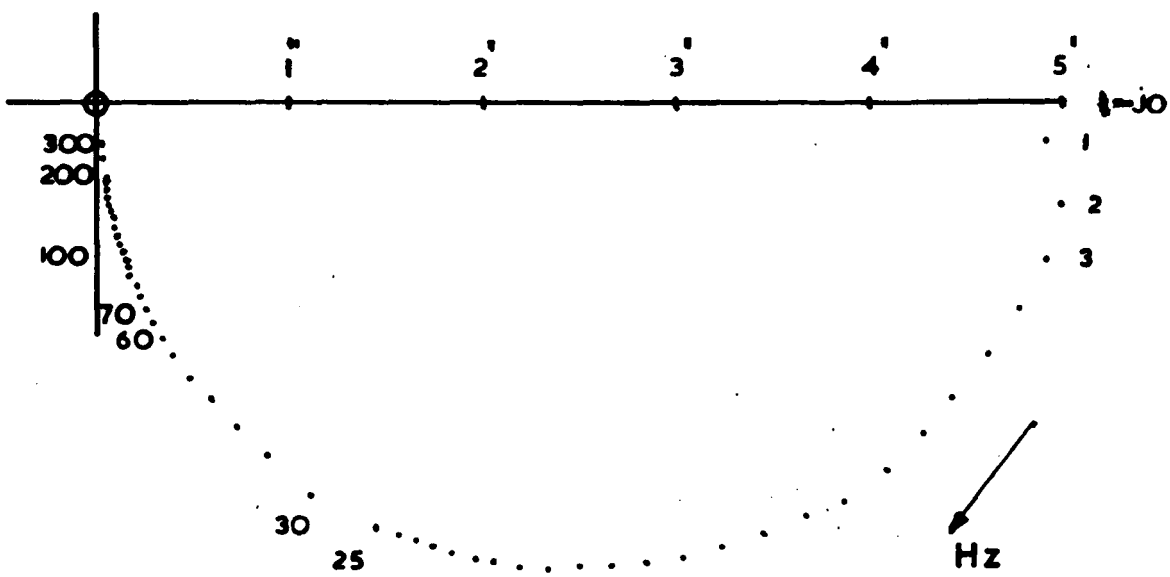

AV. TIME = 2 SECS.

B/W = 1Hz

SCALE 1" = 1VOLT

FIG. 5.4 OVERALL RESPONSE USING NEW TFA

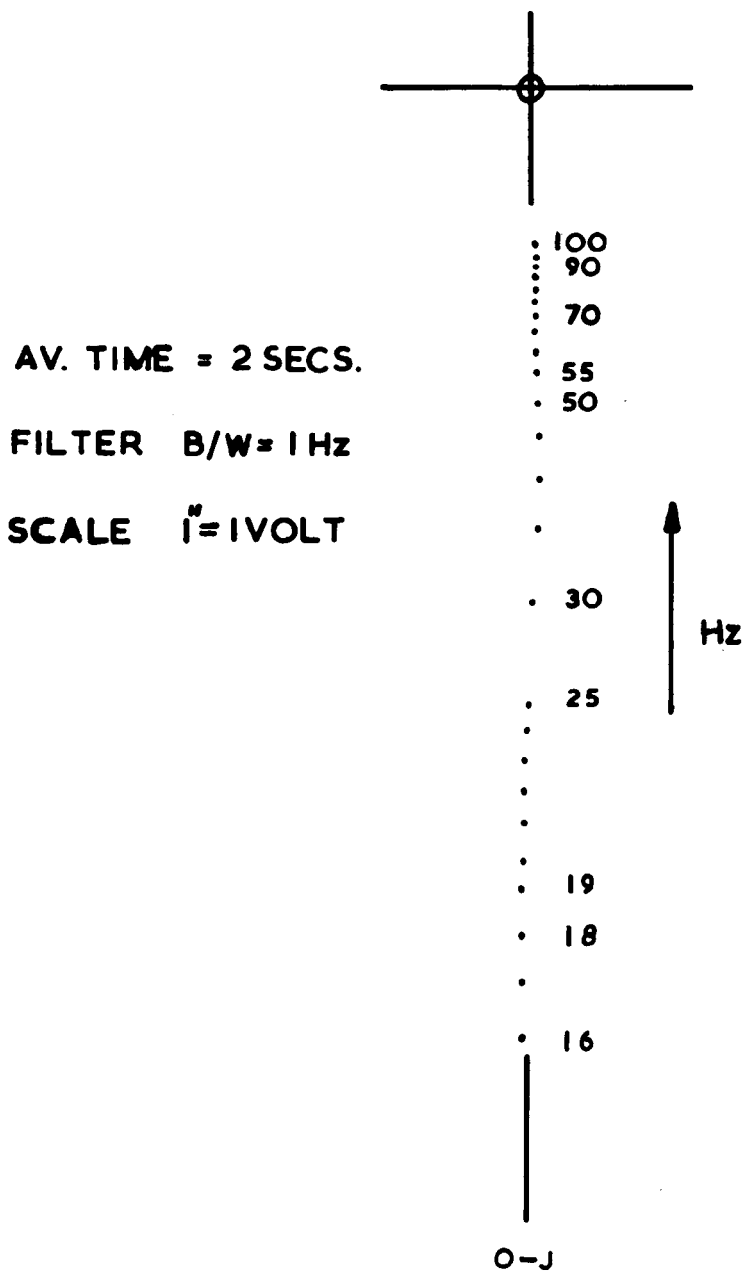

FIG. 5.5 FORWARD PATH RESPONSE USING NEW TFA

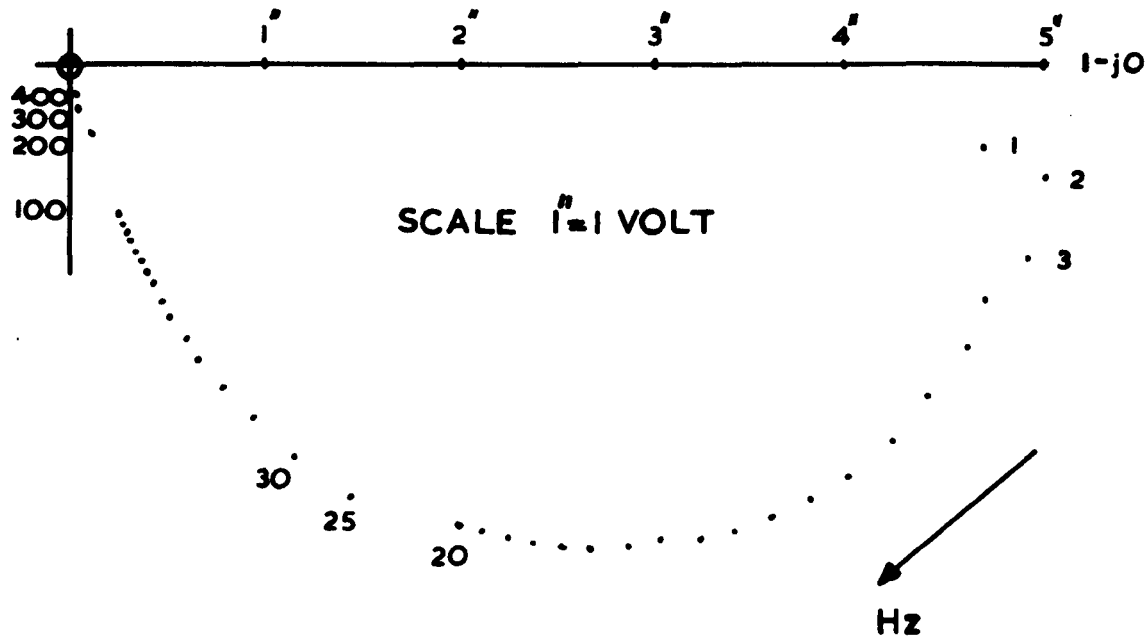

B/W 9Hz (400-100) Hz
2Hz (100- 20) Hz AV. TIME = 3 SECS.
1Hz (20- 1) Hz AV. TIME = 10 SECS.

FIG.5.6 OVERALL RESPONSE USING THE INTERNAL P.R.B.S. GENERATOR

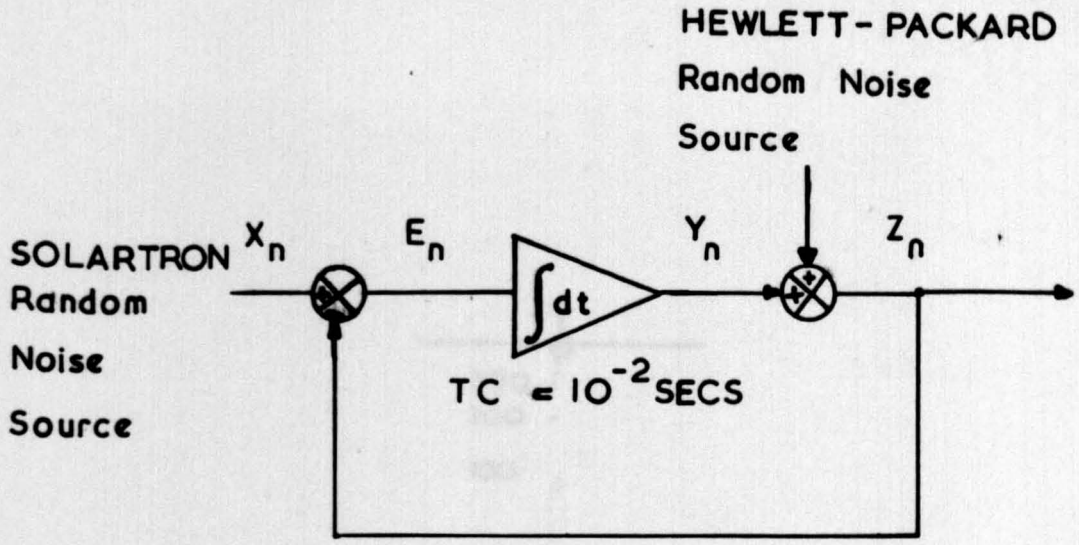

FIG. 5.7 EXPERIMENTAL NETWORK WITH ADDITIVE RANDOM NOISE

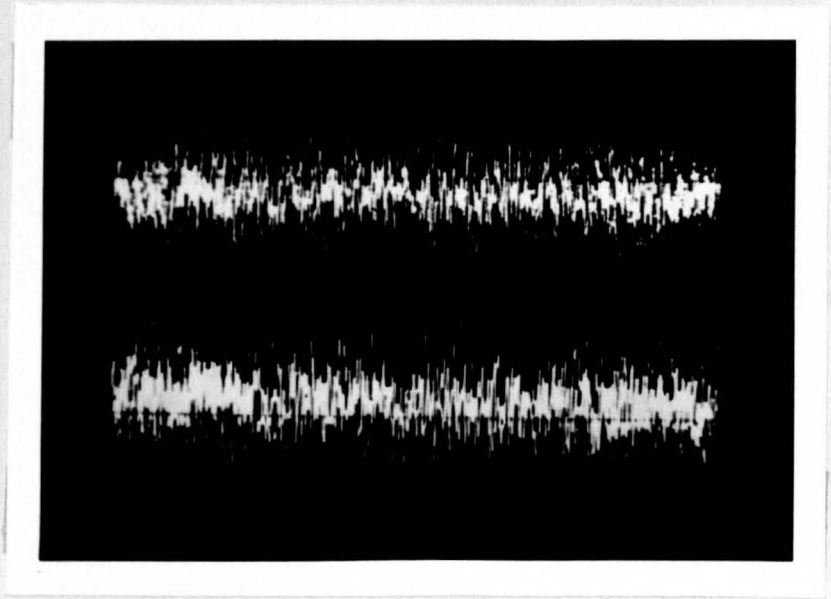

FIG. 5.8 INDEPENDENT RANDOM NOISE SOURCES

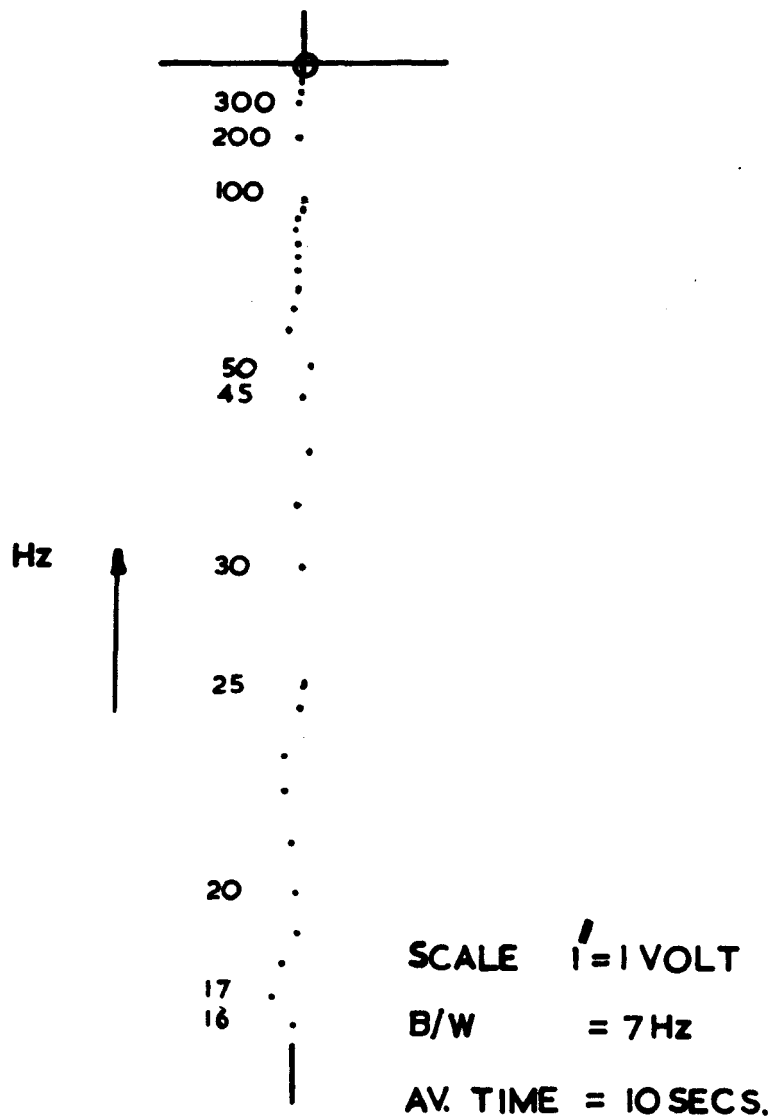

FIG. 5.9 UNBIASED ESTIMATE OF FORWARD PATH FROM RANDOM NOISE SOURCES

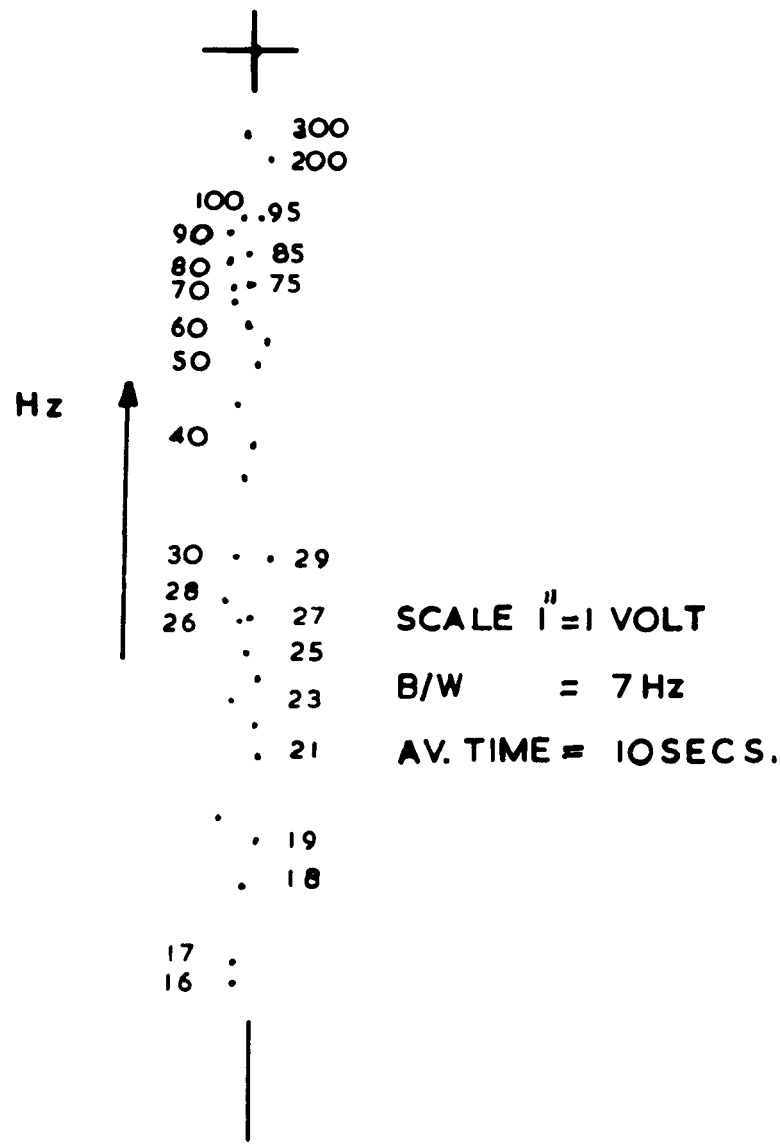

FIG.5.10 ESTIMATE OF FORWARD PATH TRANSFER FUNCTION WHEN NOISE INSERTED IN FORWARD PATH

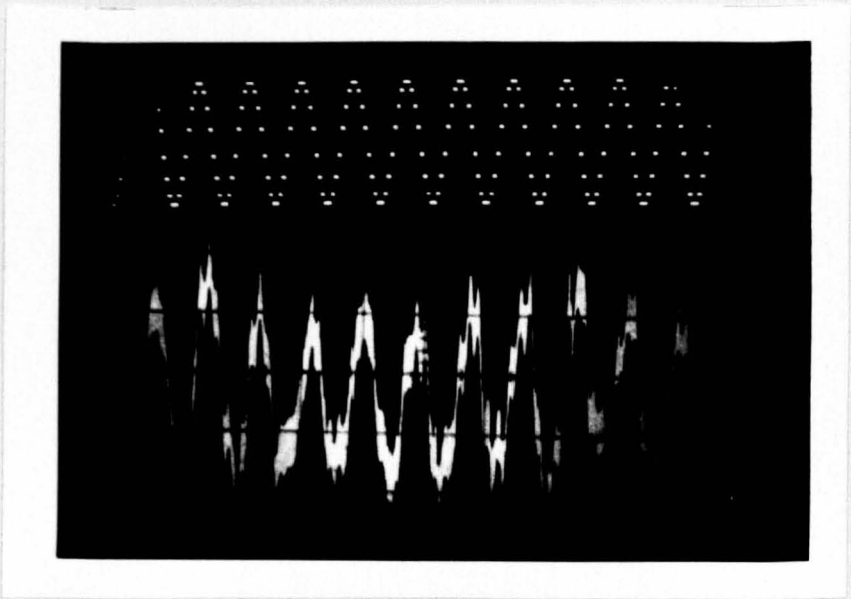

FIG. 5.11 THROTTLE/TORQUE WAVEFORMS AT 2.0Hz

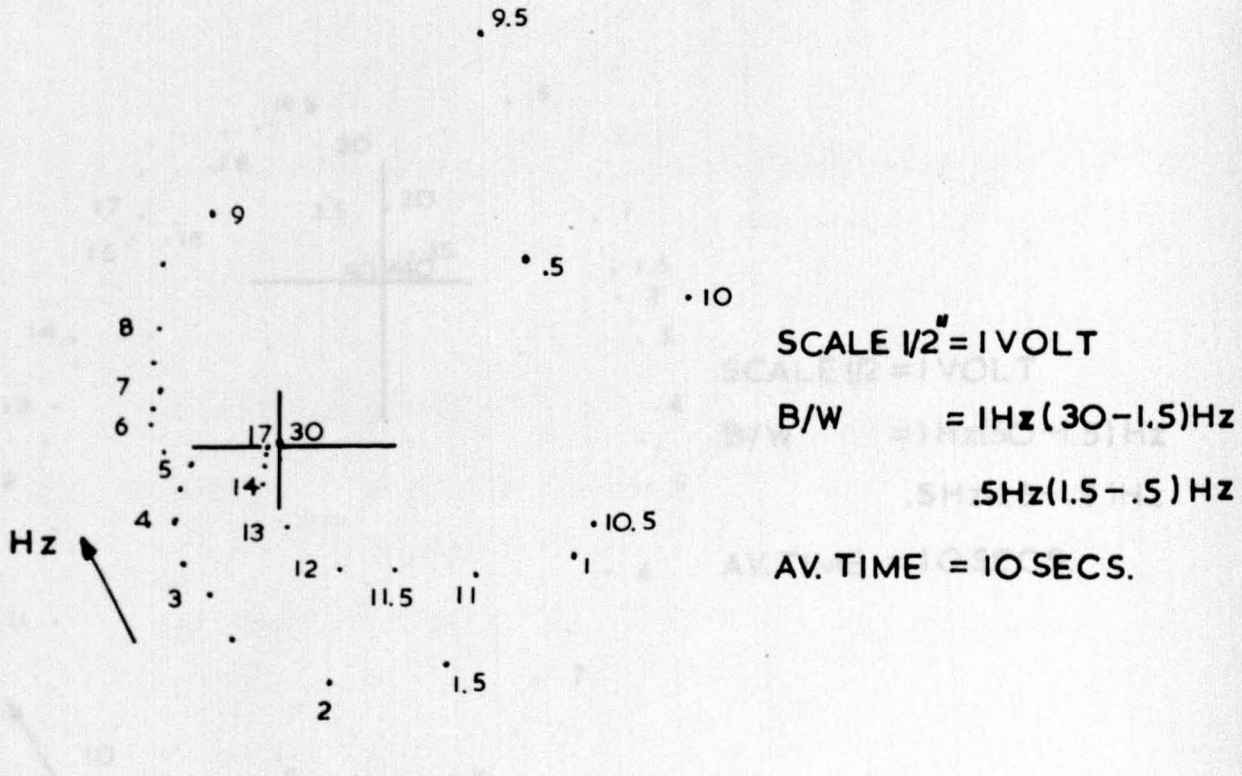

FIG. 5.12 TORQUE/THROTTLE TRANSFER FUNCTION x 1/2

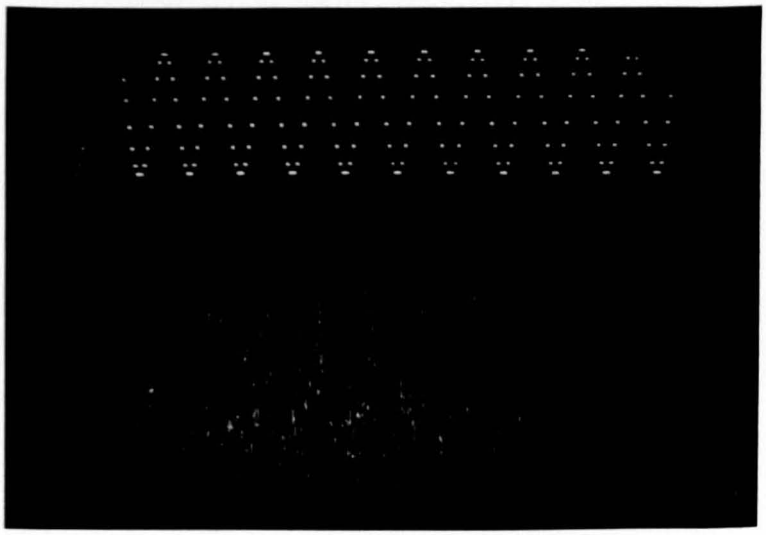

FIG. 5.13 THROTTLE/FUEL-FLOW WAVEFORMS AT 2.0Hz

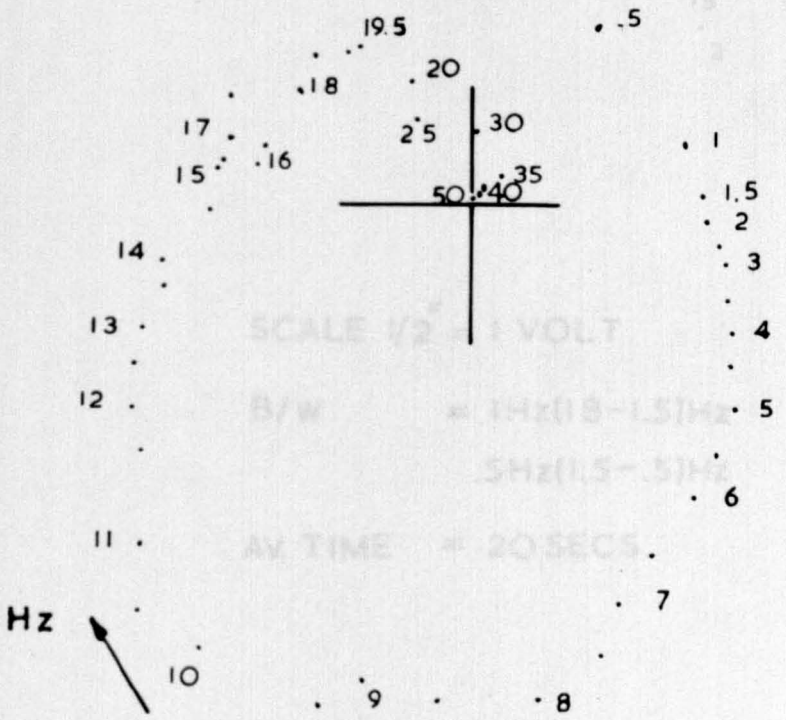

SCALE 1/2" = 1 VOLT
B/W = 1Hz(50-1.5)Hz
.5Hz(1.5-.5)Hz
AV. TIME = 10 SECS.

FIG. 5.14 FUEL-FLOW/THROTTLE TRANSFER FUNCTION x 1/2

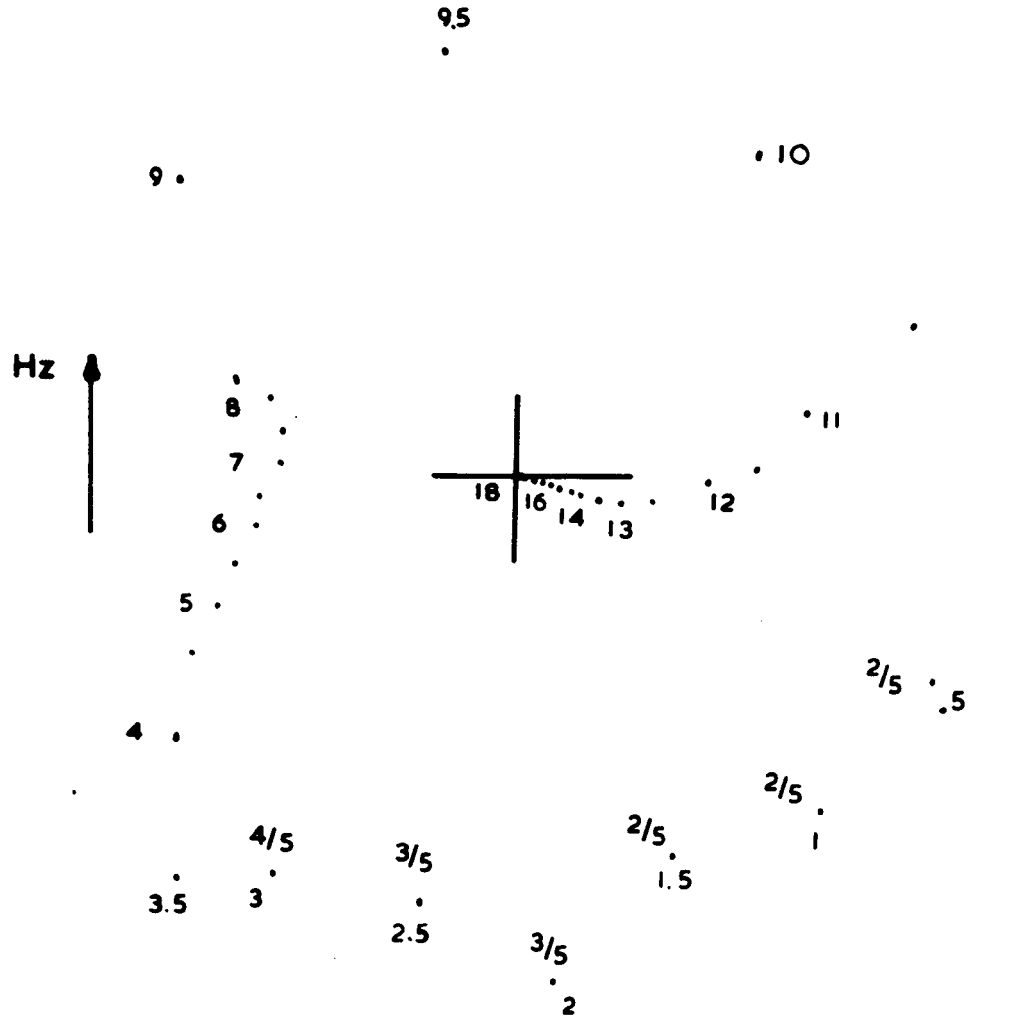

SCALE 1/2" = 1 VOLT

B/W = 1Hz(18-1.5)Hz
.5Hz(1.5-.5)Hz

AV. TIME = 20 SECS.

FIG.5.15 TORQUE/FUEL-FLOW TRANSFER FUNCTION

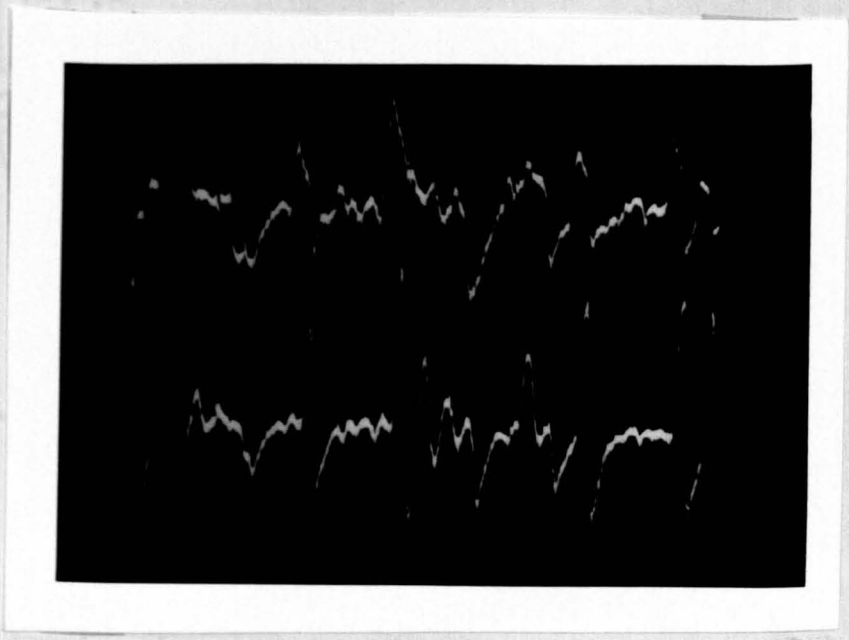

FIG. 5.16 SAMPLE OF THROTTLE, TORQUE WAVEFORMS DURING ROAD TEST

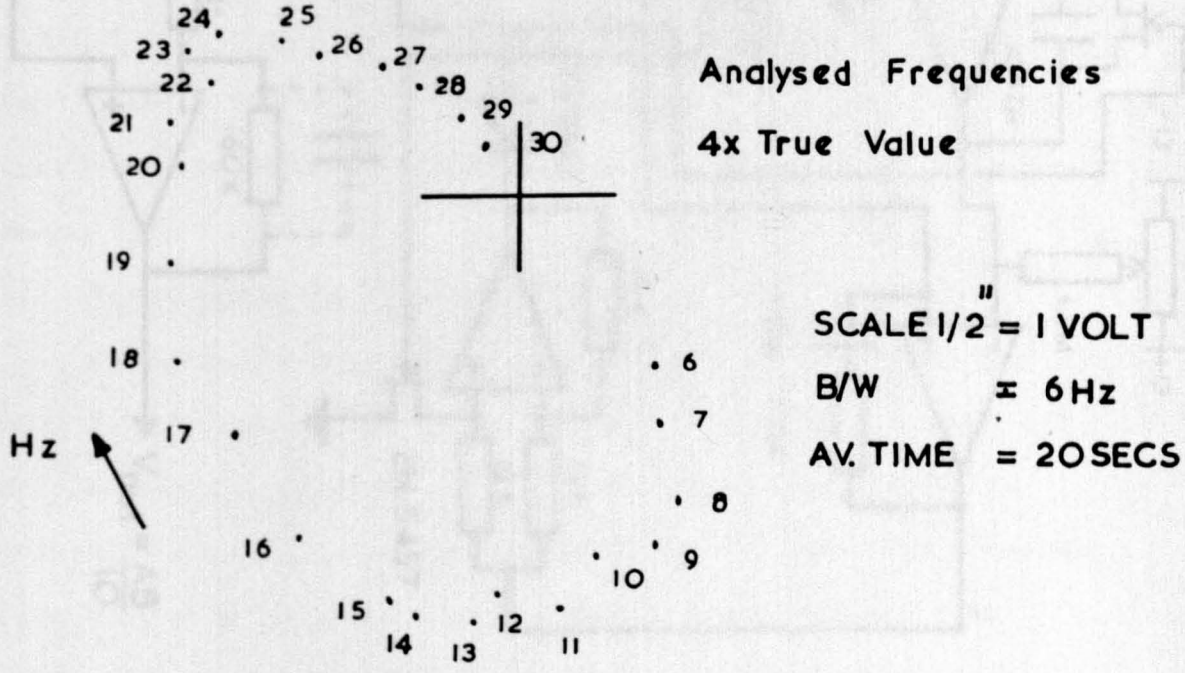

FIG. 5.17 TORQUE/THROTTLE TRANSFER FUNCTION x1/2 DURING ROAD TEST

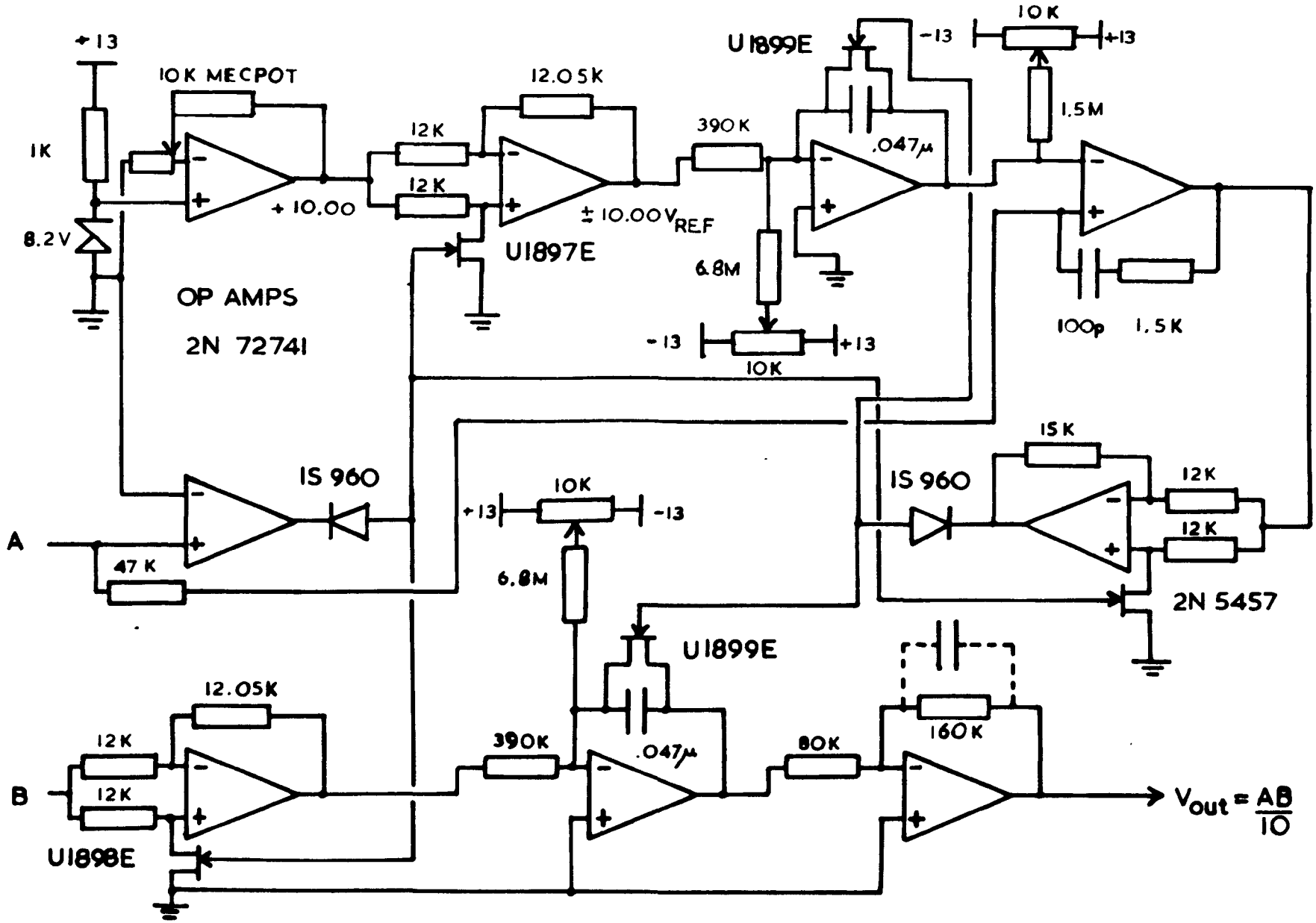

FIG. 5.18 PRECISION LOW-FREQUENCY FOUR QUADRANT MULTIPLIER

CHAPTER SIX

CONCLUSIONS

The thesis has dealt with the development of a transfer function analyser suitable for "in-situ" operation, irrespective of the nature of the available signals. Accordingly, it is the author's opinion that the instrument represents a significant advance in the state of the art, which provides an alternative to the present complex computing schemes used for similar analysis.

One advantage lies in the fact that the TFA is portable and therefore suitable for field work, as long as a mains supply is available. Hence, immediate analysis is possible, without the requirement to record information. However, if the test cannot be conducted for a sufficiently long period of time, taking the tape back to the laboratory for analysis will result in no error in the shape of the transfer function, due to varying tape speeds, during playback. Only estimates of the true analysed frequency will be in error, since the tested system does not require to be excited by a phase locked signal emanating from the instrument. The instrument's performance has been compared with currently available equipment, to illustrate that it can be used as a valuable research tool.

6.1 Suggestions for Further Work.

An immediate improvement would be the extension of this method to estimate more than one point at a time, although not necessarily all of them. Significant time savings would be possible, as it will be appreciated from the results of Chapter Five that even 80 seconds averaging per point amounts to a considerable analysis time, when well resolved features are desired. This, however, might prove to be very expensive. Certainly for low frequency analysis - below 1Hz - any recorded

data should be played back at a faster speed than it was recorded, in order to keep the analysis time to a minimum. It must, however, be remembered that this facility is limited by the maximum frequency capability of the instrument, which amounts to 2000Hz.

Secondly, at small cut-off frequencies of the commutating filters, although the drift direction is common to all, the magnitude is unfortunately not. Accurate extension of the low frequency cut-off could be obtained using a similar analysis to the construction of the adaptive loop. This would require the filter transfer function to be constructed from a number of commutating first-order or integrator circuits, arranged in a feedback loop, such that the internally generated drift could be catered for by the high loop gain.

Otherwise, apart from having better offset correction in the signum multipliers, the system appears to operate to satisfaction. Returning to the topic of the CRCF, however, it should be of further interest to develop this novel method of variable cut-off with regard to the band-pass and high-pass sections, as it would appear to provide an elegant solution to many tracking filter problems.

REFERENCES

(1) CUENOD M. SAGE A.P. "Comparison of some methods used for process identification". Identification in automatic control systems - IFAC Prague 1967.

(2) EYKHOFF P. "Process parameter and state estimation". IFAC Prague 1967.

(3) BALAKRISHNAN A.V. PETERKA V. "Identification in automatic control systems". Automatica Vol.5 pp(817-829), 1969.

(4) LEE Y.W. "Statistical theory of communication". Wiley, 1960.

(5) BALM G.J. "Crosscorrelation techniques applied to the electrocardiogram interpretation problem". Trans. IEEE Vol. BME - 14 pp (258-262), Oct. 1967.

(6) BISHOP R.E.D. GLADWELL G.M.L. "An investigation into the theory of resonance testing". Philosophical Trans. of Royal Soc. Vol.255 pp(241-280), Jan, 1963.

(7) HYDE D.W. WADE W.D. "On optimum array detection of oceanic acoustic signals". Jour. Acous. Soc. Amer. Vol.44 pp(1262-1266), 1968.

(8) PANOFSKY H.A. "Meteorological applications of cross-spectrum analysis". Spectral analysis of time series ed. Harris pp(109-132) Wiley, 1967.

(9) RICE S.O. "Mathematical analysis of random noise". Ed. Wax pp(133-294) Dover, 1954.

(10) WIENER N. "Extrapolation, interpolation and smoothing of stationary time-series". Wiley, 1949.

(11) GOODMAN T.P.
RESWICK J.B.
"Determination of system characteristics from normal operating records". Trans. ASME Vol.78 pp(258-271), Feb. 1956.

(12) BLACKMAN R.B.
TUKEY J.W.
"The measurement of power spectra". Dover publications, 1959.

(13) GOODMAN N.R.
"On the joint estimation of the spectra, cospectrum and quadrature spectrum of a two-dimensional stationary gaussian process." Scientific paper n.10 Eng. Stats. Lab. New York University, 1957.

(14) GOODMAN N.R.
KATZ S.
KRAMER B.H.
KUO M.T.
"Frequency response from stationary noise : Two case histories". Technometrics Vol. 3 No.2 pp(245-268) May, 1961.

(15) JENKINS G.M.
"An example of the estimation of a linear open loop transfer function". Technometrics Vol.5 No.2 pp(227-245), May, 1963.

(16) STANTON K.N.
"Measurement of turboalternator transfer functions using normal operating data". Proc. IEE Vol.110 pp(2001-2007), Nov. 1963.

(17) STANTON K.N.
"Estimation of turboalternator transfer functions using normal operating data". Proc. IEE Vol.112 pp(1713-1720), Sept.1965.

(18) AKAIKE H.
"Some problems in the application of the cross-spectral method". Spectral analysis of time series . Ed. Harris pp(81-107) Wiley, 1967.

(19) AKAIKE H.
"On the use of non-gaussian process in the identification of a linear dynamic system". Annals of Stat. Maths. pp(269-276) 1966.

(20) PARKS P.C. "Liapunov re-design of model reference adaptive control systems". Trans. IEEE AC-11 No.3 pp(362-367), July, 1966.

(21) MASTEN M.K.
WOMACK B.F. "Adaptive modeling of time variable systems". Info. and Control 15 pp(209-225), 1969.

(22) HSIA T.C.
VIMOLVANICH V. "An on-line technique for system identification". Trans. IEEE AC-14 pp(92-96), Feb. 1969.

(23) DWYER B. "A feedback transfer function analyser". Control pp(676-678), Dec. 1965.

(24) HUGHES M.T.G.
MAY R. "Estimation of frequency response from random data". IFAC. Prague 1967.

(25) MAY R. "Spectral analysis of engineering systems". Ph.D. thesis Univ. of Warwick, Sept. 1968.

(26) BRIGGS P.A.N.
GODFREY K.R.
HAMMOND P.H. "Estimation of process dynamic characteristics by correlation methods using pseudo - random signals". IFAC Prague 1967.

(27) PRIESTLEY M.B. "Estimation of transfer functions in closed loop stochastic systems". Automatica Vol.5 pp(623-632), 1969.

(28) JENKINS G.M.
WATTS D.G. "Spectral analysis and its applications". Holden-Day p76, 1968.

(29) ENOCHSON L.D. "Frequency response functions and coherence functions for multiple input linear systems" NASA CR-32, April, 1964.

(30) WELLSTEAD P.E. "Aspects of real-time digital spectral analysis". Ph.D. thesis Univ. of Warwick, Oct. 1970.

(31) BENDAT J.S. PIERSOL A.G. "Measurement and analysis of random data". Wiley pp(258-270), 1966.

(32) CAUGHEY T.K. DIENES J.K. "A controversy in problems involving random parametric excitation". Jour. Maths. and Physics pp(288-296), 1965.

(33) BENDAT J.S. PIERSOL A.G. "Measurement and analysis of random data". Wiley pp(264-265), 1966.

(34) JENKINS J.M. WATTS D.G. "Spectral analysis and its applications". Holden-Day pp(255-257), 1968.

(35) SHINNERS S.M. "Control systems design". Wiley pp(320-321), 1964.

(36) PAPOULIS A. "The fourier integral and its applications". McGraw-Hill pp(144-160), 1962.

(37) CAPON J. "Symposium on active networks and feedback systems". New York, pp(561-563), April, 1960.

(38) HUGHES M.T.G. "A digitally controlled sine/cosine resolver". Paper to be submitted to Electronics Letters.

(39) POWNER E.T. GREEN D.H. "Digital waveform synthesis". Electronic Eng. pp(50-54) August, 1969.

(40) DAVIES A.C. "Digital generation of low-frequency sine waves". Trans. IEEE Vol.-IM18 pp(97-105) No. 2 June, 1969.

(41) HARRIS J.N. "A programmed variable-rate counter for generating the sine function". Trans. IRE on electronic computers. pp(21-26) March, 1956.

(42) DEVINE M.L. "A.C. performance of f.e.t. analogue switch". Proc. IEE Vol.117 pp(1205-1210) July, 1970.

(43) HARTLEY M.G. "An introduction to electronic analogue computers". Methuen monograph p22, 1962.

(44) FREEMAN E.A. ABBOTT K.M. "Switch using bipolar transistors for use in analogue computing". Proc. IEE Vol.116 pp(355-364) March, 1969.

(45) BENDAT J.S. PIERSOL A.G. "Measurement and analysis of random data". Wiley pp(195-200), 1966.

(46) NOVAK D.J. SCHMIDT P.E. "Introduction to digital filters". Trans. IEEE Vol.EMC-10 pp(210-220) June, 1968.

(47) RADER C.M. GOLD. B. "Digital filter design techniques in the frequency domain". Proc. IEEE Vol.55 pp(149-171) February, 1967.

(48) HEALEY M. THOMAS J.G. "Numerical or digital filtering". Inter. Jour. Elect. Eng. Educ. Vol.7 pp(395-418), 1969.

(49) KUNTZ W. "A new sample-and-hold device and its application to the realisation of digital filters". Proc. IEEE pp(2092-2093) November, 1968.

(50) SANDBERGS L.E. FRANKS I.W. "An alternative approach to the realisation of network transfer functions: the n-path filter". Bell Syst. Tech. Jour. pp(1321-1350) September, 1960.

(51) SUN Y. FRISCH I.T. "A general theory of commutated networks". Trans. IEEE Vol.CT-16 pp(502-508) Nov.1969.

(52) M^{c}DANIEL W.L. "Fourier analysis of commutated-capacitor -type integrator output signal". Trans. IEEE Vol. AES-4 pp(637-642) July, 1967.

(53) SMITH B.D. "Analysis of commutated networks". Trans. IRE Vol.PGAE-10 pp(21-26) December, 1953.

(54) SUN Y.
FRISCH I.T.
"Analysis and synthesis of a.c. compensation filters". Trans. IEEE Vol.CT-15 pp(341-349) December, 1968.

(55) DESOER C.A.
"Transmission through a linear network containing a periodically operated switch". IRE Wescon Circuit Theory pp(34-41), 1958.

(56) HOLT A.G.J.
PULE C.
"A modified transfer function obtained from the commutating contact of an n-path filter". Int. J. of Control Vol.9, pp(425-427), 1969.

(57) TSYPYKIN Ya. Z.
"Sampling systems theory and its application". Pergamon Press Vol.1 pp(357-364), 1964.

(58) BORELLI M.T.
"Analysis of commutated networks employing feedback circuits". Trans. IEEE Vol.AES-5 pp(39-45) January, 1969.

(59) MACARIO R.C.V.
YUSEF T.
"High-Q n-path filter using diode bridges". Elect. Eng. pp(76-79) January, 1969.

(60) GLASER A.B.
HALKIAS C.C.
MEADOWS H.E.
"A tuneable, bandwidth-adjustable solid-state filter". Jour. Frank. Inst. pp(83-98) August, 1968.

(61) ASNER B.A.
"Analysis of notch networks containing synchronously commutated capacitors or RC combinations". NASA TN D-2625 Feb.,1965.

(62) HART W.G.
McGOWAN G.F.
DuPONT T.E.
"Design and application of an adaptive tracking filter control system". Trans. IEEE Vol.AES-4 pp(592-606) July, 1968.

(63) LANGER E.
"A new type of n-path filter with two pairs of complex poles". Solid-State Conf. Univ. of Pennsylvania, 1968.

(64) HOLT A.G.J.
PULE C.
"A modified transfer function obtained from the commutating contact of an n-path filter". Int. J. of Control Vol.9, pp(430-432), 1969.

(65) SUN Y.
FRISCH I.T.
"Resistance multiplication in integrated circuits by means of switching". Trans. IEEE Vol. CT-15 September, 1968.

(66) KUHLER J.A.
"Periodic - switched filter networks : a means of amplifying and varying transfer functions". Trans. IEEE Vol.SC-4 pp(225-230) August, 1969.

(67) NG K.C.
MURTHY K.K.
"Electromechanical running averager". Electr. Eng. pp(169-171) March, 1967.

(68) M^{c}KINNEY J.A.
"The periodically reverse-switched capacitor". Trans. IEEE Vol.CT-15 pp(288-290) Sept. 1968.

(69) HUELSMAN L.P.
"Theory and design of active RC circuits". M^{c}Graw-Hill, 1968.

(70) ROBROCK R.
"A digital integrator". IFAC Pulse Symposium, 1968.

(71) MOSHOS G.J.
"Error analysis of the BRM". NASA TN D3124.

(72) MANN R.
"A voltage - controlled square wave / triangular wave generator". Texas appln. report B37, 1968.

(73) LAWSON J.L.
UHLENBECK G.E.
"Threshold signals". M^{c}Graw-Hill pp(56-63), 1950.

(74) MURPHY G.J.
"Control engineering". Van Nostrand pp(62-69), 1959.

(75) COMFORT J.V.
"Studies in engine test bed automation". Ph.D Thesis U. of Warwick, 1970.

(76) ROBERTS V.C. "Integrated analogue multiplier/divider". Elect. Eng. pp(496-498) April, 1969.

APPENDIX ONE

VARIANCE OF THE REAL PART OF A TRANSFER FUNCTION.

From equations (2.24) and (2.26) we may expand as follows:-

$$\hat{K} \approx \frac{A_{yx}A_{ex} + B_{yx}B_{ex}}{(A_{ex}^2 + B_{ex}^2)} + \delta A_{yx}A_{ex}\left[A_{ex}^2 + B_{ex}^2\right]^{-1} + \delta A_{ex}A_{yx} \times \left[A_{ex}^2 + B_{ex}^2\right]^{-1} + \delta B_{yx}B_{ex}\left[A_{ex}^2 + B_{ex}^2\right]^{-1} + \delta B_{ex}B_{yx} \times \left[A_{ex}^2 + B_{ex}^2\right]^{-1} - \delta A_{ex}^2 A_{ex}\left[A_{yx}A_{ex} + B_{yx}B_{ex}\right]\left[A_{ex}^2 + B_{ex}^2\right]^{-2} - \delta B_{ex}^2 B_{ex}\left[A_{yx}A_{ex} + B_{yx}B_{ex}\right]\left[A_{ex}^2 + B_{ex}^2\right]^{-2} \quad (A\ 1.1)$$

$$\therefore \hat{K} \approx \frac{A_{yx}A_{ex}}{(A_{ex}^2+B_{ex}^2)}\left[1 + \frac{\delta A_{yx}}{A_{yx}} + \frac{\delta A_{ex}}{A_{ex}} - \frac{(2\delta A_{ex}A_{ex} + 2\delta B_{ex}B_{ex})}{(A_{ex}^2 + B_{ex}^2)}\right] + \frac{B_{yx}B_{ex}}{(A_{ex}^2+B_{ex}^2)}\left[1 + \frac{\delta B_{yx}}{B_{yx}} + \frac{\delta B_{ex}}{B_{ex}} - \frac{(2\delta A_{ex}A_{ex} + 2\delta B_{ex}B_{ex})}{(A_{ex}^2 + B_{ex}^2)}\right] \quad (A1.2)$$

Hence by taking the expected value of (A1.2) we may say

$$Av\left[\hat{K}\right] \approx \frac{A_{yx}A_{ex} + B_{yx}B_{ex}}{(A_{ex}^2 + B_{ex}^2)} \quad (A1.3)$$

by virtue of the definitions in section (2.2.2).

The variance of $\hat{K}$ can also be obtained from (A1.2).

$$\therefore \mathrm{Var}\left[\hat{K}\right] \approx \frac{(A_{yx}A_{ex})^2}{(A_{ex}^2+B_{ex}^2)^2}\left[\frac{\mathrm{Var}\left[A_{yx}\right]}{A_{yx}^2} + \frac{\mathrm{Var}\left[A_{ex}\right]}{A_{ex}^2} + \mathrm{Av}\left[\frac{2\delta A_{ex}A_{ex}+2\delta B_{ex}B_{ex}}{(A_{ex}^2 + B_{ex}^2)}\right]^2 + \frac{\mathrm{Cov}\left[A_{yx}A_{ex}\right]}{A_{yx}A_{ex}} - \mathrm{Av}\left[\frac{\delta A_{yx}2(\delta A_{ex}A_{ex}+\delta B_{ex}B_{ex})}{A_{yx}\quad(A_{ex}^2 + B_{ex}^2)}\right] + \frac{\mathrm{Cov}\left[A_{ex}A_{yx}\right]}{A_{ex}A_{yx}} - \mathrm{Av}\left[\frac{\delta A_{ex}2(\delta A_{ex}A_{ex}+\delta B_{ex}B_{ex})}{A_{ex}\quad(A_{ex}^2 + B_{ex}^2)}\right] - \frac{2\mathrm{Av}(\delta A_{ex}A_{ex}+\delta B_{ex}B_{ex})}{(A_{ex}^2 + B_{ex}^2)}\left[\frac{\delta A_{yx}}{A_{yx}} + \frac{\delta A_{ex}}{A_{ex}}\right]\right]$$

$$+ \frac{(B_{yx}B_{ex})^2}{(A_{ex}^2+B_{ex}^2)^2}\left[\frac{\mathrm{Var}\left[B_{yx}\right]}{B_{yx}^2} + \frac{\mathrm{Var}\left[B_{ex}\right]}{B_{ex}^2} + 4\mathrm{Av}\left[\frac{\delta A_{ex}A_{ex}+\delta B_{ex}B_{ex}}{(A_{ex}^2 + B_{ex}^2)}\right]^2 + \frac{\mathrm{Cov}\left[B_{yx}B_{ex}\right]}{B_{yx}B_{ex}} - \mathrm{Av}\left[\frac{\delta B_{yx}2(\delta A_{ex}A_{ex}+\delta B_{ex}B_{ex})}{B_{yx}\quad(A_{ex}^2 + B_{ex}^2)}\right] + \frac{\mathrm{Cov}\left[B_{ex}B_{yx}\right]}{B_{ex}B_{yx}} - \mathrm{Av}\left[\frac{\delta B_{ex}2(\delta A_{ex}A_{ex}+\delta B_{ex}B_{ex})}{B_{ex}\quad(A_{ex}^2 + B_{ex}^2)}\right] - \frac{2\mathrm{Av}(\delta A_{ex}A_{ex}+\delta B_{ex}B_{ex})}{(A_{ex}^2 + B_{ex}^2)}\left[\frac{\delta B_{yx}}{B_{yx}} + \frac{\delta B_{ex}}{B_{ex}}\right]\right]$$

$$+2\frac{A_{yx}A_{ex}B_{yx}B_{ex}}{(A_{ex}^2 + B_{ex}^2)^2}\left[\frac{\mathrm{Cov}\left[A_{yx}B_{yx}\right]}{A_{yx}B_{yx}} + \frac{\mathrm{Cov}\left[A_{ex}B_{ex}\right]}{A_{ex}B_{ex}} + 4\mathrm{Av}\left[\frac{\delta A_{ex}A_{ex}+\delta B_{ex}B_{ex}}{(A_{ex}^2 + B_{ex}^2)}\right]^2 + \frac{\mathrm{Cov}\left[A_{yx}B_{ex}\right]}{A_{yx}B_{ex}} - \mathrm{Av}\left[\frac{\delta A_{yx}2(\delta A_{ex}A_{ex}+\delta B_{ex}B_{ex})}{A_{yx}\quad(A_{ex}^2 + B_{ex}^2)}\right] + \frac{\mathrm{Cov}\left[A_{ex}B_{yx}\right]}{A_{ex}B_{yx}} - \mathrm{Av}\left[\frac{\delta A_{ex}2(\delta A_{ex}A_{ex}+\delta B_{ex}B_{ex})}{A_{ex}\quad(A_{ex}^2 + B_{ex}^2)}\right] - \frac{2\mathrm{Av}(\delta A_{ex}A_{ex}+\delta B_{ex}B_{ex})}{(A_{ex}^2 + B_{ex}^2)}\left[\frac{\delta B_{yx}}{B_{yx}} + \frac{\delta B_{ex}}{B_{ex}}\right]\right] \quad (A1.4)$$

(A1.4) is very much simplified, if we resort to the covariance matrix result of (A2.7). This reveals that all three square bracket terms in (A1.4) are identical such that:-

$$\mathrm{Var}\left[\hat{K}\right] \approx \left[\frac{A_{yx}A_{ex}+B_{yx}B_{ex}}{A_{ex}^2+B_{ex}^2}\right]^2 \left[\frac{1}{BT}+\frac{1}{BT}+\frac{4\left[A_{ex}^2\mathrm{Var}\left[A_{ex}\right]+2A_{ex}B_{ex}\mathrm{Cov}\left[A_{ex}B_{ex}\right]+B_{ex}^2\mathrm{Var}\left[B_{ex}\right]\right]}{(A_{ex}^2+B_{ex}^2)^2}\right.$$

$$\left.\begin{array}{lll} +\frac{1}{BT} & - & \frac{2}{BT} \\ +\frac{1}{BT} & - & \frac{2}{BT} \\ -\frac{2}{BT} & - & \frac{2}{BT} \end{array}\right] \qquad (A1.5)$$

The normalised variance has now been formed such that

$$\frac{\mathrm{Var}\left[\hat{K}\right]}{K^2} \approx \frac{1}{2BT}\left[8-16+4\left[\frac{A_{ex}^2(S_{ee}S_{xx}+A_{yx}^2-B_{yx}^2)+4A_{ex}^2B_{ex}^2}{(A_{ex}^2+B_{ex}^2)^2}\right]\right.$$

$$\left.+4\left[\frac{B_{ex}^2(S_{ee}S_{xx}-A_{ex}^2+B_{ex}^2)}{(A_{ex}^2+B_{ex}^2)^2}\right]\right] \qquad (A1.6)$$

Where $\mathrm{Var}\left[A_{ex}\right]$, $\mathrm{Var}\left[B_{ex}\right]$ have been taken from the diagonal elements of the matrix in(A2.7)

(A1.6) further reduces to

$$\frac{\mathrm{Var}\left[\hat{K}\right]}{K^2} \approx \frac{1}{2BT}\left[-8+4\left[\frac{S_{ee}S_{xx}(A_{ex}^2+B_{ex}^2)+A_{ex}^4+B_{ex}^4+2A_{ex}^2B_{ex}^2}{(A_{ex}^2+B_{ex}^2)^2}\right]\right]$$

i.e. $$\frac{\mathrm{Var}\left[\hat{K}\right]}{K^2} \approx \frac{4}{2BT}\left[\frac{1}{\gamma_{\delta e}^2}-1\right] \qquad (A1.7)$$

where $$\gamma_{\delta e}^2 = \frac{|S_{ex}|^2}{S_{ee}S_{xx}} \qquad (A1.8)$$

APPENDIX TWO

COVARIANCE MATRIX OF A CLOSED-LOOP SYSTEM.

We are interested in the matrix

$$\mathrm{Cov}[\alpha] = \mathrm{Av}\left[\left[\alpha - \mathrm{Av}(\alpha)\right]\left[\alpha - \mathrm{Av}(\alpha)\right]^{T^*}\right]$$

where T^* indicates the transposed complex conjugate and

$$\alpha = \begin{bmatrix} \hat{A}_{yx} \\ \hat{B}_{yx} \\ \hat{A}_{ex} \\ \hat{B}_{ex} \end{bmatrix}$$ is a column vector.

Further $$\hat{A}_{yx} = \tfrac{1}{2}\left(C_{yx}^{*} + C_{yx}\right) \qquad (A2.1)$$

$$\hat{B}_{yx} = \tfrac{1}{2j}\left(C_{yx}^{*} - C_{yx}\right) \qquad (A2.2)$$

It is well-known that the evaluation of the covariance matrix is weighted inversely to the product (BT), where B is the filter bandwidth of the data analysis channel and T the averaging time. Both May (25) and Jenkins (36) have evaluated the matrix for the case of an open-loop estimate and analagous to them, the covariance matrix will be derived for the closed-loop case.

1) $$\mathrm{Var}\left[\hat{A}_{yx}\right] = \frac{1}{BT}\left[\frac{1}{4}\left(S_{yx}+S_{yx}^{*}\right)\left(S_{yx}^{*}+S_{yx}\right)\right]$$

$$= \frac{1}{4BT}\left[2\left|S_{yx}\right|^2 + S_{yx}^2 + S_{yx}^{*2}\right]$$

$$\therefore \mathrm{Var}\left[\hat{A}_{yx}\right] = \frac{1}{BT}\left[\frac{1}{2}\left(S_{yy}\,S_{xx} + A_{yx}^2 - B_{yx}^2\right)\right] \qquad (A2.3)$$

2) $$\mathrm{Cov}\left[\hat{A}_{yx}, \hat{B}_{yx}\right] = \frac{1}{BT}\left[\frac{1}{4j}\left(S_{yx} + S_{yx}^{*}\right)\left(S_{yx}^{*} - S_{yx}\right)\right]$$

$$= \frac{1}{4BTj}\left[S_{yx}^{*2} - S_{yx}^{2}\right]$$

$$= \frac{1}{4BTj}\left[\left(A_{yx} + jB_{yx}\right)^2 - \left(A_{yx} - jB_{yx}\right)^2\right]$$

$$\therefore \text{Cov}\left[\hat{A}_{yx}, \hat{B}_{yx}\right] = \frac{1}{4BTj}\left[4j\, A_{yx}\, B_{yx}\right] \qquad (A2.4)$$

$$3)\ \text{Cov}\left[\hat{A}_{yx}, \hat{A}_{ex}\right] = \frac{1}{BT}\left[\frac{1}{4}(S_{yx}+S_{yx}^{*})(S_{ex}^{*}+S_{ex})\right]$$

$$= \frac{1}{4BT}\left[S_{yx}S_{ex}^{*}+(S_{yx}S_{ex}^{*})^{*}+S_{yx}S_{ex}+(S_{yx}S_{ex})^{*}\right]$$

$$= \frac{1}{4BT}\left[2(A_{yx}A_{ex}+B_{yx}B_{ex})+2(A_{yx}A_{ex}-B_{yx}B_{ex})\right]$$

$$\therefore \text{Cov}\left[\hat{A}_{yx}, \hat{A}_{ex}\right] = \frac{1}{BT}\left[A_{yx}A_{ex}\right] \qquad (A2.5)$$

$$4)\ \text{Cov}\left[\hat{A}_{yx}, \hat{B}_{ex}\right] = \frac{1}{BT}\left[\frac{1}{4j}(S_{yx}+S_{yx}^{*})(S_{ex}^{*}-S_{ex})\right]$$

$$= \frac{1}{4BTj}\left[S_{yx}S_{ex}^{*}-(S_{yx}S_{ex}^{*})^{*}-S_{yx}S_{ex}+(S_{yx}S_{ex})^{*}\right]$$

$$= \frac{1}{4BTj}\begin{bmatrix}(A_{yx}-jB_{yx})(A_{ex}+jB_{ex})\\ -(A_{yx}+jB_{yx})(A_{ex}-jB_{ex})\\ -(A_{yx}-jB_{yx})(A_{ex}-jB_{ex})\\ +(A_{yx}+jB_{yx})(A_{ex}+jB_{ex})\end{bmatrix}$$

$$= \frac{1}{4BTj}\begin{bmatrix}A_{yx}A_{ex}+B_{yx}B_{ex}-jB_{yx}A_{ex}+jB_{ex}A_{yx}\\ -A_{yx}A_{ex}-B_{yx}B_{ex}-jB_{yx}A_{ex}+jA_{yx}B_{ex}\\ -A_{yx}A_{ex}+B_{yx}B_{ex}+jB_{yx}A_{ex}+jA_{yx}B_{ex}\\ +A_{yx}A_{ex}-B_{yx}B_{ex}+jB_{yx}A_{ex}+jA_{yx}B_{ex}\end{bmatrix}$$

$$\therefore \text{Cov}\left[\hat{A}_{yx}, \hat{B}_{ex}\right] = \frac{1}{BT}\left[A_{yx}\, B_{ex}\right] \qquad (A2.6)$$

Hence the remaining individual covariances can be arrived at, following the results (A2.3) to (A2.6)

Therefore :-

$$\mathrm{Cov}\begin{bmatrix} \hat{A}_{yx} \\ \hat{B}_{yx} \\ \hat{A}_{ex} \\ \hat{B}_{ex} \end{bmatrix} = (BT)^{-1}\begin{bmatrix} \frac{1}{2}(S_{yy}S_{xx}+A_{yx}^2-B_{yx}^2) & A_{yx}B_{yx} & A_{yx}A_{ex} & A_{yx}B_{ex} \\ & \frac{1}{2}(S_{yy}S_{xx}-A_{yx}^2+B_{yx}^2) & B_{yx}A_{ex} & B_{yx}B_{ex} \\ D & & \frac{1}{2}(S_{ee}S_{xx}+A_{ex}^2-B_{ex}^2) & A_{ex}B_{ex} \\ & & & \frac{1}{2}(S_{ee}S_{xx}-A_{ex}^2+B_{ex}^2) \end{bmatrix} \qquad (A2.7)$$

where D signifies that the elements are diagonally symmetrical.

APPENDIX THREE

FOURTH - ORDER MOMENTS RELATING TO MODEL PARAMETERS.

$$a_f^* b_f c_f^* d_f = \int_0^\infty\int_0^\infty\int_0^\infty\int_0^\infty a(t-u_1)b(t-u_2)c(t-u_3)d(t-u_4)h(u_1)h(u_2)h(u_3)h(u_4)x$$
$$\exp -jw_o(u_1-u_2+u_3-u_4)\ du_1du_2du_3du_4 \qquad (A3.1)$$

Taking the expected value of the above and remembering integration and expectation to be linear operators we have:-

$$Av\left[a_f^* b_f c_f^* d_f\right] = \int_0^\infty\int_0^\infty\int_0^\infty\int_0^\infty \Big[R_{ab}(u_2-u_1)R_{cd}(u_4-u_3)+R_{ac}(u_3-u_1)R_{bd}(u_4-u_2)$$
$$+ R_{ad}(u_4-u_1)R_{bc}(u_3-u_2)\Big] h(u_1)h(u_2)h(u_3)h(u_4)x$$
$$\exp -jw_o(u_1-u_2+u_3-u_4)\ du_1du_2du_3du_4 \qquad (A3.2)$$

R_{ij} represent correlation functions obtained from decomposing the fourth moment of a function of Gaussian random variables. Evaluation of (A3.2) will proceed by separate evaluation of the constituent components of the integrand namely I_1, I_2, I_3, the order of each integration taking place in numbered sequence.

$$\therefore I_1(U) = \int_0^\infty\int_0^\infty R_{cd}(u_4-u_3)\int_0^\infty\int_0^\infty R_{ab}(u_2-u_1)\exp jw_o(u_2-u_1)h(u_1)h(u_2)du_1du_2$$
$$x\ h(u_3)h(u_4)\ \exp\ jw_o(u_4-u_3)\ du_3\ du_4 \qquad (A3.3)$$

Inverse transforming the correlation functions to their equivalent spectral densities, we have,

$$I_1(U) = \frac{1}{2\pi}\int_{-\infty}^{+\infty}\int_0^\infty\int_0^\infty S_{cd}(w-w_o)\exp j(w-w_o)(u_4-u_3)\exp\ jw_o(u_4-u_3)x$$
$$h(u_3)h(u_4)\ du_3du_4dw\ x$$
$$\frac{1}{2\pi}\int_{-\infty}^{+\infty}\int_0^\infty\int_0^\infty S_{ab}(w-w_o)\exp j(w-w_o)(u_2-u_1)\exp\ jw_o(u_2-u_1)x$$
$$h(u_1)h(u_2)\ du_1du_2dw \qquad (A3.4)$$

where S_{ij} represent the double-sided power spectral density functions.

Re-arranging the order of integration, therefore:-

$$I_1(U) = \frac{1}{4\pi^2}\int_{-\infty}^{+\infty} S_{cd}(w-w_o)\int_0^{\infty} h(u_4)\exp jwu_4 du_4 \int_0^{\infty} h(u_3)\exp -jwu_3 du_3 dw$$

$$x \int_{-\infty}^{+\infty} S_{ab}(w-w_o)\int_0^{\infty} h(u_2)\exp jwu_2 du_2 \int_0^{\infty} h(u_1)\exp -jwu_1 du_1 dw \qquad (A3.5)$$

$$\therefore I_1(U) = \frac{1}{4\pi^2}\int_{-\infty}^{+\infty} S_{cd}(w-w_o)H_4^*(jw)H_3(jw)dw \int_{-\infty}^{+\infty} S_{ab}(w-w_o)H_2^*(jw)H_1(jw)dw \qquad (A3.6)$$

Again from (A3.3) we may say,

$$I_2(U) = \int_0^{\infty}\int\int R_{bd}(u_4-u_2)\exp jw_o(u_4+u_2)h(u_2)h(u_4)\, du_2\, du_4\, x$$

$$\int_0^{\infty}\int\int R_{ac}(u_3-u_1)\exp - jw_o(u_3+u_1)h(u_1)h(u_3)\, du_1 du_3 \qquad (A3.7)$$

Transforming (A3.7) in like manner to (A3.4):-

$$I_2(U) = \frac{1}{2\pi}\int_{-\infty}^{+\infty}\int_0^{\infty}\int\int S_{bd}(w-w_o)\exp j(w-w_o)(u_4-u_2)\exp jw_o(u_4+u_2)\, x$$

$$h(u_2)h(u_4)du_2 du_4 dw$$

$$x \frac{1}{2\pi}\int_{-\infty}^{+\infty}\int_0^{\infty}\int\int S_{ac}(w-w_o)\exp j(w-w_o)(u_3-u_1)\exp -jw_o(u_3+u_1)\, x$$

$$h(u_1)h(u_3)du_1 du_3 dw \qquad (A3.8)$$

(A3.8) may be re-arranged similarly to (A3.5) to yield:-

$$I_2(U) = \frac{1}{4\pi^2}\int_{-\infty}^{+\infty} S_{bd}(w-w_o)\int_0^{\infty} h(u_4)\exp jwu_4 du_4 \int_0^{\infty} h(u_2)\exp -j(w-2w_o)u_2 du_2 dw$$

$$x \int_{-\infty}^{+\infty} S_{ac}(w-w_o)\int_0^{\infty} h(u_3)\exp j(w-2w_o)u_3 du_3 \int_0^{\infty} h(u_1)\exp -jwu_1 du_1 dw \qquad (A3.9)$$

$$\therefore I_2(U) = \frac{1}{4\pi^2}\int_{-\infty}^{+\infty} S_{bd}(w-w_o)H_4^*(jw)H_2(jw-j2w_o)dw$$

$$x \int_{-\infty}^{+\infty} S_{ac}(w-w_o)\, x\, H_3^*(jw-j2w_o)H_1(jw)dw \qquad (A3.10)$$

Similarly,

$$I_3(U) = \int_0^{\infty}\int\int R_{ad}(u_4-u_1)\exp jw_o(u_4-u_1)h(u_1)h(u_4)du_1 du_4\, x$$

$$\int_0^{\infty}\int\int R_{bc}(u_3-u_2)\exp -jw_o(u_3-u_2)h(u_2)h(u_3)du_2 du_3 \qquad (A3.11)$$

Transforming as before we have:-

$$I_3(U) = \frac{1}{2\pi}\int_{-\infty}^{+\infty}\iint_{0}^{\infty} S_{ad}(w-w_o)\,\mathrm{expj}(w-w_o)(u_4-u_1)\,\mathrm{expj}w_o(u_4-u_1)\ x$$

$$h(u_1)h(u_4)du_1du_4dw$$

$$x\ \frac{1}{2\pi}\int_{-\infty}^{+\infty}\iint_{0}^{\infty} S_{bc}(w-w_o)\,\mathrm{expj}(w-w_o)(u_3-u_2)\,\mathrm{exp}-jw_o(u_3-u_2)$$

$$x\ h(u_2)h(u_3)du_2du_3dw \qquad \text{(A3.12)}$$

$$\therefore I_3(U) = \frac{1}{4\pi^2}\int_{-\infty}^{+\infty} S_{ad}(w-w_o)H_4^*(jw)H_1(jw)dw \int_{-\infty}^{+\infty} S_{bc}(w-w_o)H_3^*(jw-j2w_o)\ x$$

$$H_2(jw-j2w_o)dw$$

(A3.13)

APPENDIX FOUR

EQUIVALENT BANDWIDTH OF SECOND-ORDER BUTTERWORTH LOW-PASS FILTER

$$\frac{1}{2\pi}\int_{-\infty}^{+\infty}|H(jw)|^2 dw = \frac{1}{2\pi j}\int_{-\infty}^{+\infty}\frac{g_n(w)}{h_n(w)h_n(-w)}\,dw$$

where $h_n(w) = A_o w^n + A_1 w^{n-1} + A_2 w^{n-2} + \ldots\ldots\ldots A_n$

$g_n(w) = B_o w^{2n-2} + B_1 w^{2n-4} + B_2 w^{2n-6} + \ldots\ldots B_{n-1}$

For two second-order Butterworth polynomial configurations in cascade

$$h_n(w) = (-w^2 + j\sqrt{2}\, w_c w + w_c^2)^2$$

$$h_n(-w) = (-w^2 - j\sqrt{2} w_c w + w_c^2)^2$$

Therefore:-

$$A_o = 1; A_1 = -j\sqrt{w_c}; A_2 = -3w_c^2; A_3 = j\sqrt{2} w_c^3; A_4 = w_c^4$$

Also, $g_n(w) = jw_c^8$

Therefore:-

$$B_o = B_1 = B_2 = 0;\ B_3 = jw_c^8$$

The general form of the integral for n = 4 is :-

$$I_4 = \frac{(A_o B_3 A_4^{-1})(A_o A_3 - A_1 A_2)}{2A_o(A_o A_3^2 + A_1^2 A_4 - A_1 A_2 A_3)}$$

Substituting the above values for A_n and B_n we have :-

$$I_4 = \frac{(jw_c^8 w_c^{-4})(j\sqrt{2} w_c^3 - j3\sqrt{2} w_c^3)}{2(-2w_c^6 - 2w_c^6 + 6w_c^6)} = \frac{w_c}{\sqrt{2}}$$

APPENDIX FIVE.

Evaluation of Time Varying Offset Current.

Consider a general R_n in the feedback i.e. an analysis during a period with the system time-invariant.

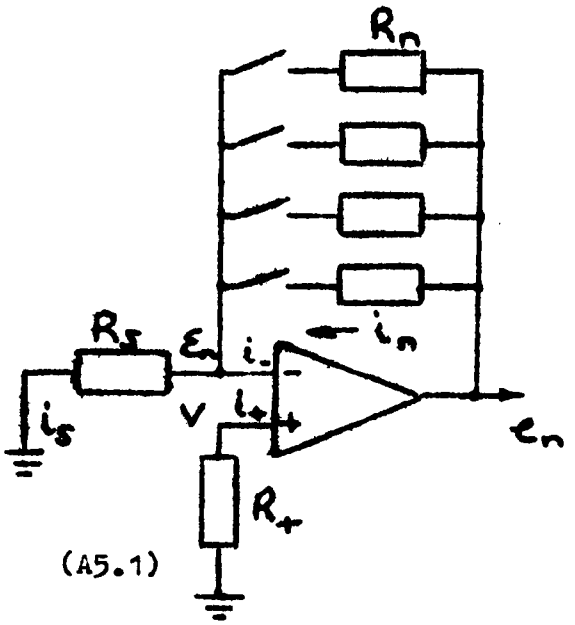

$$\therefore e_n = A(V - \varepsilon_n) \qquad (A5.1)$$

$$\text{or } e_n = A\left[(i_+ - i_-)Zin\right] \qquad (A5.2)$$

where A is the open-loop gain. Zin is the differential input impedance.

$$-V = i_+ R_i$$

$$\varepsilon_n = - i_s R_s$$

$$i_s = i_- - i_n$$

$$i_n = (e_n - \varepsilon_n)R_n^{-1}$$

using (A5.1)

$$e_n\left[1+A\frac{R_s}{R_n}\right] = A\left[-i_+R_+ + R_s\left(i_- + \frac{\varepsilon_n}{R_n}\right)\right] \qquad (A5.3)$$

Further from(A5.1)

$$\varepsilon_n = (- e_n + AV)A^{-1}$$

$$\therefore e_n\left[1 + \frac{AR_s}{R_n} + \frac{R_s}{R_n}\right] = A\left[-i_+R_+ + R_s\left(i_- + \frac{V}{R_n}\right)\right] \qquad (A5.4)$$

Multiply throughout by R_n and using $AR_s \gg R_s + R_n$

Then,

$$e_n = - \frac{i_+R_+R_n}{R_s} + \frac{i_-R_sR_n}{R_s} - \frac{i_+R_sR_+}{R_s} \qquad (A5.5)$$

Over one complete cycle of the stage, the expectation of $e_n = 0$.

Hence $0 = i_- \, Av\,(R_n) - i_+ \frac{R_+}{R_s} \left[R_s + Av(R_n) \right]$ (A5.6)

But the $Av(e_n) = 0$ implies $i_- = i_+$

$\therefore \overline{R_n} = \frac{R_+}{R_s} \left[R_s + \overline{R_n} \right]$ where the bar indicates expectation.

Hence, $R_+ = \frac{R_s \overline{R_n}}{R_s + R_n}$ and R_+ is then the required setting.

APPENDIX SIX

Resynthesised Second-Order Butterworth Polynomial

From Fig (3.10) using the symbols V_0, V_1, V_2 as voltage points, it can be stated that :-

$$V_2 = V_0 + \frac{1}{(sC_1R+1)}(V_1 - V_0) \qquad (A6.1)$$

But $$V_0 = \frac{1}{(sC_2R+1)} V_2 \qquad (A6.2)$$

Substitute for V_2 and remove denominators hence :-

$$V_0(sC_2R+1)(sC_1R+1) = V_0(sC_1R+1) + V_1 - V_0 \qquad (A6.3)$$

Simplifying (A6.3)

Therefore $$\frac{V_0}{V_1} = \frac{1}{s^2C_2C_1R^2+sC_2R+1} \qquad (A6.4)$$

Substituting; $C_2 = \frac{1}{2}C_1$, $F_1(s) = \dfrac{2}{s^2C_1^2R^2+sC_1R+2}$ (A6.5)

$C_2 = C_1$, $F_2(s) = \dfrac{1}{s^2C_1^2R^2+sC_1R+1}$ (A6.6)

$C_2 = 2C_1$, $F_3(s) = \dfrac{1}{2s^2C_1^2R^2+2sC_1R+1}$ (A6.7)

Equations (A6.5) to (A6.7) may be rephrased as conventional polynomials in s, w_o such that :-

$$F_1(s) = \frac{w_o^2}{s^2+\frac{w_o}{2}s+w_o^2} \qquad F_2(s) = \frac{w_o^2}{s^2+w_os+w_o^2} \qquad F_3(s) = \frac{w_o^2}{s^2+\sqrt{2}sw_o+w_o^2}$$

where $w_o = \dfrac{\sqrt{2}}{C_1R}$ $\qquad w_o = \dfrac{1}{C_1R}$ $\qquad w_o = \dfrac{1}{\sqrt{2}C_1R}$

$\left|F_1(s)\right|_{s=w_o} = \sqrt{2}$ $\qquad \left|F_2(s)\right|_{s=w_o} = 1$ $\qquad \left|F_3(s)\right|_{s=w_o} = \dfrac{1}{\sqrt{2}}$